AD-A070 004 BELL AEROSPACE TEXTRON BUFFALO N Y F/G 17/5
BEHAVIOR OF INFRARED WINDOW MATERIALS EXPOSED TO RAIN DROP ENVI--ETC(U)
SEP 78 J V HACKWORTH, L H KOCHER F33615-77-C-5069
UNCLASSIFIED AFML-TR-78-184 NL

1 OF 2
AD A070004

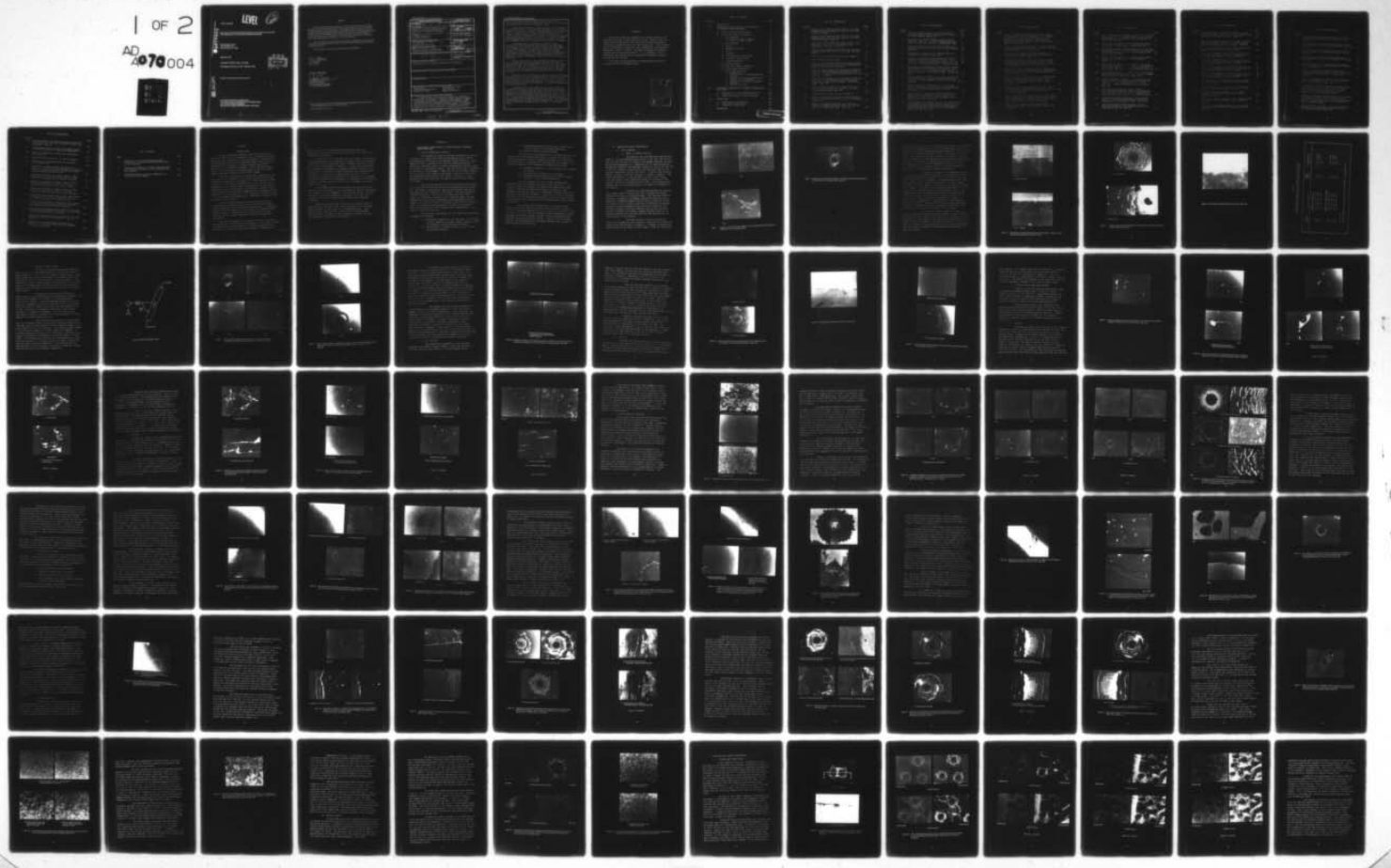

LEVEL II

AFML-TR-78-184

AD A070004

BEHAVIOR OF INFRARED WINDOW MATERIALS EXPOSED TO RAIN DROP ENVIRONMENTS AT VELOCITIES TO 2000 FPS (610 M/S)

Bell Aerospace Textron
Post Office Box One
Buffalo, New York 14240

September 1978

TECHNICAL REPORT AFML-TR-78-184

Final Report for Period July 1977 - September 1978

Approved for public release; distribution unlimited.

AIR FORCE MATERIALS LABORATORY
AIR FORCE WRIGHT AERONAUTICAL LABORATORIES
AIR FORCE SYSTEMS COMMAND
WRIGHT-PATTERSON AIR FORCE BASE, OHIO 45433

NOTICE

When Government drawings, specifications, or other data are used for any purpose other than in connection with a definitely related Government procurement operation, the United States Government thereby incurs no responsibility nor any obligation whatsoever; and the fact that the government may have formulated, furnished, or in any way supplied the said drawings, specifications, or other data, is not to be regarded by implication or otherwise as in any manner licensing the holder or any other person or corporation, or conveying any rights or permission to manufacture, use, or sell any patented invention that may in any way be related thereto.

This report has been reviewed by the Information Office (ASD/OIP) and is releasable to the National Technical Information Service (NTIS). At NTIS, it will be releasable to the general public, including foreign nations.

This technical report has been reviewed and is approved for publication.

T. L. Peterson

T.L. PETERSON
Project Monitor

FOR THE COMMANDER

J.M. KELBLE, CHIEF
Nonmetallic Materials Division
Air Force Materials Laboratory

Copies of this report should not be returned unless return is required by security considerations, contractual obligations, or notice on a specific document.

AIR FORCE/56780/11 May 1979 — 150

Unclassified

SECURITY CLASSIFICATION OF THIS PAGE (When Data Entered)

REPORT DOCUMENTATION PAGE

READ INSTRUCTIONS BEFORE COMPLETING FORM

1. REPORT NUMBER: AFML-TR-78-184	2. GOVT ACCESSION NO.
3. RECIPIENT'S CATALOG NUMBER	
4. TITLE (and Subtitle): Behavior of Infrared Window Materials Exposed to Rain Drop Environments at Velocities to 2000 FPS (610 M/S)	5. TYPE OF REPORT & PERIOD COVERED: Final Report. July 1977 - Sept 1978
	6. PERFORMING ORG. REPORT NUMBER
7. AUTHOR(s): J. Vaughn Hackworth, Lawrence H. Kocher	8. CONTRACT OR GRANT NUMBER(s): F33615-77-C-5069
9. PERFORMING ORGANIZATION NAME AND ADDRESS: Bell Aerospace Textron, P.O. Box One, Buffalo, New York 14240	10. PROGRAM ELEMENT, PROJECT, TASK AREA & WORK UNIT NUMBERS: P.E. 62102F, Project: 2422, Task: 242201
11. CONTROLLING OFFICE NAME AND ADDRESS: MBE, Air Force Materials Laboratory, Wright-Patterson AFB, Ohio 45433	12. REPORT DATE: September 1978
	13. NUMBER OF PAGES: 152 (166 p.)
14. MONITORING AGENCY NAME & ADDRESS (if different from Controlling Office): 2422, 01	15. SECURITY CLASS. (of this report): Unclassified
	15a. DECLASSIFICATION/DOWNGRADING SCHEDULE

16. DISTRIBUTION STATEMENT (of this Report)

Approved for public release; distribution unlimited.

17. DISTRIBUTION STATEMENT (of the abstract entered in Block 20, if different from Report)

18. SUPPLEMENTARY NOTES

19. KEY WORDS (Continue on reverse side if necessary and identify by block number)

Rain Erosion
Infrared Window Materials
Single Drop Impact
Multiple Drop Impact
Stress Waves
Damage Mechanisms

20. ABSTRACT (Continue on reverse side if necessary and identify by block number)

An experimental and analytical program was performed to investigate the behavior of infrared window materials exposed to rain drop environments. Materials investigated included polycrystalline CVD zinc selenide and zinc sulfide; single crystalline silicon, magnesium fluoride, spinel, and sapphire; and fusion cast spinel. Rain drop environments consisted of single 0.080 in. (2.0 mm) drops; a standard rainfield with

DD FORM 1 JAN 73 1473 EDITION OF 1 NOV 65 IS OBSOLETE

UNCLASSIFIED

SECURITY CLASSIFICATION OF THIS PAGE (When Data Entered)

408 855

JQB

0.070 in. (1.8 mm) drops and rainfall rate of 1.0 in/hr (2.5 cm/hr); and a small drop rainfield with 0.030 in. (0.75 mm) drops and rainfall rate of 0.4 in/hr (1 cm/hr).

Single drop experiments established the following damage threshold velocities: zinc selenide - between 450 and 500 fps (137 and 152 m/s); zinc sulfide - approximately 575 fps (175 m/s); silicon - approximately 900 fps (274 m/s); magnesium fluoride - between 900 and 1120 fps (274 and 340 m/s), but closer to 1120 fps; spinel - approximately 1300 fps (396 m/s); and sapphire-between 1500 and 1750 fps (457 and 535 m/s). Additional single drop experiments demonstrated that reducing the grain size of zinc selenide significantly increased its resistance to damage.

Single drop impact experiments proved that anti-reflection coatings can modify the response of the substrate to drop impact. A thorium fluoride coating prevented damage to zinc sulfide, although the coating fractured and/or debonded at the site of impact. A proprietary coating on gallium arsenide also prevented damage to the substrate, although it too was removed by the impact. A lanthanum fluoride coating, which appeared to suffer no damage by single drop impact, did not improve the erosion resistance of zinc sulfide in the small drop rainfield.

Thin, outer layers of zinc sulfide were found to protect zinc selenide substrates from damage. Ring fractures from a single drop impact just penetrated a 0.005 in. (0.13 mm) thick layer at 730 fps (222 m/s) and a 0.020 in (0.50 mm) thick layer at 1120 fps (340 m/s). A bilayered specimen with a 0.020 in. (0.50 mm) thick zinc sulfide layer gave performance comparable to that of thick, homogeneous zinc sulfide in the small drop rainfield.

Comparison of the results from the small drop rainfield experiments with those from standard rainfield experiments showed erosion resistance of zinc sulfide, relative to that of zinc selenide, was less in the small drop rainfield than in the standard rainfield. A simple equivalency of total mass of water impacted per unit area was not adequate to correlate damage rates in the two rainfields.

A modification of the analytical drop impact model to incorporate a decay with time in the impact pressure gave more realistic stress-time curves than were computed by the original model in which pressure remained constant as the contact area expanded. The modified model predicted tensile stresses of 11.5 to 14.5 ksi (80 to 100 MPa) in zinc selenide impacted by a 0.080 in. (2.0 mm) diameter water drop at 500 fps (152 m/s) which is just slightly above the damage threshold velocity. The predicted stresses were close to the ultimate strength of 8.5 ksi (58.6 MPa) for zinc selenide, demonstrating the validity of the modified model.

FOREWORD

This final report was prepared by J. Vaughn Hackworth and Lawrence H. Kocher of Bell Aerospace Textron, Buffalo, New York under Contract F33615-77-C-5069 with the Air Force Materials Laboratory, Wright-Patterson Air Force Base, Ohio. This contract was initiated under Project No. 7340 "Nonmetallic and Composite Materials", Task No. 734007, "Coatings for Energy Utilization, Control and Protective Functions". T. L. Peterson, of the Elastomers and Coatings Branch, Nonmetallic Materials Division was the project monitor.

This report covers research performed during the period 25 July 1977 to 25 September 1978.

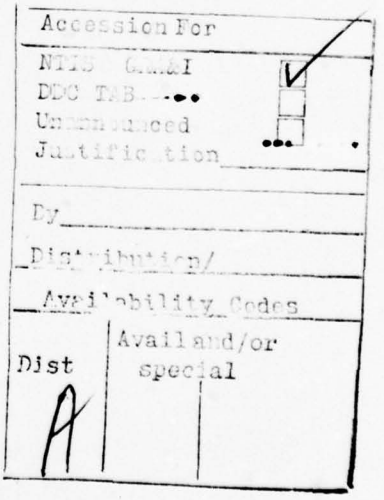

TABLE OF CONTENTS

LIST OF ILLUSTRATIONS

LIST OF ILLUSTRATIONS

LIST OF ILLUSTRATIONS

LIST OF ILLUSTRATIONS

LIST OF ILLUSTRATIONS

LIST OF ILLUSTRATIONS

LIST OF ILLUSTRATIONS

LIST OF TABLES

SECTION I

INTRODUCTION

Infrared-transparent windows, fabricated from brittle materials, are subject to damage and loss of transmittance when exposed at high velocities to rain environments. Development of infrared window materials with improved erosion resistance and development of techniques to protect the more susceptible materials can be aided by knowledge of the mechanism by which erosion is initiated and an understanding of the relationship between infrared transmission and erosion damage.

A previous investigation has provided information on the behavior of zinc selenide, zinc sulfide, and gallium arsenide subjected to water drop environments.[1] The response of these materials to impact by a water drop at 730 fps (222 m/s) was determined using a single water drop generator installed in the AFML/Bell erosion test facility. The results of these initial single drop impact experiments suggested ways to improve erosion resistance of these materials, e.g., reduction of the grain size of zinc selenide and introduction of compressive stresses in the surfaces of the materials.

Rainfield experiments performed during the previous investigation provided insight into the relationship between erosion damage and loss of infrared transmittance. A relatively simple analytical model of rain drop impact also demonstrated promise based on a comparison between the predicted stress patterns and the fracture patterns obtained in single drop experiments.

The work described in this report builds on, and extends, that performed in the previous investigation. The objectives were to determine the erosion behavior of current infrared window materials; describe the mechanisms and modes of degradation of

material properties; and identify suitable techniques for development of more erosion resistant materials for future infrared window requirements.

In addition to zinc selenide and zinc sulfide, the materials studied included silicon, magnesium fluoride, spinel, and sapphire. These additional four materials are of interest for applications at velocities between Mach 1 and Mach 2. Single drop experiments were performed to determine the damage threshold velocity for all the materials; the effect of impact angle for zinc selenide; the improvement to be gained by reducing the grain size of zinc selenide; the response of antireflection coatings on zinc selenide and gallium arsenide; the performance of bilayered zinc sulfide/zinc selenide specimens; and the feasibility of a bimedia protective layer concept.

A small drop rainfield was designed and installed in the AFML/Bell erosion facility. This rainfield was used to investigate the progress of erosion damage on zinc selenide and zinc sulfide. Exploratory experiments were also performed in the small drop rainfield to evaluate antireflection coatings and bilayered specimens.

Modifications were made to the analytical model used for predicting the transient stress state introduced in an infrared window material by the impact of a single water drop. These modifications, involving the introduction of time-dependent functions which allowed the impact pressure to decay, improved the predictive capabilities of the model.

SECTION II

EXPERIMENTAL INVESTIGATION OF RAIN EROSION OF INFRARED WINDOW MATERIALS

A. General Experimental Details

The response of selected infrared transmitting materials to impact by a single water drop was determined using a liquid drop generator installed in the AFML/Bell erosion facility. This generator and its operation have been described previously.[1] Basically, individual drops of water are generated by gravity feed at the end of a hypodermic needle. The size of the drop is governed by the bore of the hypodermic needle and the rate of drop formation is controlled by the length of the needle. For all of the single drop experiments described in this report, 0.080 in. (2.0 mm) diameter drops were used with a formation rate of about one drop per second.

The rotating arm with the attached specimen was brought up to the selected velocity before the drop generator was turned on. The number of drops which impacted the specimen depended on the length of time (number of revolutions of the arm) before the flow was terminated. The size of the drops and their rate of impact on a specimen at a given set of conditions were verified periodically by tests with specimens of polymethylmethacrylate. Except for a series of tests to investigate the effects of impact angle, all specimens were impacted at an angle of 90 degrees. That is, the surfaces of the specimens were perpendicular to the plane of rotation of the arm.

The materials investigated in the single drop experiments included the following:

(1) Homogeneous materials - zinc selenide, zinc sulfide, silicon, magnesium fluoride, spinel, sapphire, and a developmental fine-grained zinc selenide.

(2) Antireflection coatings applied to zinc sulfide and gallium arsenide.

(3) Bilayered specimens with thin zinc sulfide outer layers bonded to zinc selenide substrates.

(4) Simulated bimedia window specimen.

The multiple drop experimentation included impacting zinc selenide with overlapping single drops to follow the progress of erosion damage, and exposure of several specimens to a small-drop rainfield especially designed and installed for this program. The specimens exposed to this rainfield included the following:

(1) Homogeneous materials - zinc selenide, zinc sulfide, and spinel.

(2) Antireflection coating on zinc sulfide.

(3) Bilayered specimen with thin zinc sulfide layer bonded to a zinc selenide substrate.

The zinc selenide and zinc sulfide specimens were polycrystalline and produced by chemical vapor deposition. The silicon, magnesium fluoride, and sapphire specimens were single crystals. The gallium arsenide specimen consisted of a few extremely large grains and can be considered a single crystal with respect to the size of the drops. Single crystal spinel specimens were used for the single drop experiments while both single crystal and polycrystalline, fusion-cast spinel were used for the rainfield experiments.

All specimens were procured with a polished finish having a scratch-to-dig ratio better than 60-40 and a flatness of 1 to 2λ. They were normally 0.875 in. x 0.875 in. x 0.375 in. thick (2.22 cm x 2.22 cm x 0.95 cm), except for the bilayered and bimedia specimens which were somewhat thicker, and the fine-grained zinc selenide specimens which were thinner. Details of the bilayered, bimedia, and fine-grained zinc selenide specimens are included in the appropriate section below.

B. Single Drop Impact Experiments

1. Zinc Selenide

a. Effect of Impact Velocity

Specimens of zinc selenide were impacted with 0.080 in. (2.0 mm) diameter water drops at 300, 400, and 500 fps (91, 122, and 152 m/s) to establish the damage threshold velocity. Microscopic examination at a magnification of 135X disclosed no evidence of damage on the specimens impacted at 300 or 400 fps (91 or 122 m/s); however, ring fracture patterns were found on the specimen impacted at 500 fps (152 m/s). A typical ring fracture formed by impact at 500 fps (152 m/s) is shown in Figure 1. The cracks penetrated to a maximum depth of about 0.0016 inches (0.04 mm) based on their projected length on the plane of the specimen surface at a magnification of 640X. This approximation assumes that the cracks penetrated at an angle of 45 degrees to the surface.

A fourth zinc selenide specimen was impacted with single drops at 450 fps (137 m/s) to define the damage threshold velocity to a narrower range. This specimen showed no evidence of damage, so the damage threshold velocity for zinc selenide is somewhere between 450 and 500 fps (137 and 152 m/s). This seems about as close as practical to establish the damage threshold velocity because of the statistical nature of the fracture strength of brittle materials such as zinc selenide. Fracture strength, and thereby damage threshold velocity, is strongly dependent on the nature and the size distribution of flaws present in the material.

Raising the impact velocity to 730 fps (222 m/s) increased both the number of cracks and their depth as shown by the ring fracture in Figure 2. Attempts to examine the cross section of the impact site in Figure 2 were not successful.

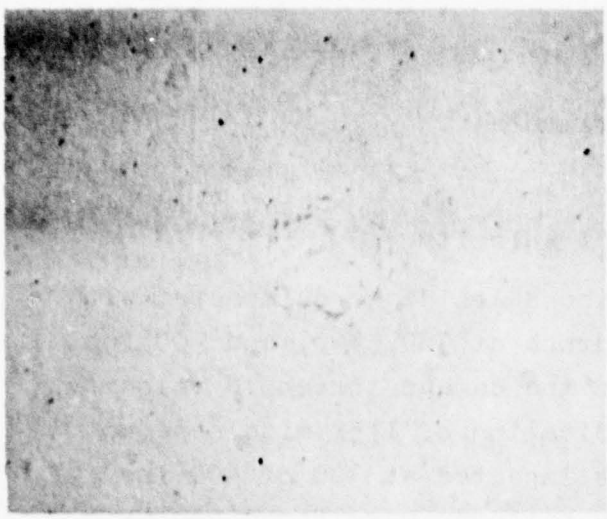

40X

135X

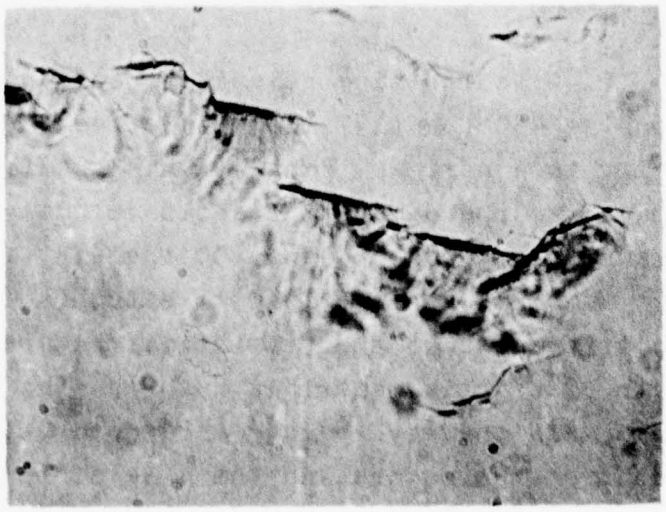

640X

Figure 1. Damage on Zinc Selenide from 0.080 in. (2.0 mm) Diameter Water Drop Impact at 500 fps (152 m/s). Transmitted Light

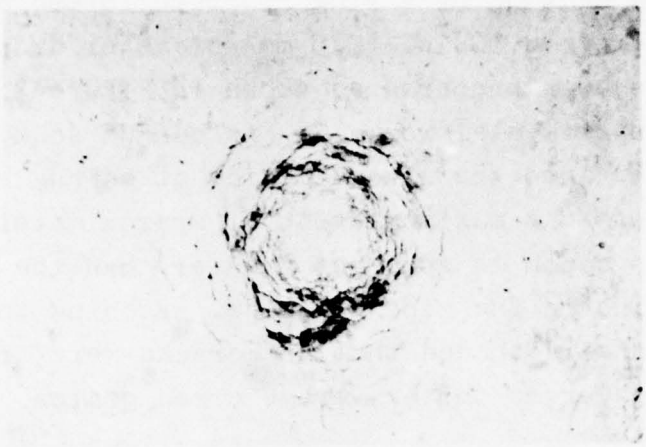

Figure 2. Damage on Zinc Selenide from 0.080 in. (2.0 mm) Diameter Water Drop Impact at 730 fps (222 m/s). Transmitted Light. Mag. 30X

However, a cross section of a ring fracture formed on zinc selenide by a slightly larger 0.10 in. (2.5 mm) diameter drop impacting at 730 fps (222 m/s) was prepared as shown in Figure 3. This specimen was from past experimental work.[1] As can be seen, the surface cracks propagated into the zinc selenide at an angle of approximately 45 degrees to a maximum depth of approximately 0.006 inches (0.14 mm). This depth is somewhat greater than the diameter of the largest grains in the zinc selenide. Etching the cross sectioned impact site showed that the cracks were transgranular and typically traversed three average sized grains.

A dramatic increase in the damage produced by a 0.080 in. (2.0 mm) diameter drop was obtained when the impact velocity was raised still higher to 1120 fps (340 m/s) as shown by the ring fracture in Figure 4. The dark shadow in the upper right hand corner of Figure 4b was caused by a crack formed by the impact of several drops to the right of the impact site shown in the figure. This large crack angularly penetrated to the back surface of the specimen directly below the impact site in the figure and thus was apparent when transmitted light was used. A cross section of this impact site is shown in Figure 5. As can be seen, the ring fractures propagated at an angle of approximately 45 degrees to a maximum depth of approximately 0.027 in. (0.68 mm). Based on the results of these experiments, the depth of penetration of the ring fractures appeared to be proportional to the velocity raised to the 3.5 power.

The effect of impact velocity on the size of the annulus where ring fracturing occurred is shown in Table 1. Raising the velocity from 500 fps (152 m/s) to 730 fps (222 m/s) increased the outer radius of the annulus of fracture with little effect on the inner radius. Raising the velocity to 1120 fps (340 m/s) increased the inner radius as well as the outer radius. The outer radius appeared to be approximately proportional to velocity squared.

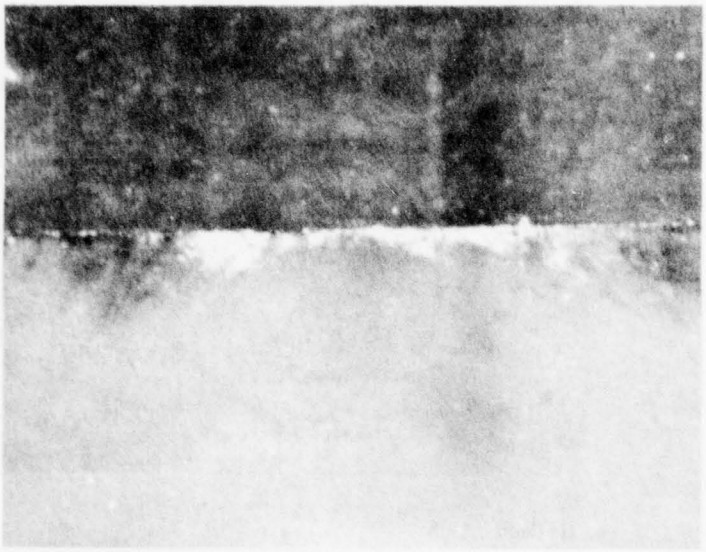

a. Unetched - Mag 110X

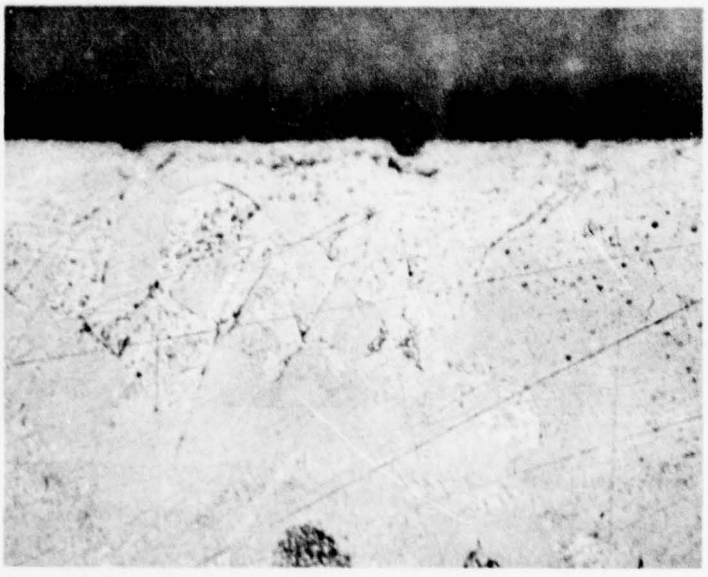

b. Etched - Mag 440X

Figure 3. Cross Section of Single Drop Impact Site on Zinc Selenide. 1.00 in. (2.5 mm) Diameter Drop Impacting at 730 fps (222 m/s).

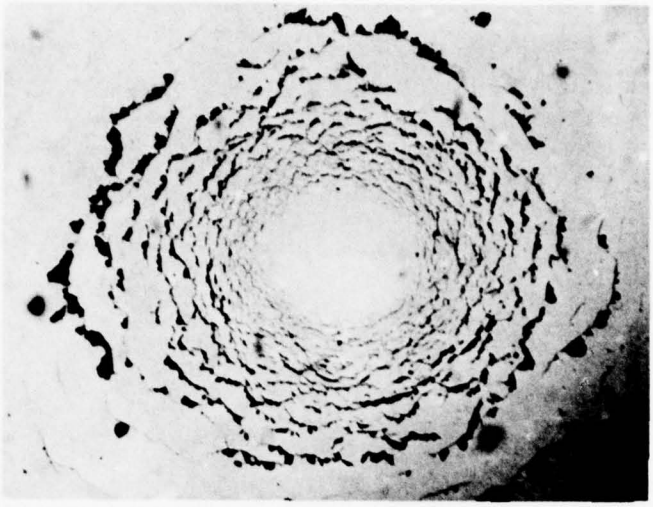

a. Reflected Light

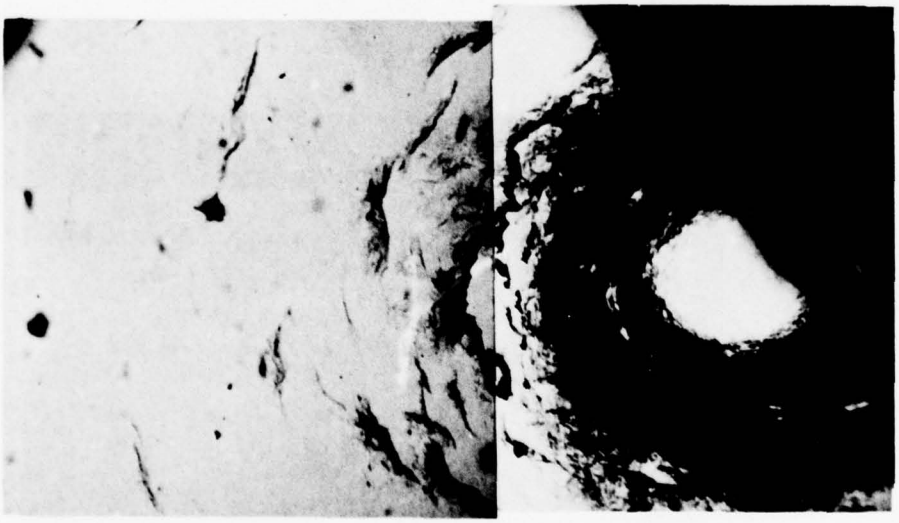

b. Transmitted Light

Figure 4. Damage on Zinc Selenide from 0.080 in. (2.0 mm) Diameter Water Drop Impact at 1120 fps (340 m/s). Mag. 30X

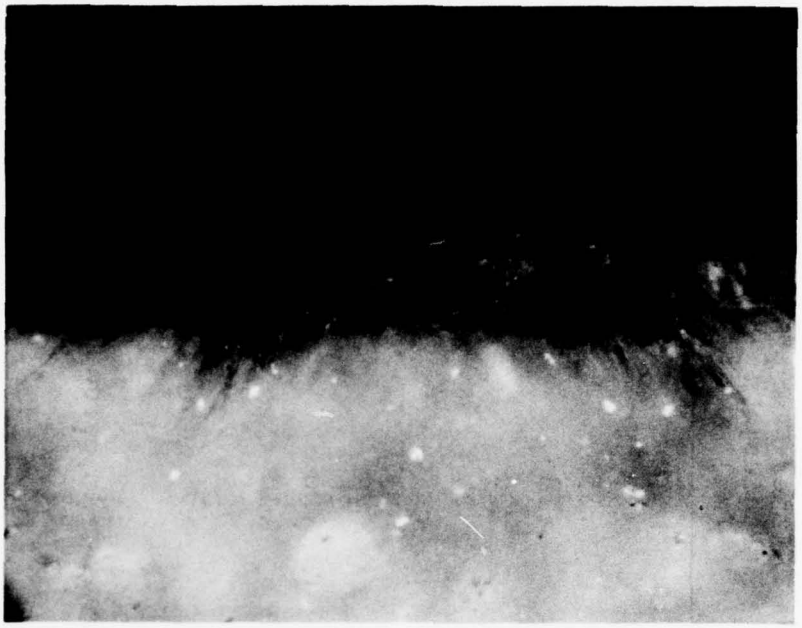

Figure 5. Cross Section of Impact Site Shown in Figure 4. Mag. 35X

TABLE 1

DIMENSIONS OF ANNULUS OF RING FRACTURES PRODUCED BY 2.0 MM DIAMETER WATER DROP IMPACT ON ZINC SELENIDE

Impact Angle	Impact Velocity	Inner Radius (mm)	Outer Radius (mm)
	Effect of Velocity		
90°	1120 fps (341 m/s)	.35	1.41 (.60)[a]
90°	730 fps (222 m/s)	.18	.71 (.48)[a]
90°	500 fps (152 m/s)	.20	.32
	Effect of Impact Angle		
90°	730 fps (222 m/s)	.18	.71 (.48)[a]
75°	730 fps (222 m/s)	.20	.60 (.35)[a]
60°	730 fps (222 m/s)	.18	.55 (.35)[a]
45°	730 fps (222 m/s)	.22	.25

[a] Major extent of cracking is within radius in parenthesis.

b. Effect of Impact Angle

Four zinc selenide specimens were impacted with 0.080 in. (2.0 mm) diameter drops at 730 fps (222 m/s) at impact angles of 75, 60, 45 and 30 degrees, respectively. Impact angle is defined as the angle between the specimen surface and the velocity vector of the specimen as shown in Figure 6. This definition of impact angle neglects the contribution of vertical velocity of the drop which is small relative to the horizontal velocity of the specimen since the drop falls only a few inches before impact.

Micrographs illustrating the effects of impact angle on the ring fractures are presented in Figure 7. The ring fracture formed at 90 degrees is the same one shown previously in Figure 2. The ring fracture formed at an impact angle of 45 degrees is shown at a magnification of 135X because the cracks were not readily visible at the lower magnification of 30X. No evidence of damage was detected on the specimen impacted at an angle of 30 degrees. The top of each micro-photograph as shown is oriented in the same direction as the top edge of the specimen during the test.

The ring fracture patterns at impact angles less than 90 degrees were circular and surprisingly symmetrical, although there was some evidence of more extensive damage in the area toward the top of the specimen. This trend was most evident in the fractures formed at an impact angle of 60 degrees. A polymethylmethacrylate specimen was subsequently impacted at an angle of 60 degrees to investigate further the effect of impact angle. The assymmetrical nature of the loads generated by impact are quite apparent in a typical impact site shown in Figure 8a. Both the inner and outer boundaries of the indented area are approximately circular; however, they are not concentric as was the case for impact at 90 degrees (Figure 8b).

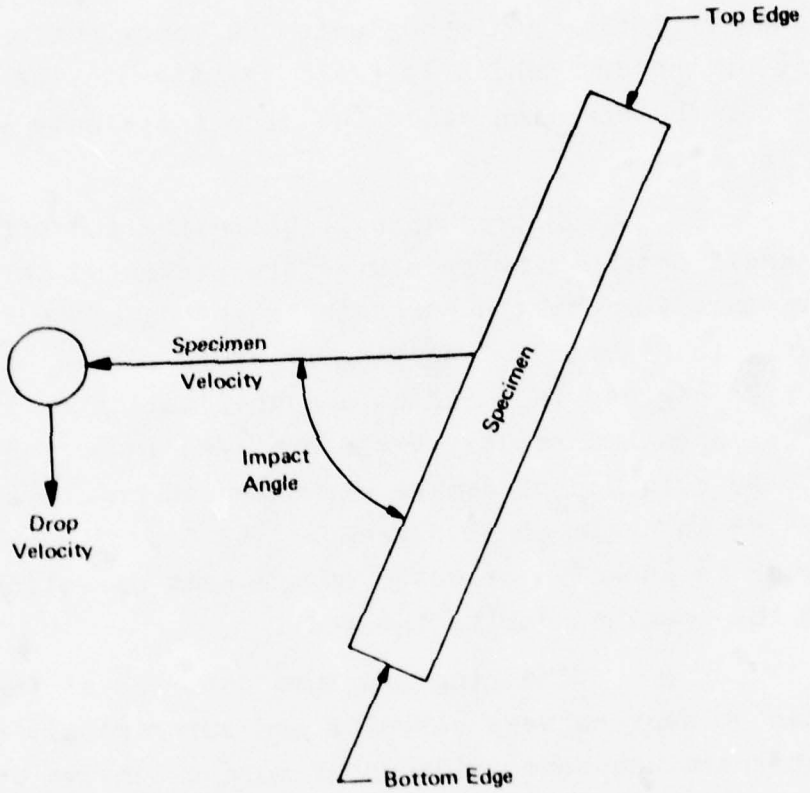

Figure 6. Sketch Defining Impact Angle

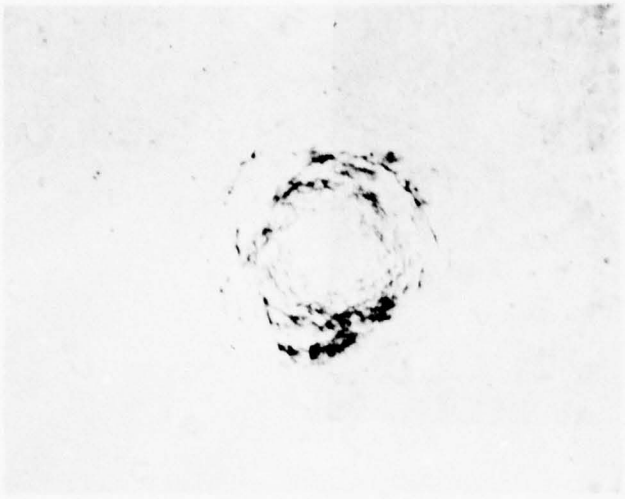

30X

a. 90°

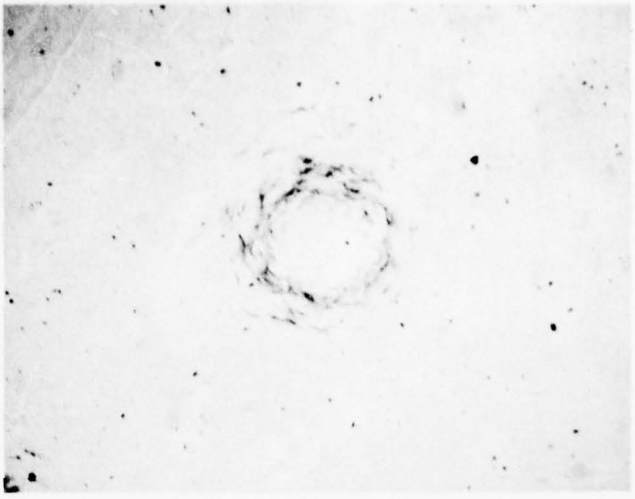

b. 75°

30X

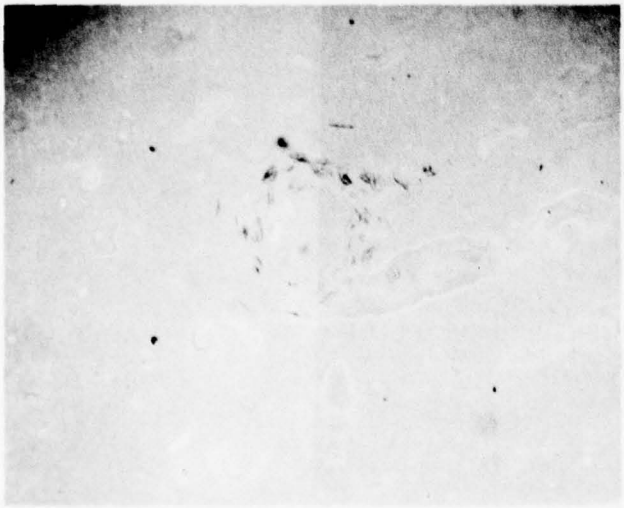

30X

c. 60°

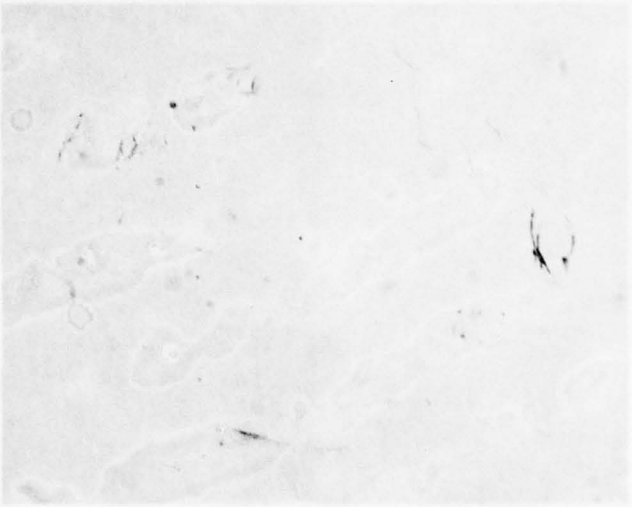

d. 45°

135X

Figure 7. Effect of Impact Angle on Ring Fracturing of Zinc Selenide Impacted by 0.080 in. (2.0 mm) Diameter Water Drops at 730 ft/sec (222 m/s)

a. 60°

b. 90°

Figure 8. Effect of Impact Angle on Assymmetry of Damage as Shown on Polymethlymethacrylate Impacted by a 0.080 in. (2.0 mm) Diameter Water Drop at 730 ft/sec (222 m/s). Mag. 40X

The effects of impact angle on the radii of the annular areas of ring fractures on zinc selenide are shown in Table 1. As can be seen from the data in this table, the inner radius remains essentially constant while the outer radius decreases significantly as the angle of impact is lowered from 90 degrees to 45 degrees. The same trend is also apparent in Table 1 when the impact velocity is decreased from 730 fps (222 m/s) to 500 fps (152 m/s) at an impact angle of 90 degrees. In fact, the ring fracture pattern in Figure 1 which was formed by a 0.080 in. (2.0 mm) drop impacting at 500 fps (152 m/s) and an angle of 90 degrees is quite similar to that in Figure 7d which was formed by a similar drop impacting at 730 fps (222 m/s) and an angle of 45 degrees. For the later case, the component of the velocity perpendicular to the surface of the specimen is 516 fps (157 m/s).

The component of the velocity perpendicular to the surface of the specimen appears to control the impact damage, at least to a first approximation. This assumption was subsequently verified by impacting a zinc selenide specimen with 0.080 in.(2.0 mm) diameter drops at 630 fps (192 m/s) and an impact angle of 90 degrees. As shown in Figure 9, the ring fractures obtained for this case were comparable to those previously obtained at a velocity of 730 fps (222 m/s) and an impact angle of 60 degrees. The component of velocity perpendicular to the surface was 632 fps (193 m/s) for this latter case. Additional experimentation is required to establish the usefulness of this approximation, particularly for predicting the rate of transmittance loss in a rainfield as a function of angle.

2. Zinc Sulfide

The single drop experiments on zinc sulfide reported in Reference 1 were extended by impacting specimens at 1120 fps (340 m/s) with 0.080 in. (2.0 mm) diameter drops.

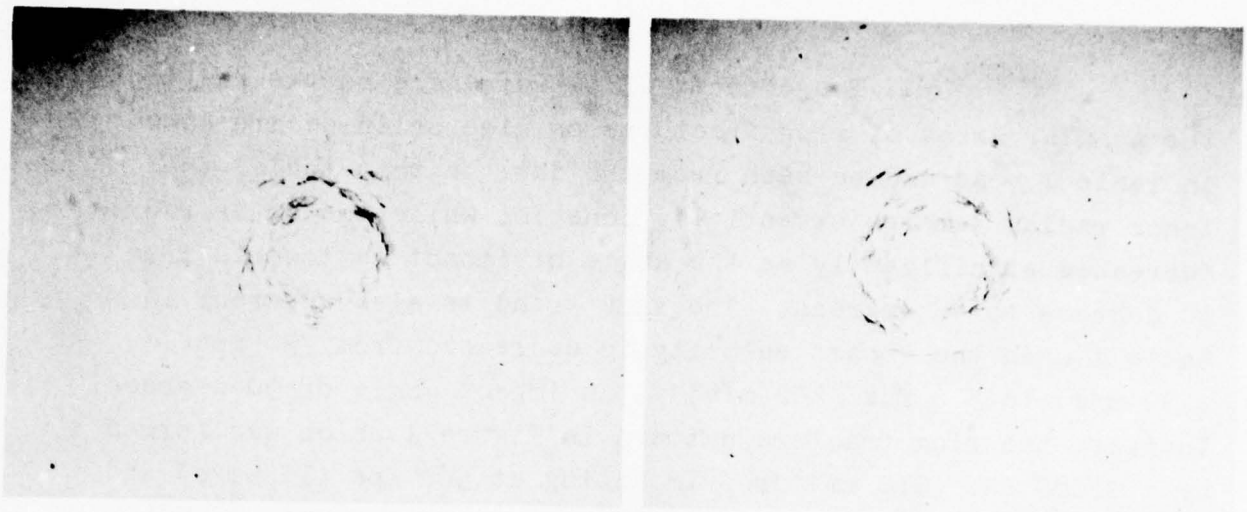

a. 630 fps (192 m/s) at 90° Impact Angle

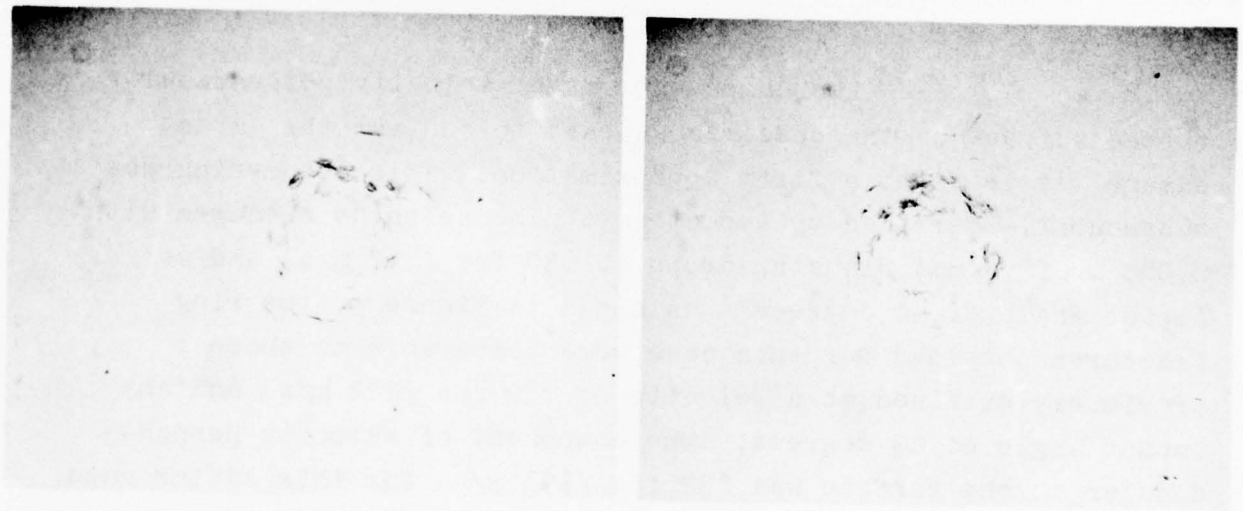

b. 730 fps (222 m/s) at 60° Impact Angle.
Component of Velocity Normal to Surface
is 632 fps (193 m/s).

Figure 9. Similarity of Damage on Zinc Selenide Impacted by 0.080 in. (2.0 mm) Diameter Drops when Normal Components of Velocity are Equal. Transmitted Light. Mag. 30X.

Figure 10 compares the ring fracture formed at 1120 fps (340 m/s) with that formed at 730 fps (222 m/s) obtained from the prior work. The increase in the extent of damage with the increase in velocity is dramatic. Additional tests at 630 and 575 fps (192 and 175 m/s) showed the damage threshold velocity was just below 575 fps (175 m/s).

The ring fracture produced on zinc sulfide by an impact velocity of 1120 fps (340 m/s) is similar in appearance to that produced on the lower strength zinc selenide by a lower impact velocity of 730 fps (222 m/s) shown previously in Figure 2. For zinc sulfide impacted at 1120 fps (340 m/s), the inner radius of the annulus of fracture was 0.008 in. (0.20 mm). The major extent of cracking was encompassed within an outer radius of 0.020 in. (0.50 mm), although cracks were found out to a radius of 0.040 in. (1.0 mm). For zinc selenide impacted at 730 fps (222 m/s), the corresponding dimensions for the annulus of fracture were 0.007 in. (0.18 mm) for the inner radius, and 0.019 in. (0.48 mm) and 0.028 in. (0.71 mm) for the outer radii.

Figure 11 presents the cross section of the 1120 fps (340 m/s) impact site shown in Figure 10b. The surface cracks propagated at an angle of approximately 45 degrees to a maximum depth of approximately 0.008 inches (0.20 mm). The similarity between the damage to zinc sulfide by a drop impacting at 1120 fps (340 m/s) and the damage to zinc selenide by a drop impacting at a lower velocity of 730 fps (222 m/s) is again apparent when Figure 11 is compared to Figure 3.

3. Silicon

Specimens of single crystal silicon were impacted at 900 and 1120 fps (274 and 340 m/s) with 0.080 in. (2.0 mm) diameter drops. Microscopic examination of the specimen impacted at 900 fps (274 m/s) disclosed only the single crack shown in Figure 12a. The damage threshold velocity for silicon impacted with this size

a. 730 ft/sec (222 m/s)

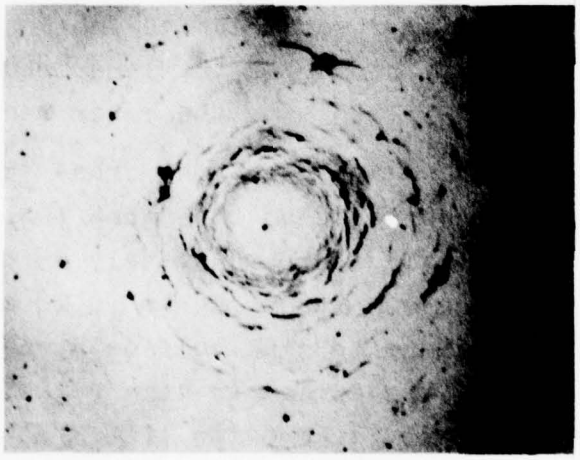

b. 1120 ft/sec (340 m/s)

Figure 10. Effect of Impact Velocity on Ring Fracturing of Zinc Sulfide Impacted by a 0.080 in. (2.0 mm) Diameter Water Drop. Mag. 30X

Figure 11. Cross Section of Impact Site in Figure 10. Mag. 55X

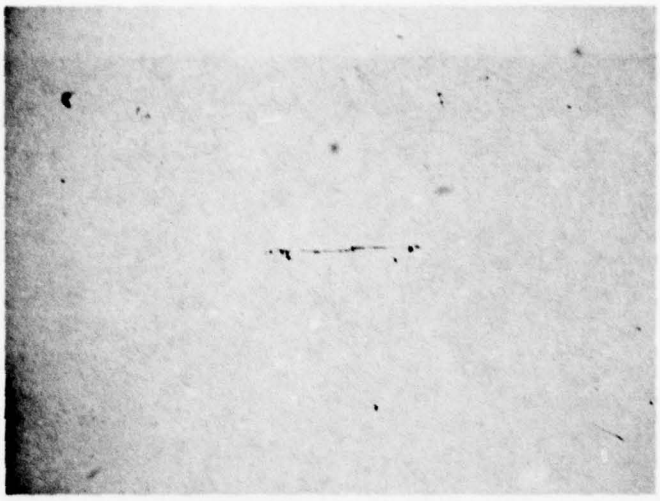

a. 900 ft/sec (274 m/s). Mag. 30X

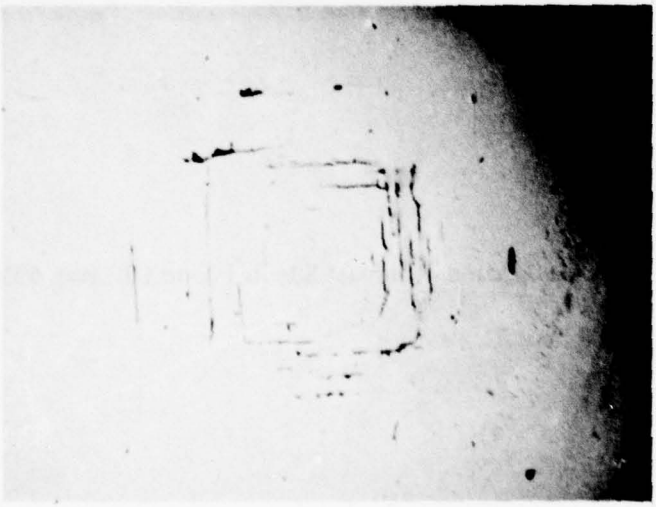

b. 1120 ft/sec (340 m/s). Mag. 40X

Figure 12. Effect of Impact Velocity on Ring Fracturing of Silicon Impacted by a 0.080 in. (2.0 mm) Diameter Water Drop.

drop appears to be slightly below 900 fps (274 m/s). A complete ring fracture pattern was formed by a single drop impact at 1120 fps (340 m/s) as illustrated in Figure 12b. This ring fracture pattern is characteristic of the cubic crystal structure of silicon. The face of the specimen is the (100) plane and the fractures represent cleavage of the {010} and {001} planes.

4. Single Crystal Magnesium Fluoride

Figure 13 shows the ring fracture pattern formed on magnesium fluoride by impact with a 0.080 in. (2.0 mm) diameter drop at 1120 fps (340 m/s). The pattern reflects the cubic crystal lattice of magnesium fluoride. The face of the specimen is the (100) plane and the fractures are cleavage of the {010} and {001} planes, as was the case with silicon.

The specimen had been first impacted on the opposite surface with similar diameter drops at 900 fps (274 m/s) with no detectable damage produced. Additional tests were not performed to establish the damage threshold velocity. Judging by the extent of the fracture in Figure 13, the threshold velocity is probably close to, but somewhat less than, 1100 fps (335 m/s).

5. Spinel

Specimens of single crystal spinel of stoichiometric composition ($MgO \cdot Al_2O_3$) were impacted at velocities of 1300, 1500, and 1750 fps (396, 457, and 533 m/s) with 0.080 in. (2.0 mm) diameter drops. Examples of the damage formed at each velocity are presented in Figures 14a, b, and c. A single fracture was detected on the specimen impacted at 1300 fps (396 m/s) as shown in Figure 14a. The damage threshold velocity for this material can therefore be taken as 1300 fps (396 m/s). Figure 14b shows one of several sites of damage formed by drop impact at 1500 fps (457 m/s). The fracturing at these sites was considerably more extensive than that formed by drop impact at 1300 fps (396 m/s).

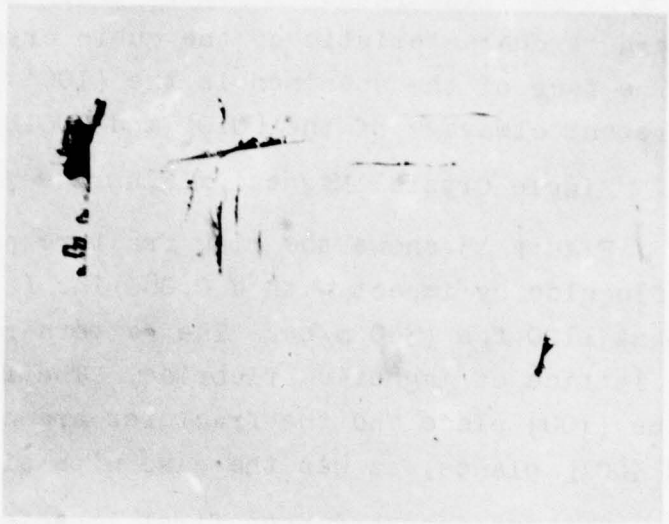

Figure 13. Damage on Magnesium Fluoride from 0.080 in. (2.0 mm) Diameter Water Drop Impact at 1120 fps (340 m/s). Reflected Light. Mag. 30X

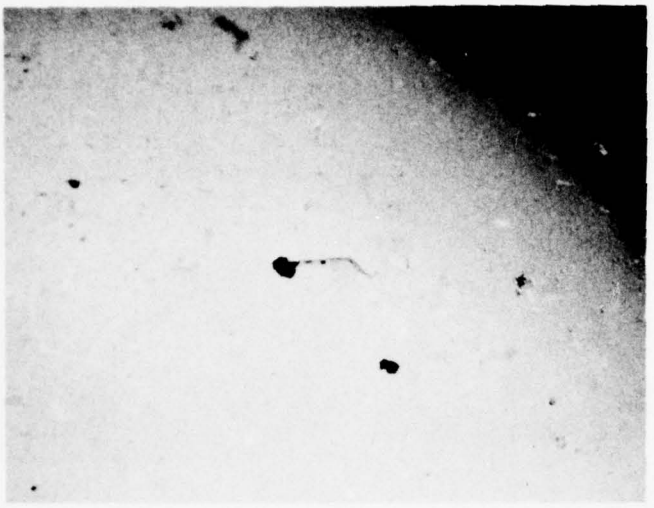

40X

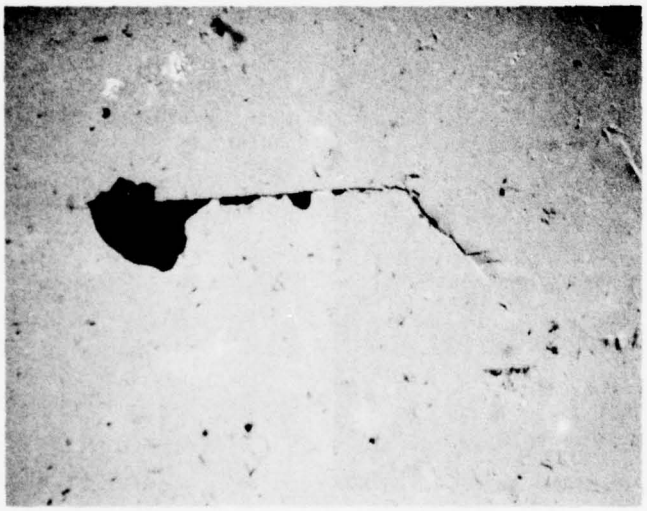

165X

a. 1300 fps (396 m/s) Impact Velocity.
Reflected Light with Nomarski Contrast

Figure 14. Effect of Impact Velocity on Ring Fracturing of Single Crystal Spinel Impacted by a 0.080 in. (2.0 mm) Diameter Water Drop. Continued.

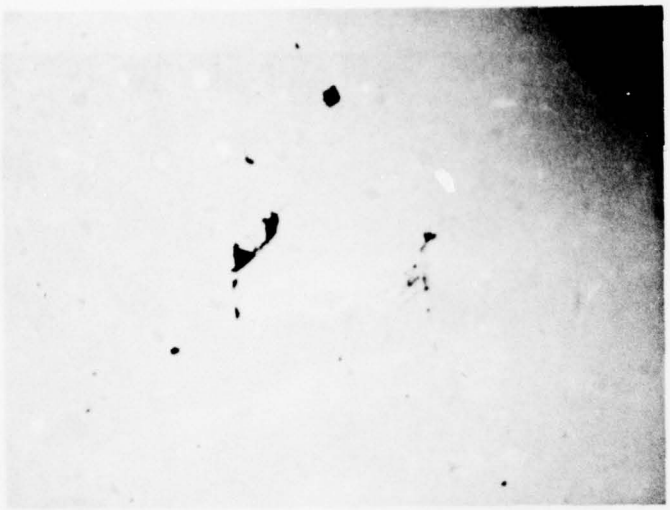

40X

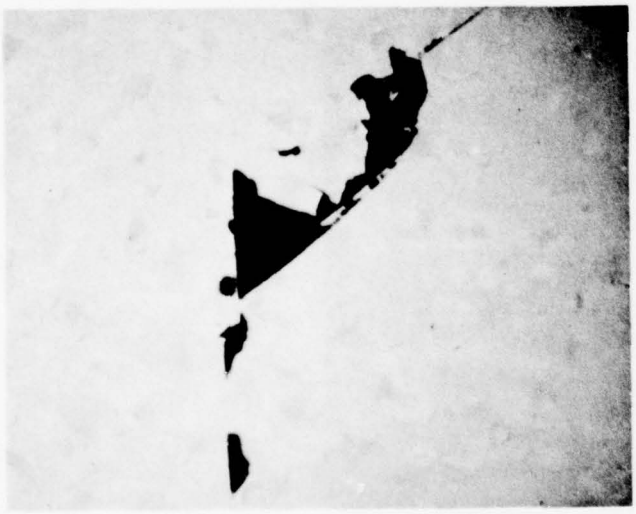

165X

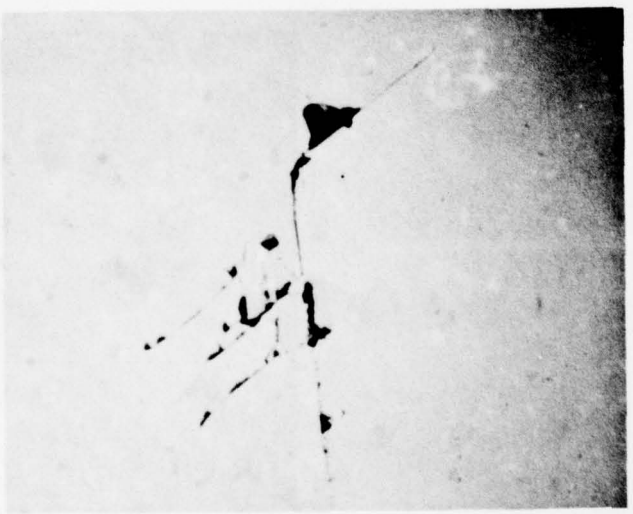

165X

b. 1500 fps (457 m/s) Impact Velocity.
Reflected Light with Nomarski Contrast.

Figure 14. Continued.

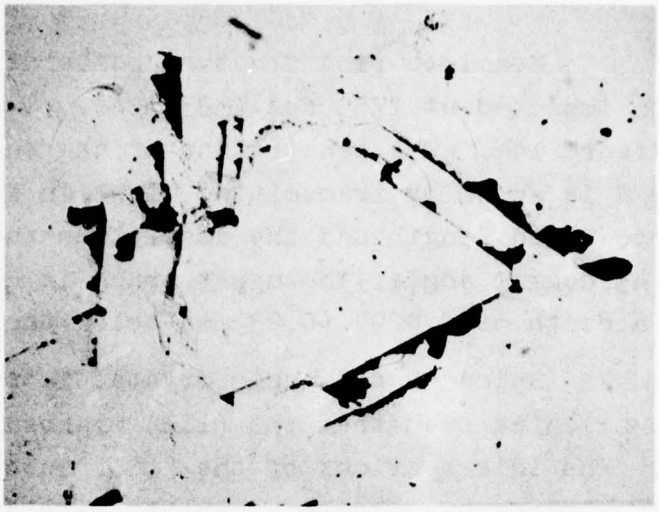

Site A, Mag. 30X

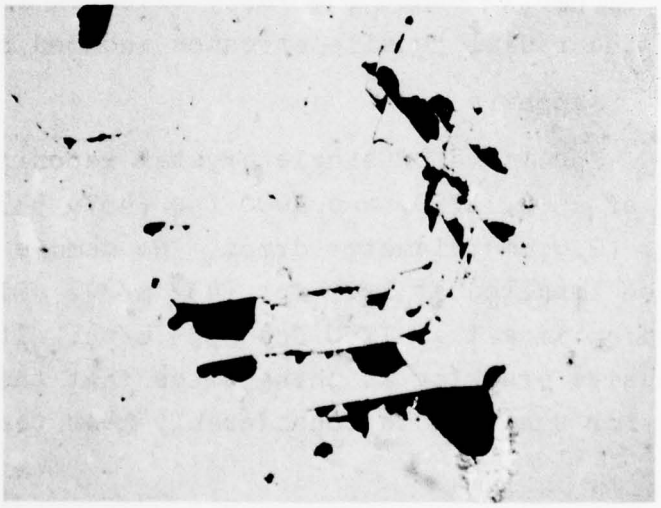

Site B, Mag. 30X

c. 1750 fps (533 m/s) Impact Velocity.
Transmitted Light.

Figure 14. Concluded.

Complete ring fracture patterns were formed on the specimen impacted at 1750 fps (533 m/s). Two such sites are shown in Figure 14c. The penetration of the surface crack at impact Site A is shown by transmitted light in Figure 15. Based on its projected length and the assumption that it penetrates at 45 degree angle, the upper crack in Figure 15b penetrates to a depth of 0.009" (0.23 mm) below the surface.

Spinel has a cubic crystal lattice and the specimens were oriented such that the (111) planes formed the outer surface. The intersections of the {100} cube planes with the specimen surface would then exhibit 3-fold symmetry such as is apparent at Site A in Figure 14c. Thus, the fracture of spinel appears to be cleavage of the cubic face planes. The {111} planes are the preferential cleavage planes for spinel; however these planes were not favorably oriented for cleavage to occur from the radial tensile stresses induced by drop impact.

6. Sapphire

Specimens of single crystal sapphire were impacted at velocities of 1500, 1750, and 2000 fps (457, 535, and 610 m/s) with 0.080 in. (2.0 mm) diameter drops. No damage was detected on the specimen impacted at 1500 fps (457 m/s). Figure 16a shows two sites of drop impact at 1750 fps (533 m/s). It is apparent from the extensive cracking at these sites that the damage threshold velocity for sapphire is considerably less than 1750 fps (533 m/s).

An almost complete ring fracture formed by a drop impact at 2000 fps (610 m/s) is shown in Figure 16b. Cracks can be seen forming four sides of a hexagonal shaped pattern. Figure 16c shows another example of damage produced by a drop impact at 2000 fps (610 m/s). The cracks at this site also exhibit the three-fold symmetry of a hexagon, although cracks are present on only two of the six sides.

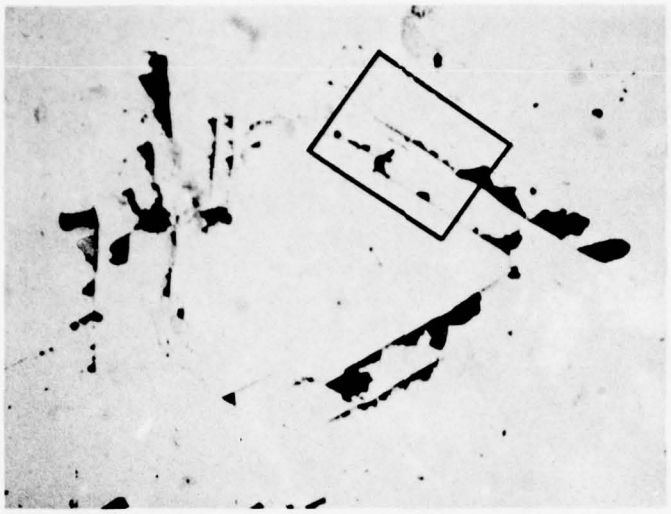

a. Impact Site A, Mag. 30X

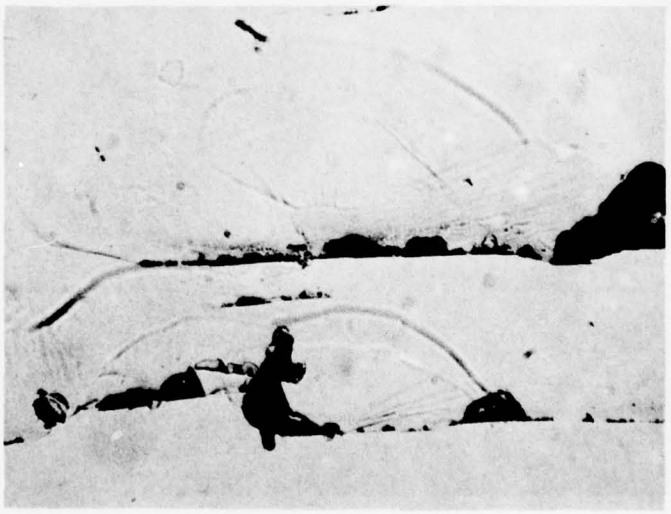

b. Area Outlined in a, above. Mag. 135X

Figure 15. Penetration of Cracks formed on Single Crystal Spinel by 0.080 in. (2.0 mm) Diameter Water Drop Impact at 1750 fps (533 m/s). Transmitted Light.

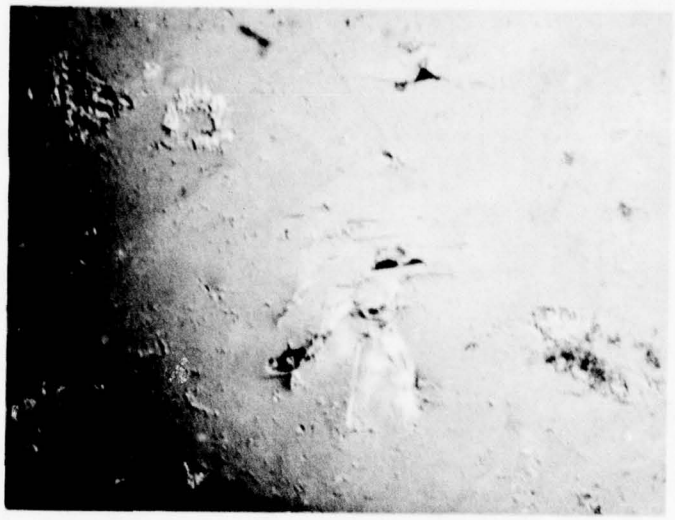

Site A, Mag. 160X

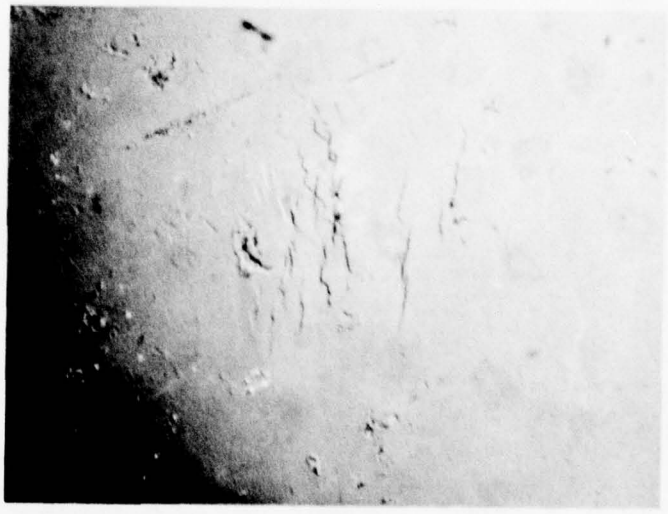

Site B, Mag. 300X

a. 1750 fps (533 m/s) Impact Velocity.
Reflected Light with Nomarski Contrast.

Figure 16. Effect of Impact Velocity on Ring Fracturing of Sapphire Impacted by a 0.080 in. (2.0 mm) Diameter Water Drop. (Continued)

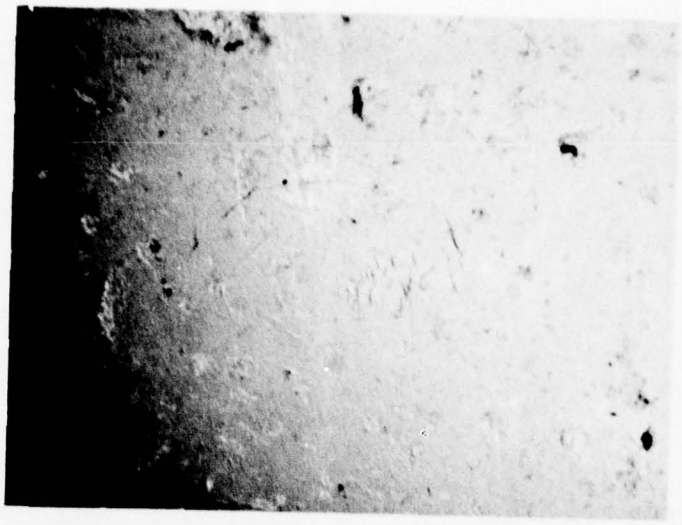

Reflected Light with Nomarski Contrast, Mag. 40X

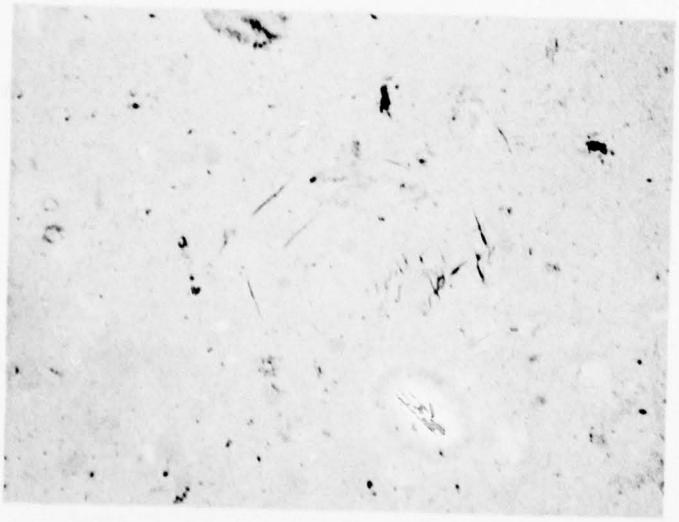

Transmitted Light, Mag. 40X

b. Site A - 2000 fps (610 m/s) Impact Velocity

Figure 16. Continued

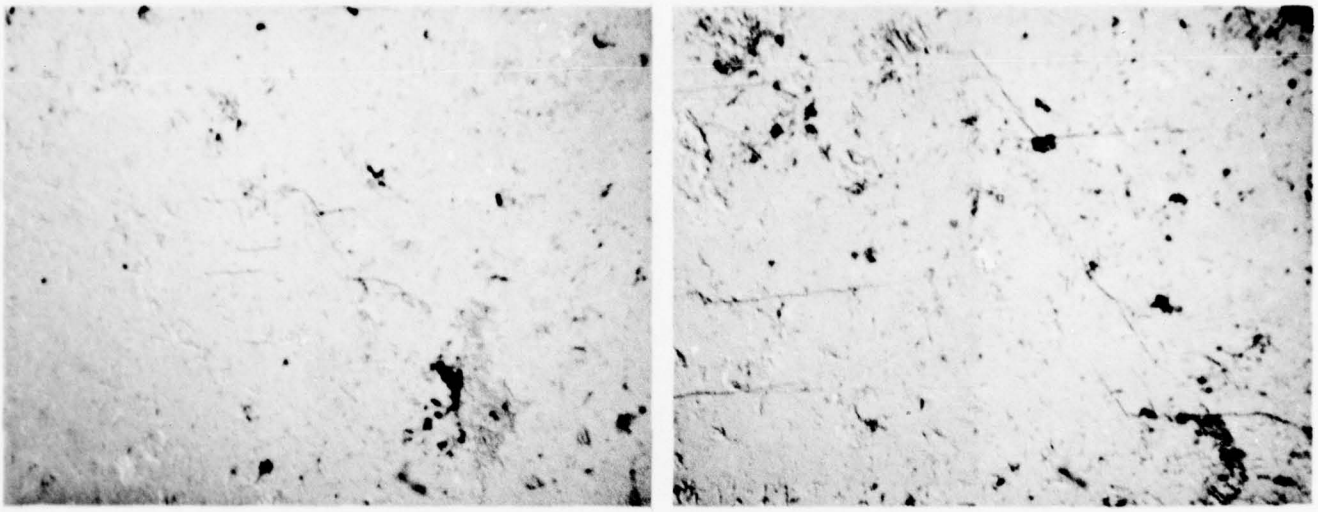

Mag. 40X

Mag. 160X

Reflected Light with Nomarski Contrast

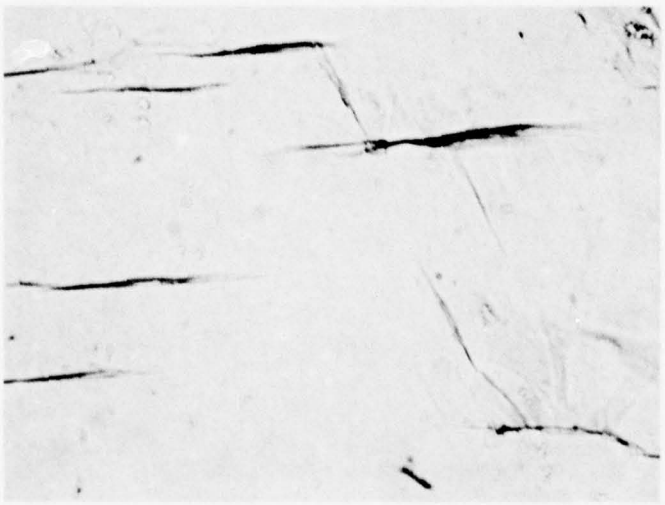

Transmitted Light, Mag. 160X

c. Site B - 2000 fps (610 m/s) Impact Velocity

Figure 16. Concluded.

The sapphire specimens had a hexagonal crystal lattice and were reported by the vendor to have the c-axis at an angle of 60 degrees from the normal to the specimen surface. Sapphire preferentially parts on the {1011} rhombohedral planes. The intersection of these planes with the specimen surface would form a foreshortened hexagon because of the tilt of the c-axis. The partial hexagonal pattern formed by the cracks in Figure 16b does not appear to be particularly foreshortened. In fact, the angles of intersection of the planes of the cracks in both Figures 16b and 16c are about 120 degrees which indicates the absence of foreshortening.

7. Fine-Grained Zinc Selenide

Prior single drop experiments had indicated that much of the superior erosion resistance of zinc sulfide as compared to zinc selenide was a result of the order of magnitude smaller grain size of the zinc sulfide.[1] The small grains would limit the depth of the cleavage cracks because they must traverse grain boundaries and undergo directional changes in neighboring grains which have different crystallographic orientations. It was concluded that the erosion resistance of zinc selenide could be improved by a reduction of its grain size. A development effort to produce fine grained zinc selenide was subsequently initiated at the Research Division of the Raytheon Company.

Specimens of the initial fine-grained zinc selenide produced by this development effort were received for evaluation by single drop impact tests. These specimens were 0.116 in. (2.95 mm) thick, as compared to the thickness of 0.375 in. (9.5 mm) for all prior single drop experiments, so comparably thin specimens of standard grain size zinc selenide and standard zinc sulfide were included for comparison. Figure 17 compares the microstructures of the fine-grained zinc selenide specimens to that of the thin, standard zinc selenide. The

a. Standard Grain Size, Thin Specimen

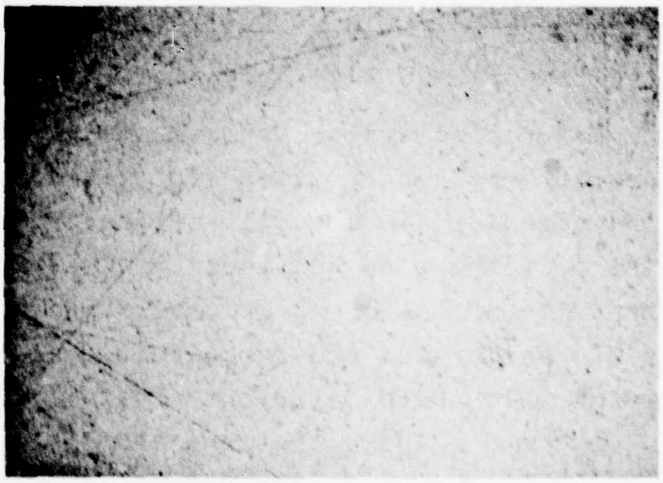

b. Fine Grained, Lot 6

c. Fine Grained, Lot 12

Figure 17. Comparison of Grain Size of Standard and Fine Grained Zinc Selenide. Mag. 135X

specimen from Lot 6 had an extremely fine grain size that could not be resolved at a magnification of 135X. The specimen from Lot 12 exhibited a mixed grain size. The smallest grains were not as small as those of the specimen from Lot 6 and the largest grains were not as large as those of the thin specimen of standard zinc selenide.

Ring fractures produced on the zinc selenide specimens by impact with single 0.080 in. (2.0 mm) diameter drops at 730 fps (222 m/s) are shown in Figure 18. The reduction in grain size significantly improved the erosion resistance of zinc selenide as can be seen by comparing Figure 18b with Figure 18a. All of the ring fractures produced by single drop impact on the fine-grained specimen from Lot 6 were less extensive than those on the thin, standard grain size specimen. The depth of penetration of the cracks was also decreased by the reduction in grain size as can be seen by comparing the projections of the cracks under transmitted light in the microphotographs at 135X magnification.

The fine-grained specimen from Lot 12 exhibited site-to-site variation in damage corresponding to the variation in grain size. Some of the ring fractures on this material, e.g., Site A in Figure 18c, were comparable to those on the specimen from Lot 6. Others, e.g., Site B in Figure 18c, were more extensive and comparable to those on the thin, standard grain size specimen.

Figure 19 compares a ring fracture on fine-grained zinc selenide with those on standard zinc sulfide. The appearance of the fractures were enhanced by etching the specimens in a heated solution containing 50% by volume HCl in water. The resistance to drop impact damage of fine-grained zinc selenide approached that of zinc sulfide; however, zinc sulfide was still significantly more resistant. The impact sites on fine-grained zinc selenide appeared to exhibit a greater number of cracks than did the

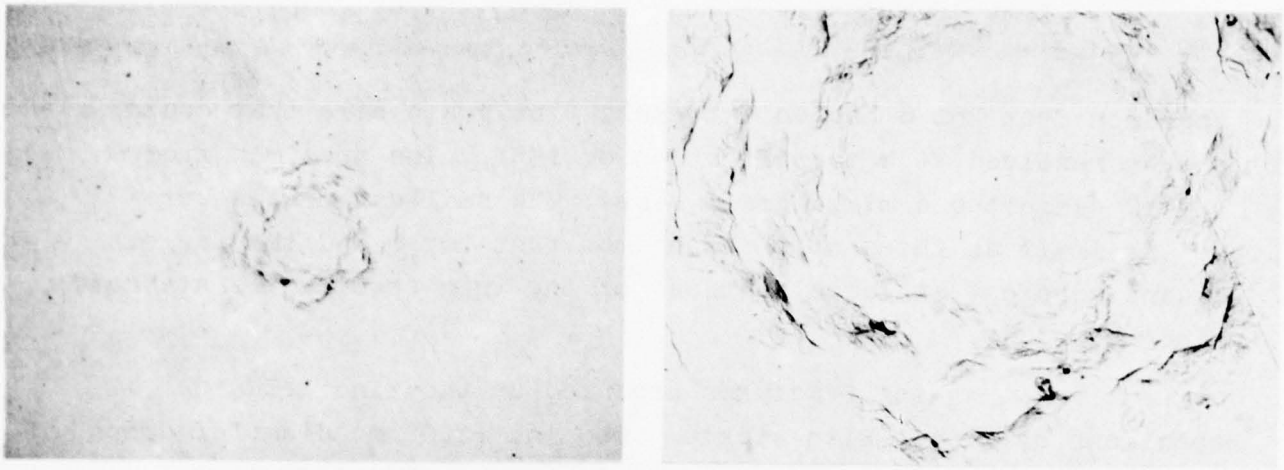

30X Site A 135X

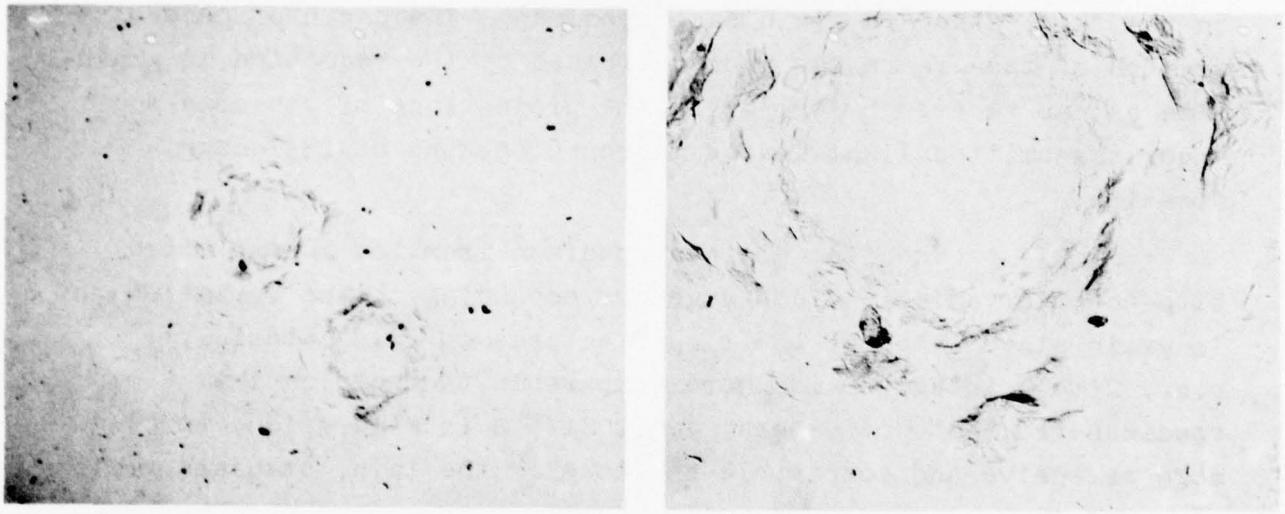

30X Site B 135X

a. Standard Grain Size, Thin Specimen

Figure 18. Comparison of Ring Fractures Formed on Standard and Fine Grained Zinc Selenide by Impact of a 0.080 in. (2.0 mm) Diameter Water Drop at 730 fps (222 m/s). Specimens Unetched. Transmitted Light. Continued.

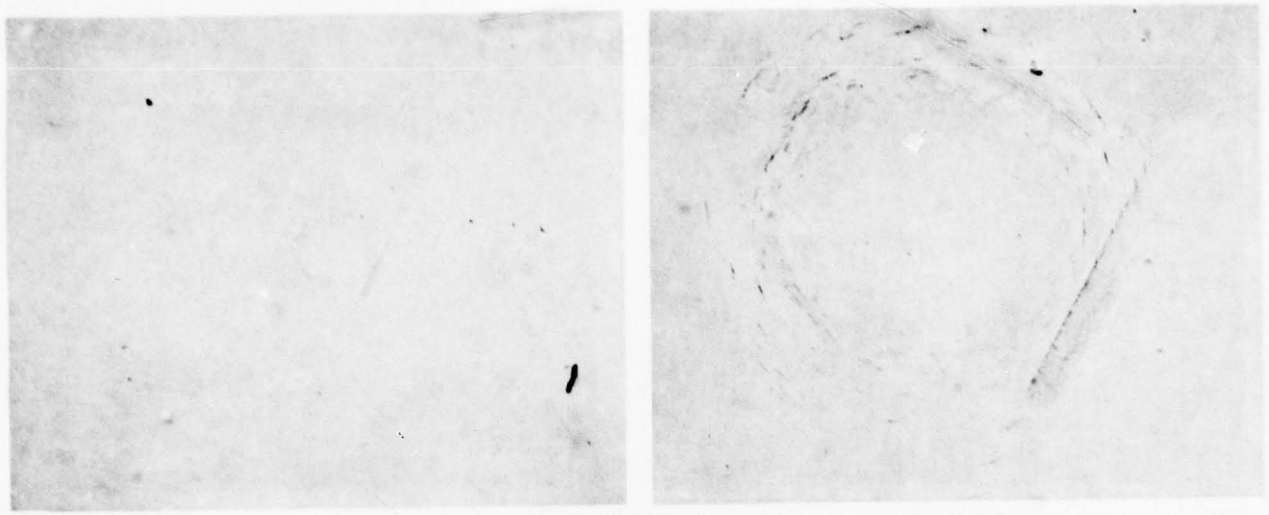

30X Site A 135X

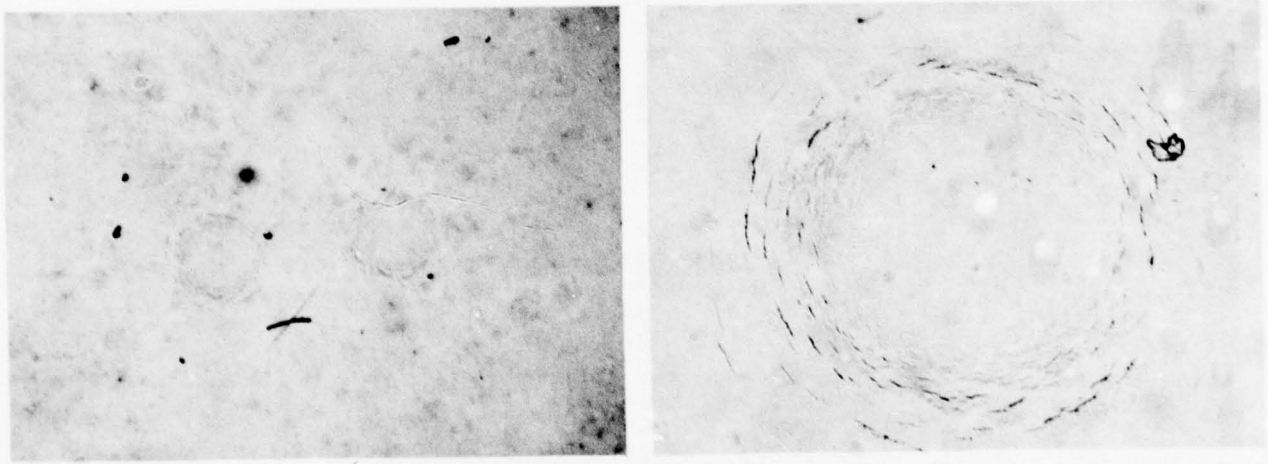

30X Site B 135X

b. Fine Grain Size, Lot 6

Figure 18. Continued.

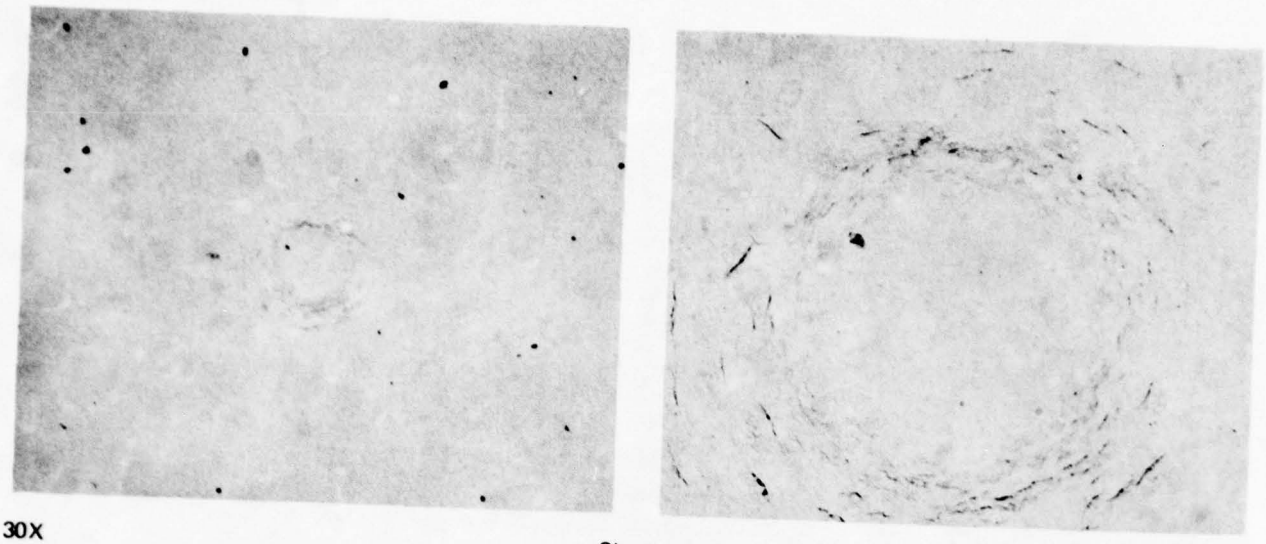

30X

Site A

135X

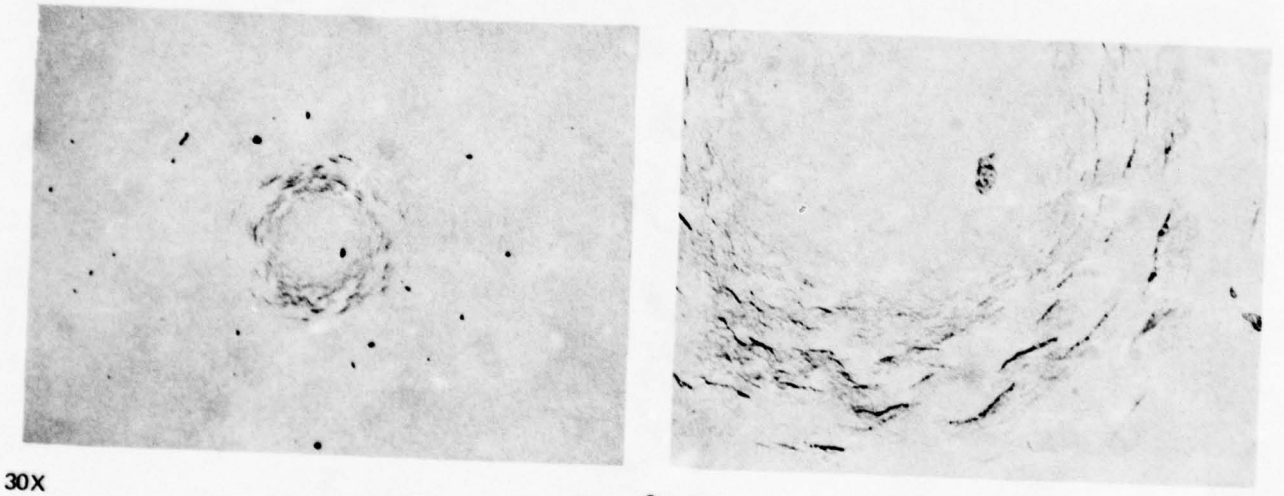

30X

Site B

135X

c. Fine Grain Size, Lot 12

Figure 18. Concluded.

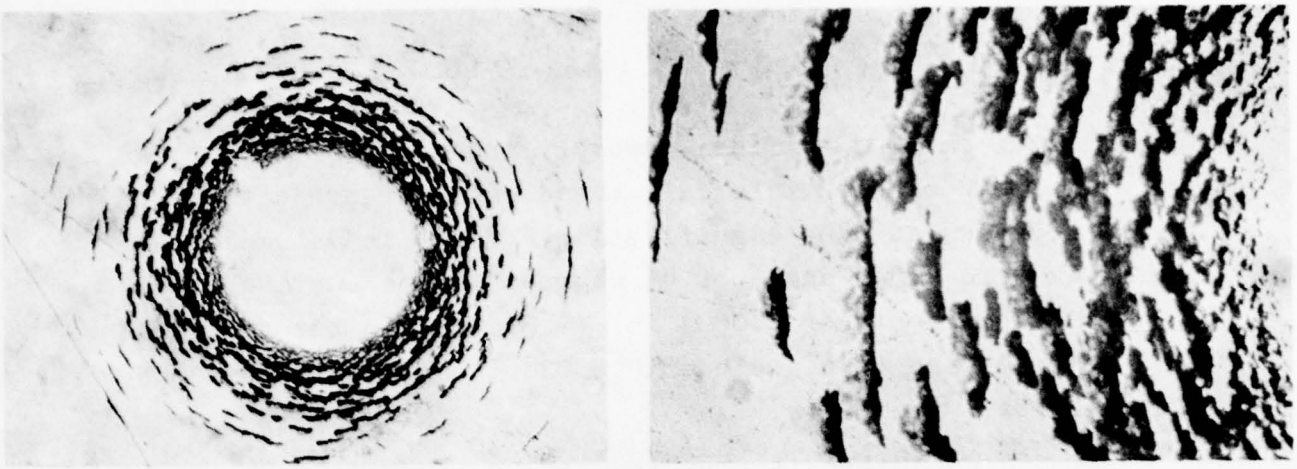

135X a. Fine-Grained Zinc Selenide, Lot 6. 640X

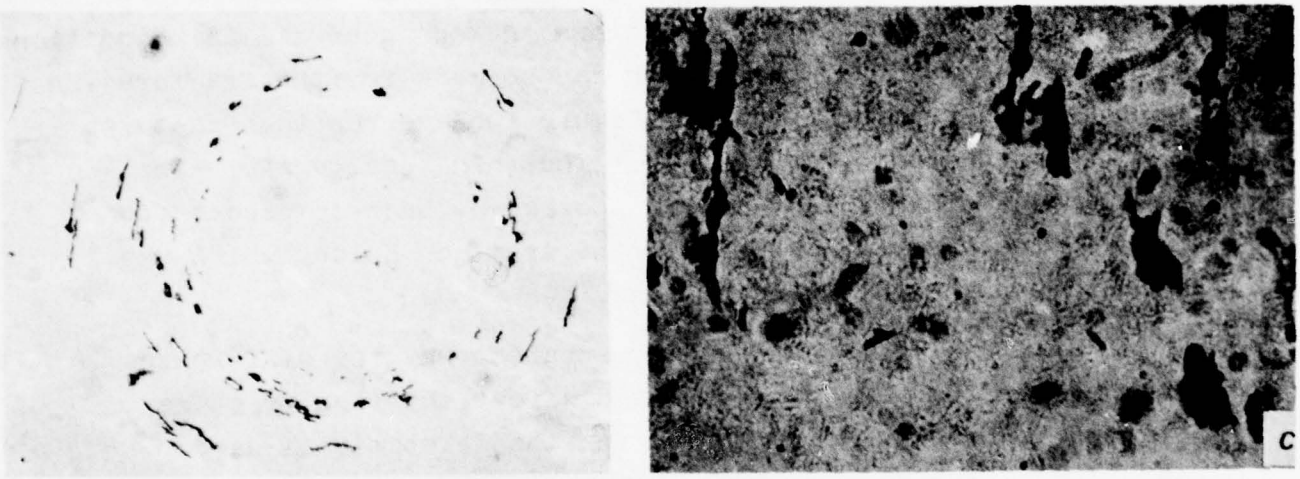

135X b. Standard Zinc Sulfide, Thick Specimen 640X

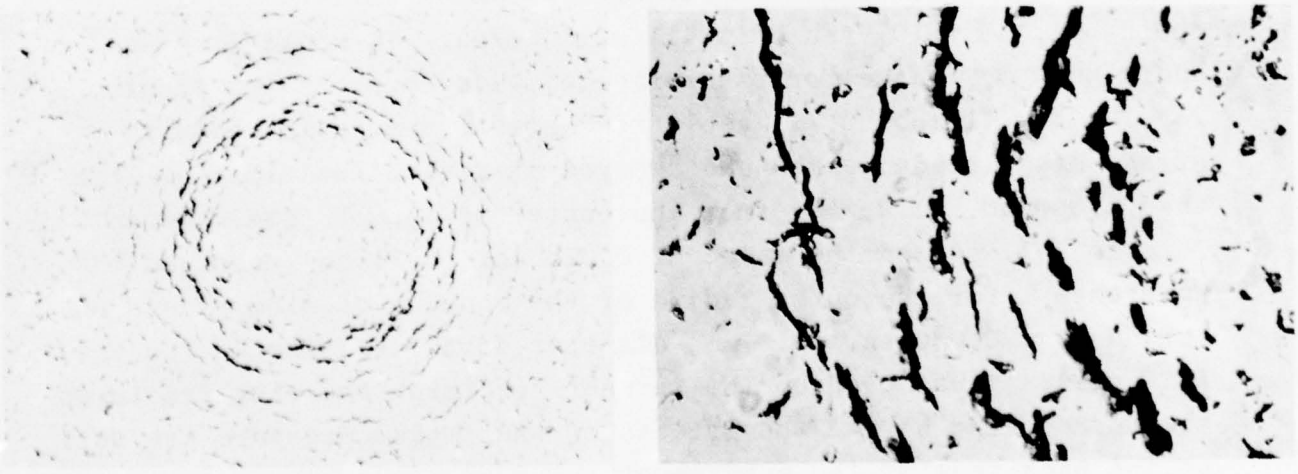

135X c. Standard Zinc Sulfide, Thin Specimen 640X

Figure 19. Comparison of Ring Fracture Formed on Fine-Grained Zinc Selenide and Standard Zinc Sulfide by Impact of a 0.080 in. (2.0 mm) Diameter Water Drop at 730 fps (222 m/s). Specimens Etched. Transmitted Light.

impact sites on zinc sulfide; however, the depth of the cracks are comparable on both materials based on their projections in the micrographs at 640X magnification. If it is assumed that the cracks are at an angle of 45 degrees to the surface, they penetrate to a depth of 0.0004 in. (0.010 mm) in the fine-grained zinc selenide and to a depth of 0.00028 in. (0.007 mm) in the zinc sulfide.

Interestingly, the ring fractured annulus on the thin standard zinc selenide specimen (Figure 19a) was considerably smaller than that on a thick specimen tested under similar conditions (Figure 2). A similar conclusion can be made for the fractures on the thin zinc sulfide specimen (Figure 19c) versus the fractures on a thick specimen (Figure 19b). The thin specimens of zinc selenide and zinc sulfide were supported by back-up pieces of polymethylmethacrylate (PMMA) in the specimen holder which was designed for the thicker specimens.

It is not readily apparent why the differences in thickness or the PMMA back-up would affect the ring fracture patterns. For examine, the time for the dilatational wave generated by the drop impact to reach the back face of the thin specimen would be 0.71 μsec for zinc selenide (Dilatational Wave Speed = 1.360×10^4 fps or 0.411×10^4 m/s). It would take an additional 0.71 μsec for the reflected wave to reach the front face. At a time of 0.71 μsec after impact, the radial tensile stress has already peaked and decayed at radial locations of less than 0.050 in. (1.25 mm) from the center of impact (see Figure 72). This is well beyond the value of 0.028 in. (0.71 mm) reported in Reference 1 for the outer radius of the annulus of ring fractures formed by a 0.080 in. (2.0 mm) diameter drop impacting at 730 fps (222 m/s). Thus, even on the thinner specimen, the ring fractures are formed long before the effects of the impact pressure are felt at the back face of the specimen.

Differences in the materials from which the thick and thin specimens were fabricated could possibly account for the difference in sizes of the ring fractured annuli; however, this appears unlikely for two reasons. First, the microstructures of the thin standard grain size zinc selenide and zinc sulfide specimens were comparable to those of the thicker specimens of each material previously tested and it is logical that the specimens would have similar response to drop impact. Second, the same effect of thickness was apparent for both zinc selenide and zinc sulfide. It does not seem probable that the same unknown material difference between the thin and thick specimens would be present in both materials.

The purpose of this series of tests was to evaluate the effect of reduced grain size for zinc selenide rather than the effect of specimen thickness. Additional experiments with specimens from the same batch of material are required to establish definitely that the observed effect of thickness is real.

8. Antireflection Coatings

A series of single drop impact experiments were performed to investigate the response of antireflection coatings applied to zinc sulfide and gallium arsenide. The coatings listed below were applied to four zinc sulfide specimens by Honeywell, Inc., who developed them under Air Force Contract.[2]

- Lanthanum fluoride (LaF_3) monolayer
- Neodymium fluoride (NdF_3) monolayer
- Thorium fluoride (ThF_4) monolayer
- Zinc selenide (inner) and neodymium fluoride (outer) bilayer ($ZnSe/NdF_3$)

A proprietary coating of unknown composition was applied to one gallium arsenide specimen by Laser Optics, Inc.

The coated specimens were exposed to impact by 0.080 in. (2.0 mm) diameter water drops at 730 fps (222 m/s). The zinc sulfide specimen coated with LaF_3 showed no evidence of water drop impact damage so a second test was performed on this specimen. Again, no evidence of impact damage was found. All other specimens tested in both series of experiments in which the LaF_3 coated specimen was included did exhibit evidence of water drop impact. This suggests that the LaF_3 coating somehow prevented damage from water drop impact at 730 fps (222 m/s). Such a conclusion must be tentative since it is still possible that there could have been a malfunction of the single drop generator during both tests of the LaF_3 coated specimen. As will be discussed in a subsequent section on rainfield experiments, the LaF_3 coated specimen did not appear to be more erosion resistant than uncoated zinc sulfide when exposed to a rainfield environment.

Ring fractures similar in appearance and size to those formed on uncoated zinc sulfide were found on the specimen coated with NdF_3 as shown in Figure 20. There appeared to be no loss of adhesion of the coating at the impact sites. An example of the impact sites found on the zinc sulfide specimen coated with ThF_4 is shown in Figure 21. The ring fractures in the ThF_4 coating at the ten o'clock position are somewhat similar to those formed on uncoated zinc sulfide. A spiral pattern of cracking of the coating can be seen on the opposite side at the four o'clock position. This type of pattern, found only on the specimen coated with ThF_4, may be related to the mechanism of growth of the coating during deposition. It bears a resemblance to the growth of a crystal around a screw dislocation.

Other examples of spiral crack patterns on the ThF_4 coating are shown in Figure 22. A portion of the coating was also removed at the impact site shown in Figure 22a. No evidence of damage to the zinc sulfide was apparent in the area where the coating was removed. There were also other relatively

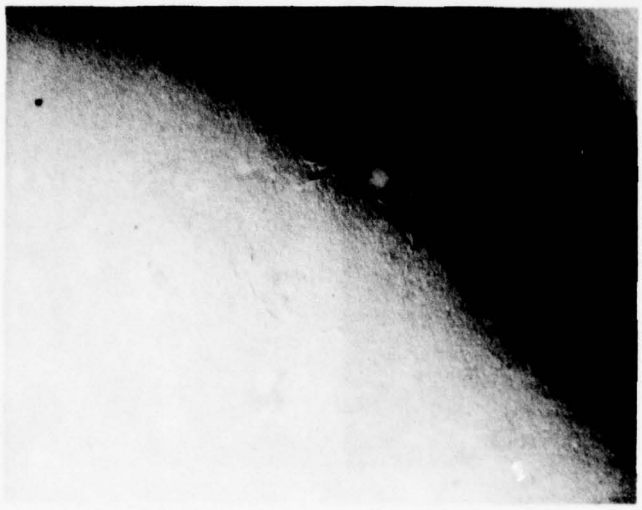

a. Reflected Light with Nomarski Contrast. Mag. 40X

b. Transmitted Light. Mag. 40X

Figure 20. Site of Impact of a Water Drop on Zinc Sulfide with an Antireflection Coating of Neodymium Fluoride. 0.080 in. (2.0 mm) Diameter Drop at 730 fps (222 m/s). Mag. 40X

a. Reflected Light with Nomarski Contrast. Mag. 40X

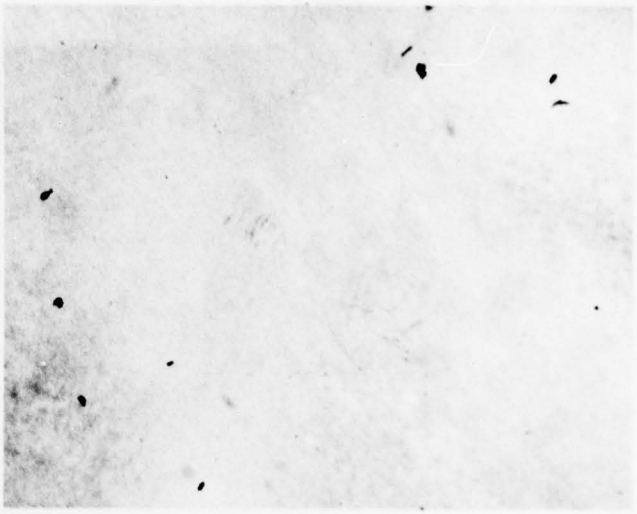

b. Transmitted Light. Mag. 40X

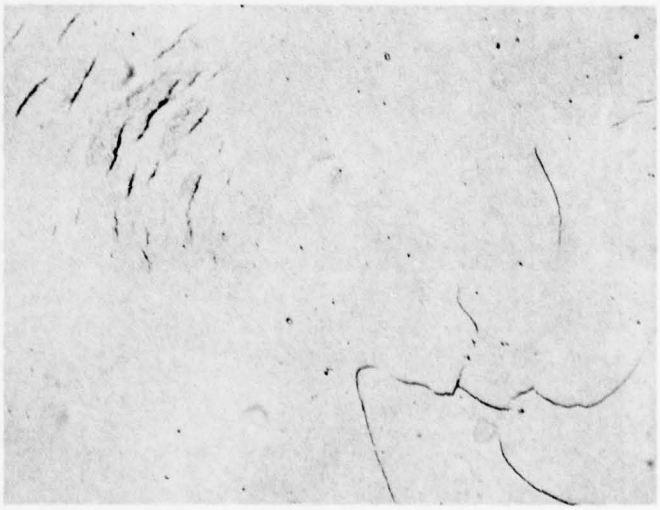

c. Transmitted Light. Mag. 130X

Figure 21. Site of Impact of a Water Drop on Zinc Sulfide with an Antireflection Coating of Thorium Fluoride. 0.080 in. (2.0 mm) Diameter Drop at 730 fps (222 m/s)

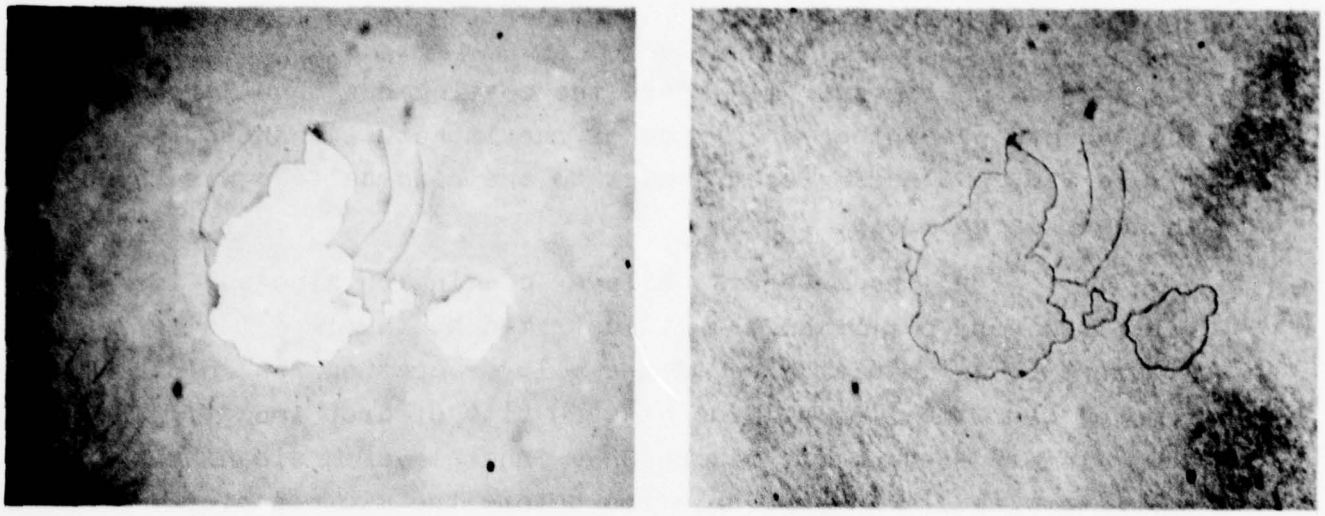

Reflected Light Transmitted Light

a. Site No. 1

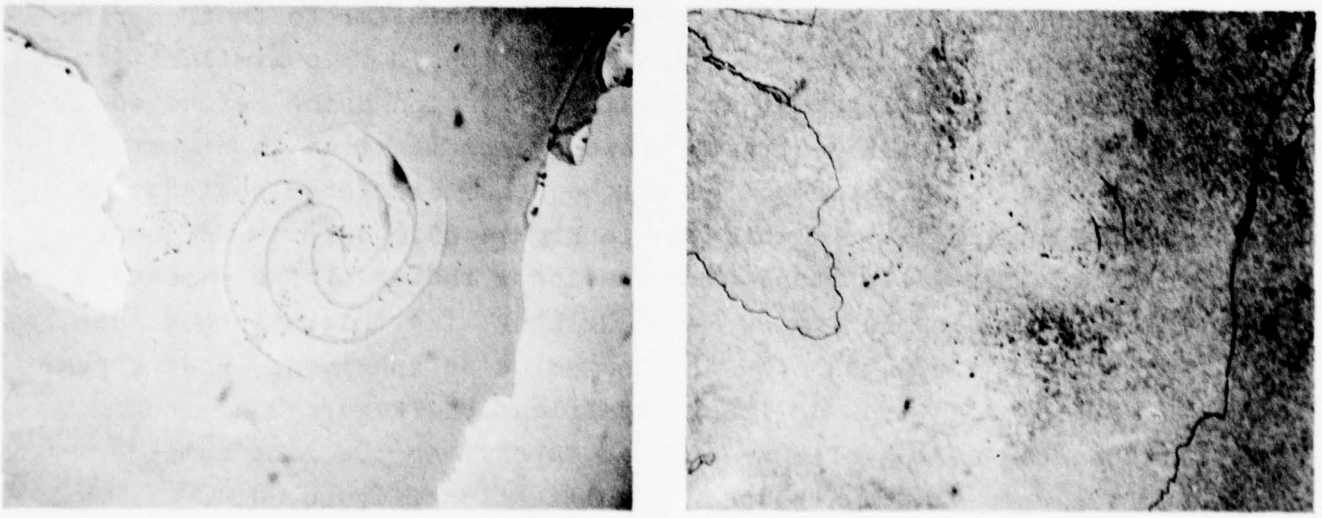

Reflected Light Transmitted Light

b. Site No. 2

Figure 22. Spiral Cracks in Thorium Fluoride Antireflection Coating on Zinc Sulfide at Site of Impact of a Water Drop. 0.080 in. (2.0 mm) Diameter Drop at 730 fps (222 m/s). Mag 40X

large areas on the specimen where the coating has been removed, such as are present on each side of the impact site shown in Figure 22b. No evidence of damage to the zinc sulfide was found in these large areas.

The $ZnSe/NdF_3$ bilayer coating on zinc sulfide exhibited poor performance as illustrated by the impact site in Figure 23. An annular area of the bilayer coating was completely removed from the zinc sulfide at each site of drop impact. The NdF_3 also adhered poorly to the ZnSe inner layer: cleaning the specimen with a mild soap solution before the microscopic examination removed most of the NdF_3.

The response of the $ZnSe/NdF_3$ coated zinc sulfide was considerably different from that of uncoated zinc sulfide, although some impact sites had a few isolated surface cracks such as can be seen in Figure 23c. At first glance, the damage on the coated zinc sulfide appeared to be similar to that on zinc selenide impacted under identical conditions. This similarity was particularly apparent at low magnification using reflected light with Nomarski contrast. However, examination at higher magnification established the unique behavior of the coated zinc sulfide specimen as illustrated in Figure 24. Surface features that look like slip steps near the inner radius of the damaged area can be seen in Figure 24b. Nothing like this has been seen before on any zinc sulfide or zinc selenide specimen. What appear to be ring fractures at lower magnification (Figure 24a) look like narrow strips of some sort of deposit on the zinc sulfide surface when viewed at higher magnification (Figure 24c).

The antireflection coating was removed from the gallium arsenide over a large annular region surrounding the center of drop impact as shown in Figure 25a. Within this region there was a smaller annulus that at first appeared to be a ring fracture pattern. This pattern, shown at higher magnification in Figure 25b, had an unusual appearance and did not resemble

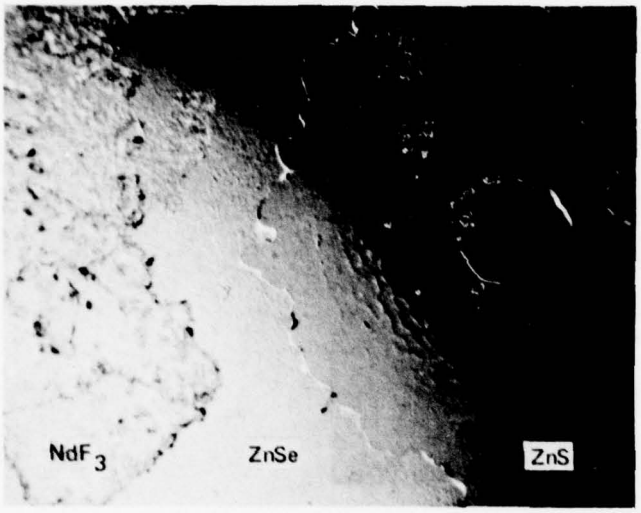

a. Site No. 1. Reflected Light with Nomarski Contrast. Mag. 40X

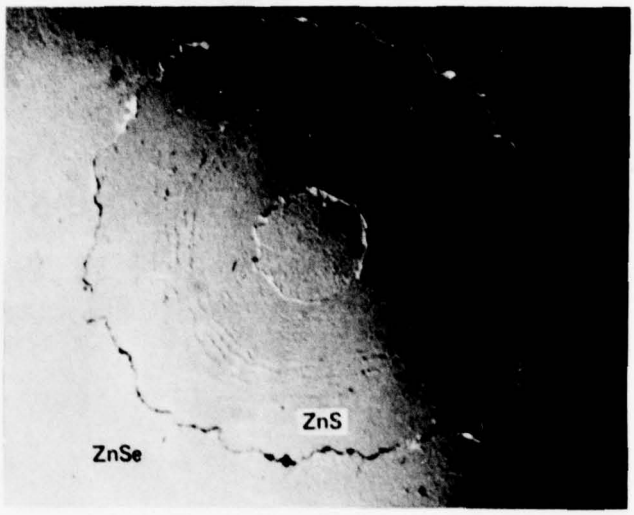

b. Site No. 2. Reflected Light with Nomarski Contrast. Mag. 40X

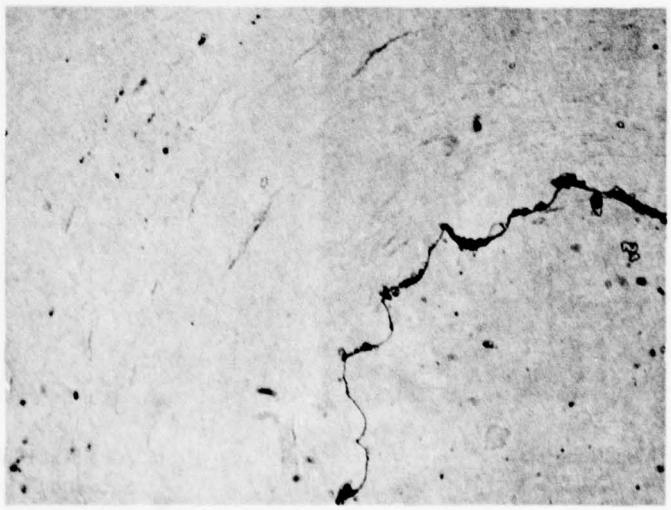

c. Site No. 2. Transmitted Light. Mag 160X

Figure 23. Sites of Impact of a Water Drop on Zinc Sulfide with a Bilayered Antireflection Coating Consisting of an Inner Layer of Zinc Selenide and an Outer Layer of Neodymium Fluoride. 0.080 in. (2.0 mm) Diameter Drop at 730 fps (222 m/s).

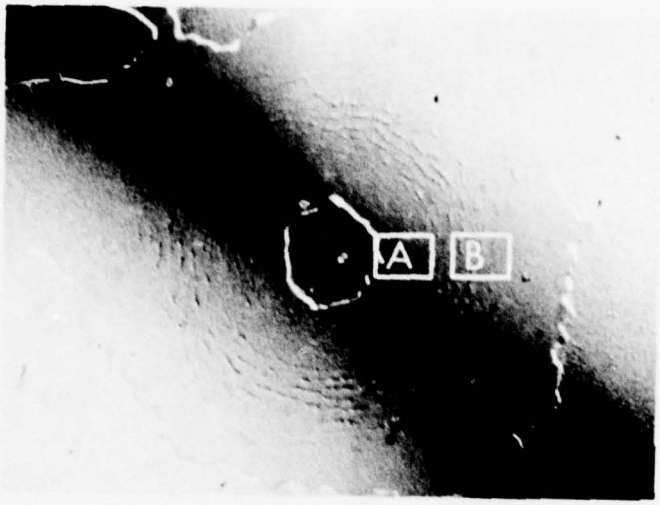

a. Overall View of Impact Site. Mag. 40X

b. Area A at Higher Magnification Showing Slip Steps. Mag. 620X

c. Area B at Higher Magnification Showing Strips of Coating Remaining on Zinc Sulfide Surface. Mag. 620X

Figure 24. Details of Features Found at The Site of Impact of a Water Drop on Zinc Sulfide with a Bilayered Antireflection Coating Consisting of an Inner Layer of Zinc Selenide and an Outer Layer of Neodymium Fluoride. 0.080 in. (2.0 mm) Diameter Drop at 730 fps (222 in/s).

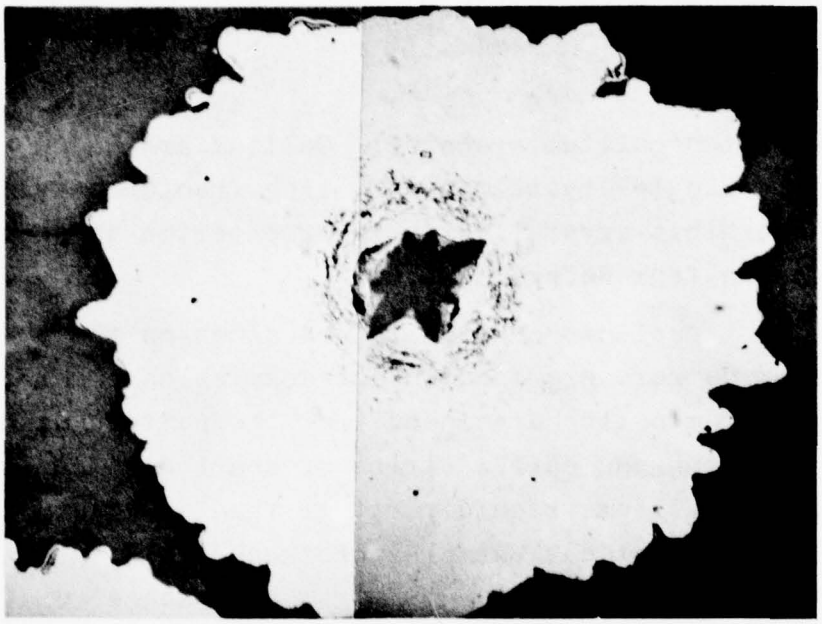

a. Mag 30X

b. Mag 135X

Figure 25. Site of Impact of a Water Drop on Gallium Arsenide with an Antireflection Coating. 0.080 in. (2.0 mm) Diameter Drop at 730 fps (222 m/s)

those on uncoated gallium arsenide. Gallium arsenide is essentially a single crystal and the ring fractures from water drop impact exhibit crystallographic orientation as shown in Figure 26 taken from Reference 1.

Replicas of drop impact sites on the coated gallium arsenide were examined in a transmission electron microscope. This examination disclosed that the pattern was made up of relatively long and narrow strips of coating remaining on the surface of the gallium arsenide, rather than cracks in the surface of the gallium arsenide. Examples of these strips are shown in the electron micrographs in Figure 27. The presence of a ring pattern comprised of strips of the coating is an unusual phenomena for which there is no explanation at this time.

Figure 28 shows an interesting impact site where portions of the antireflection coating remained bonded to the gallium arsenide substrate in the region of highest tensile stresses. The ring pattern formed on the gallium arsenide by the narrow strips of coating can be seen in the three areas where the coating was removed by the impact. Examination of the intact regions of the coating at 620X magnification with Nomarski contrast revealed no fractures of the coating as illustrated in Figure 28.

Figure 29 shows a site where part of the coating that remained bonded after a drop impact was subsequently removed by a second drop which impacted nearby. The site of impact of this second drop just appears in the upper right-hand corner of Figure 29. As can be seen, the ring pattern at the first drop impact site had not formed in the area where the coating was not removed by the first impact.

No evidence of damage to the gallium arsenide was found during the optical and electron microscopic examination of impact sites. The specimen was tested a second time to obtain a

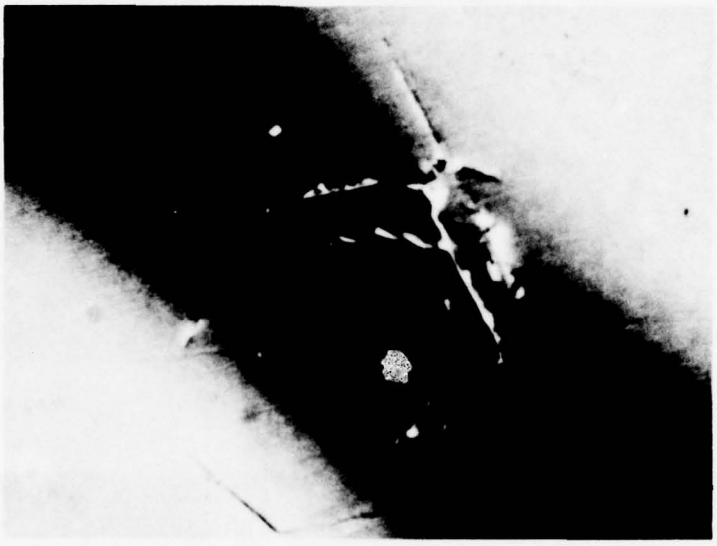

Figure 26. Ring Fracture formed on Gallium Arsenide by a 0.080 in. (2.0 mm) Diameter Water Drop Impacting at 730 fps (222 m/s). Mag. 60X

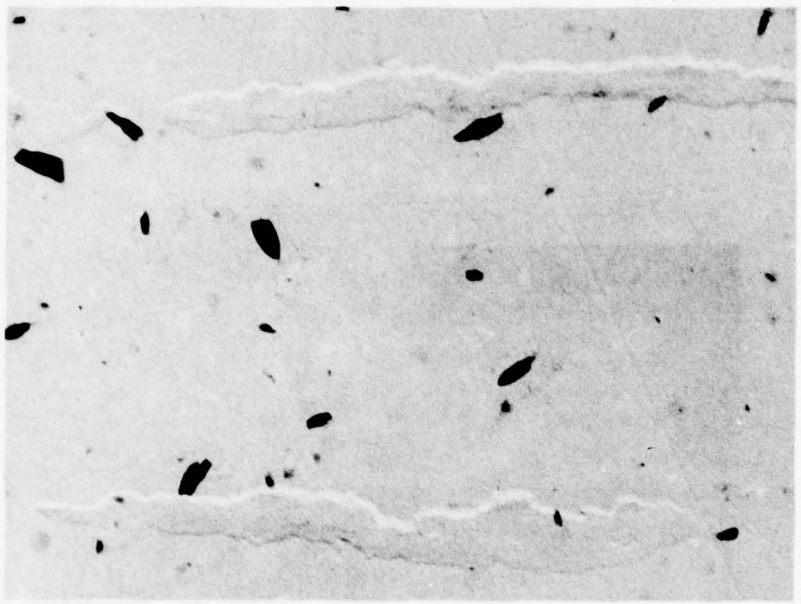

Mag. 5000X

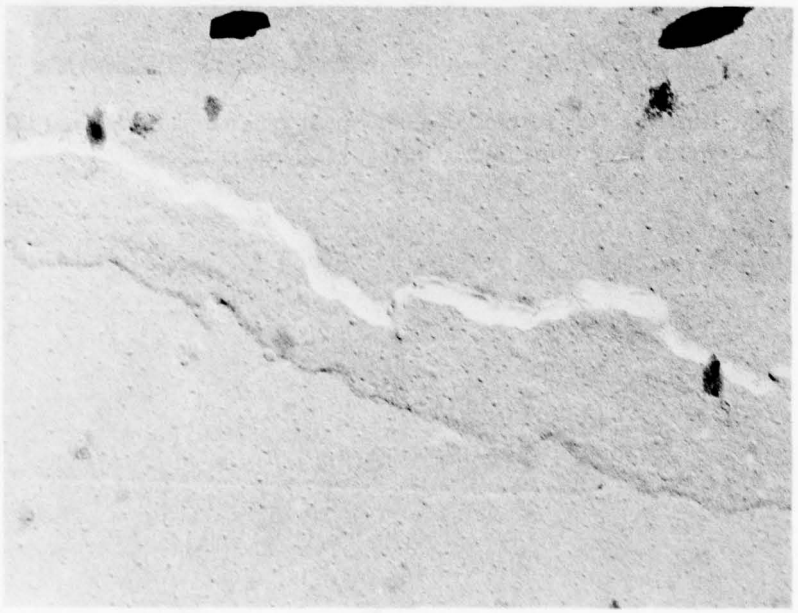

Mag. 12,000X

Figure 27. Electron Micrographs of the Ring Pattern Formed at the Site of Impact of a Water Drop on Gallium Arsenide with an Antireflection Coating. 0.080 in. (2.0 mm) Diameter Drop at 730 fps (222 m/s).

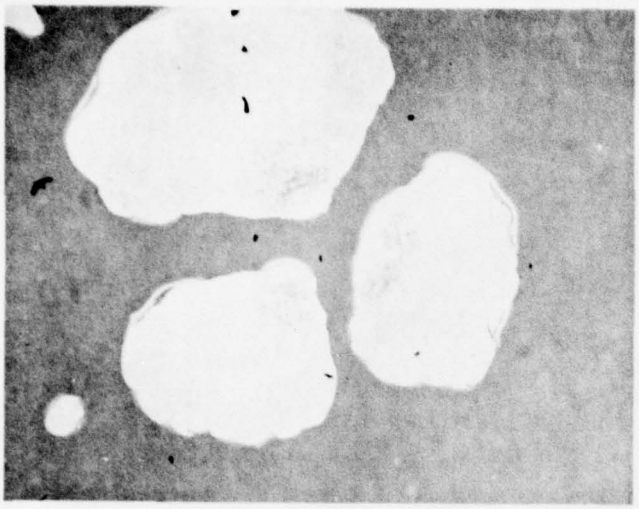

30X

135X

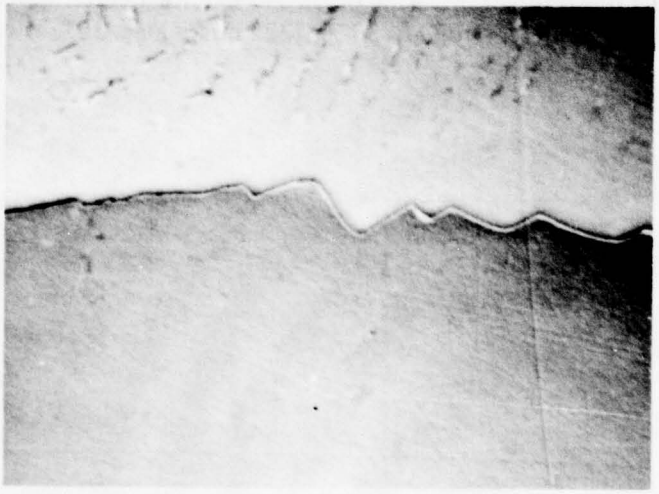

620X

Figure 28. Partial Removal of Coating at Site of Impact of a Water Drop on Gallium Arsenide with an Antireflection Coating. 0.080 in. (2.0 mm) Diameter Water Drop at 730 fps (222 m/s).

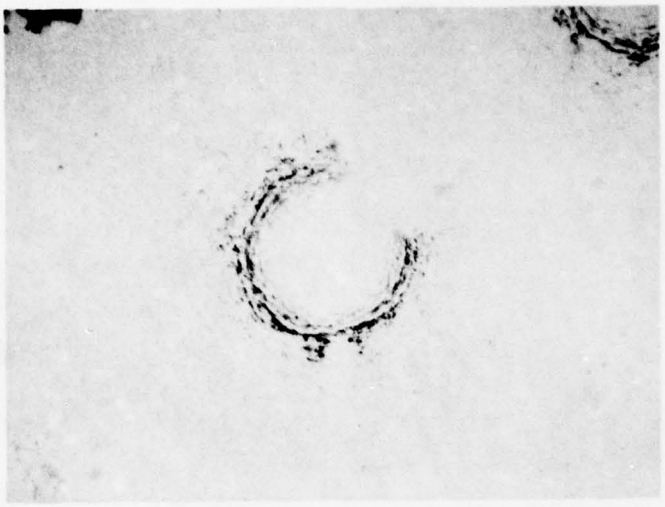

Figure 29. Site of Impact of a Water Drop on Gallium Arsenide with an Antireflection Coating Illustrating Formation of Incomplete Ring Pattern. 0.080 in. (2.0 mm) Diameter Drop at 730 fps (222 m/s). Mag. 30X

drop impact in an area where the coating had been previously removed by the impact of several single drops. This second test produced Site B in Figure 30 which was typical for uncoated gallium arsenide. The two sites in Figure 30 are dramatic evidence of the change in response of gallium arsenide to water drop impact caused by the presence of the antireflection coating.

This series of experiments demonstrated the fact that an antireflection coating can modify the response of the substrate to water drop impact even though the coating is very thin, on the order of a few microns. It is not certain how such a thin coating can modify the behavior of the substrate material even though the impact of a water drop is a surface phenomenon. For example, the maximum radial tensile stress induced in zinc sulfide by the impact at 730 fps (222 m/s) of a 0.080 in. (2.0 mm) diameter water drop has been computed to be less than the fracture strength at depths below 0.002 in. (50μm),[1]

Possibly, the process by which a coating is applied leaves residual stresses in the surface which can affect the response of the material. Resistance to impact would be increased by compressive stresses and decreased by tensile stresses. The antireflection coating may also have less severe defects than the surface of the substrate and be effectively stronger. It is also possible that the coatings render inoperative the surface flaws in the substrates. Regardless, the coatings are effective only as long as they remain on the surface. This series of experiments indicates that lack of adhesion is a problem which requires more attention.

9. Bilayered Materials

One approach to improve the erosion resistance of an infrared window is to protect it with an outer layer of an erosion resistant material. This approach has been evaluated initially in a previous series of single drop experiments on bilayered specimens having thin layers of zinc sulfide cemented to zinc selenide substrates.[1] It was found that the ring

Site A - AR Coating Sound when Drop Impacted
Site B - AR Coating Removed by Nearby Prior Impacts before Drop Impacted

Figure 30. Sites of Impact of Two Water Drops on Gallium Arsenide with an Antireflection Coating. 0.080 in. (2.0 mm) Diameter Drops Impacting at 730 fps (222 m/s) Mag. 40X

fractures produced by a 0.080 in. (2.0 mm) diameter drop impacting at 730 fps (222 m/s) did not penetrate through a 0.010 in. (0.25 mm) thick layer of zinc sulfide.

This prior work was extended to include a decrease in layer thickness and an increase in impact velocity. Four bilayered specimens were prepared with zinc sulfide outer layer thicknesses of 0.005, 0.010, 0.020 and 0.040 in. (0.12, 0.25, 0.50 and 1.00 mm) bonded to zinc selenide substrates. Lens cement was used for bonding the layers so they could be removed in decementing solution after the impact experiments.

The specimen with the layer thickness of 0.005 in. (0.12 mm) was impacted with 0.080 in. (2.0 mm) diameter water drops at 730 fps (222 m/s). The ring fractures appeared to just penetrate the zinc sulfide layer as shown in Figure 31. Examination of the back face of the layer after it was removed from the zinc selenide substrate verified this conclusion as shown in Figure 32. The large crack running across the impact site in Figure 32a resulted from handling of the thin layer after it was removed. Microscopic examination of the front face of the substrate after the outer layer was removed revealed no damage to the zinc selenide.

The three specimens with zinc sulfide layer thicknesses of 0.010, 0.020, and 0.040 in. (0.25, 0.50 and 1.00 mm) were impacted with 0.080 in. (2.0 mm) diameter water drops at 1120 fps (340 m/s). The damage produced by a single drop impact on the specimen with the 0.010 in. (0.25 mm) thick layer is shown in Figure 33 as observed from the front surface of the specimen before the zinc sulfide layer was removed. The extent of damage on the zinc sulfide layer as revealed by reflected light (Figure 33c) was more extensive than that on homogeneous bulk zinc sulfide tested under similar conditions (Figure 10b).

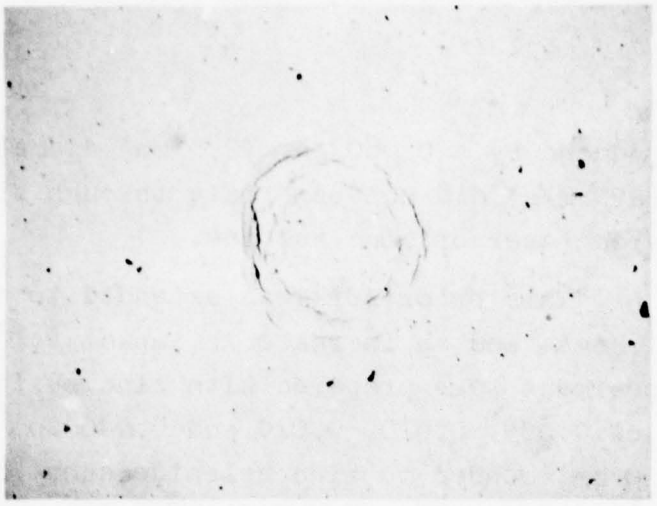

Mag. 30X

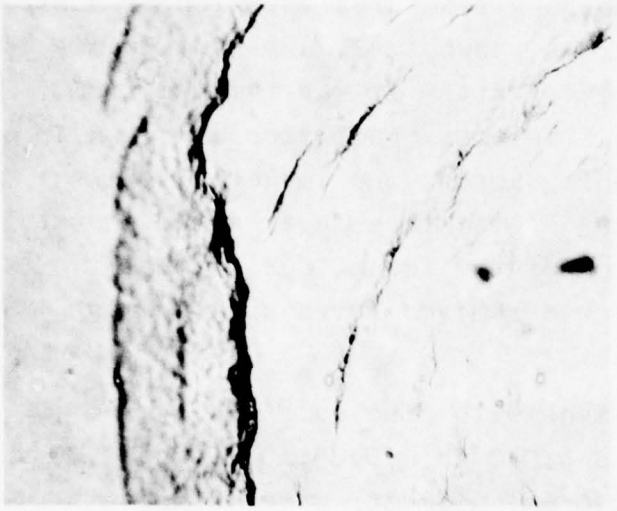

Mag. 250X. Focused on Front Face

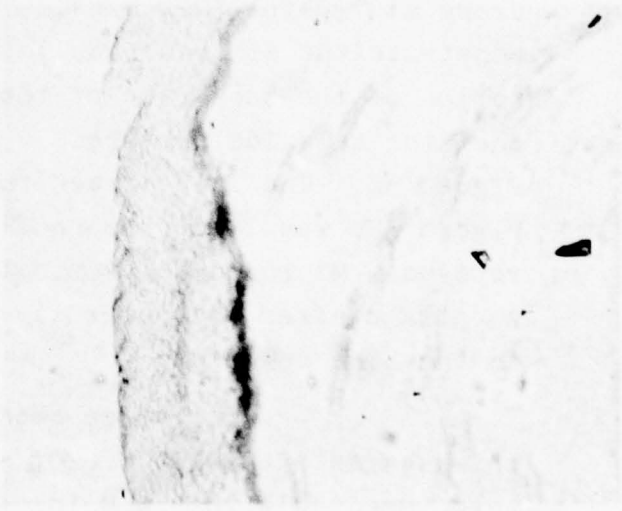

Mag. 250X. Focused on Zinc Selenide Substrate.

Figure 31. Impact Site on Front Face of 0.005 in. (0.12 mm), Thick Layer of Zinc Sulfide Bonded to Zinc Selenide. Surface Impacted by 0.080 in. (2.0 mm) Water Drop at 730 fps (222 m/s). Transmitted Light.

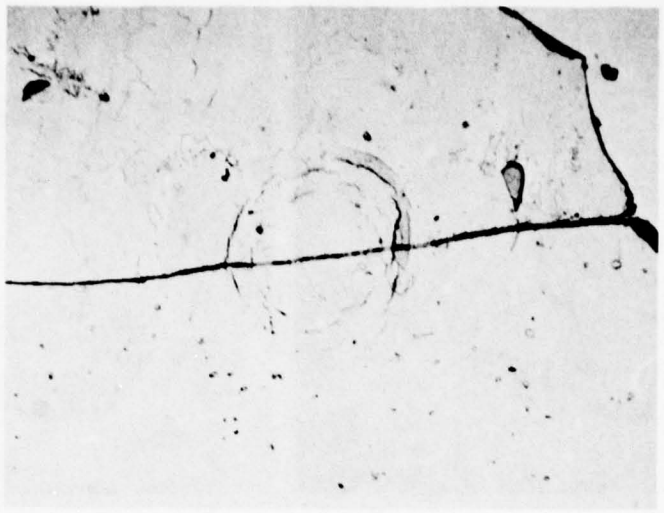

a. Transmitted Light. Mag. 30X

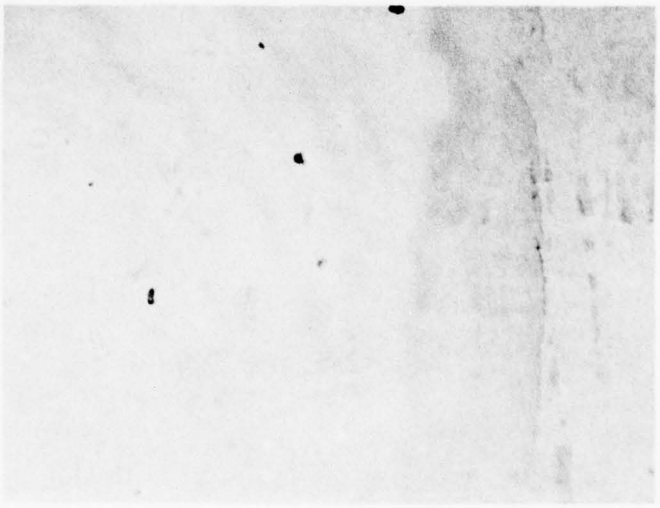

b. Focused on Back Face. Reflected Light. Mag. 250X

Figure 32. Impact Site in Figure 31 as Observed after Removal of the Zinc Sulfide Layer. Mirror Image of Figure 31.

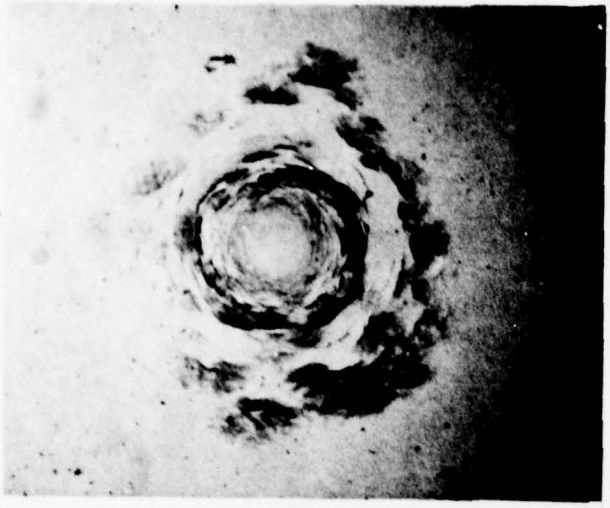

a. Transmitted Light, Mag. 18X

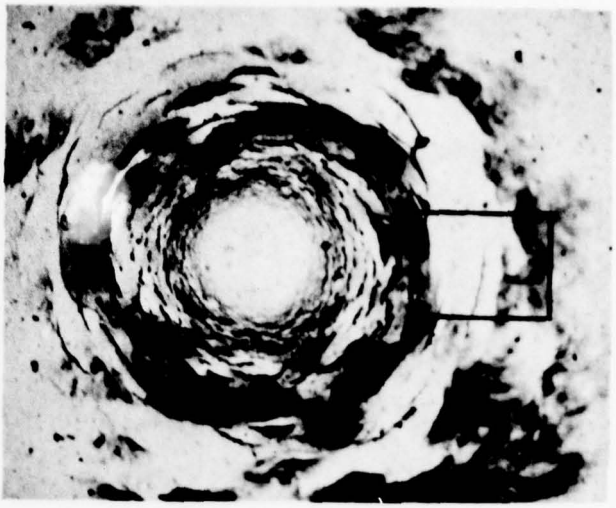

b. Transmitted Light, Mag. 30X

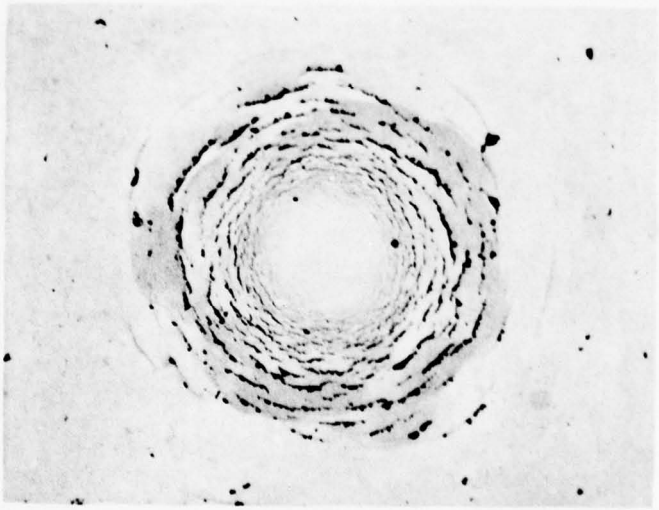

c. Reflected Light, Mag. 30X

Figure 33. Impact Site on Front Surface of 0.010 in. (0.25 mm) Thick Layer of Zinc Sulfide Bonded to Zinc Selenide. Surface Impacted by 0.080 in. (2.0 mm) Diameter Water Drop at 1120 fps (342 m/s). Continued.

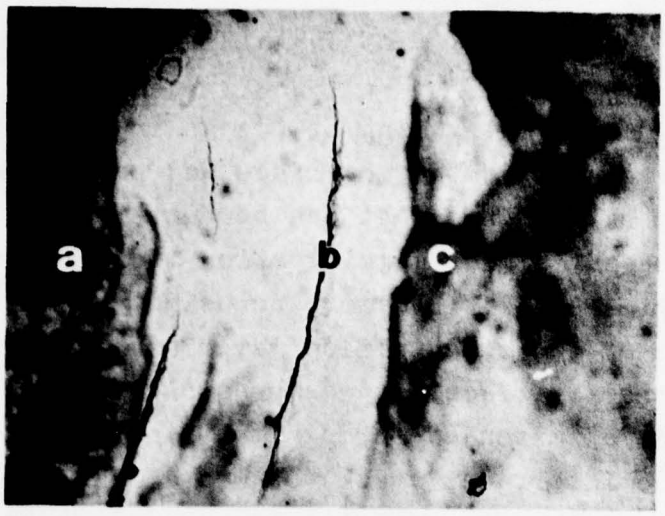

d. Area Outlined in Fig. b, Focused on
Front Surface. Transmitted Light. Mag. 135X

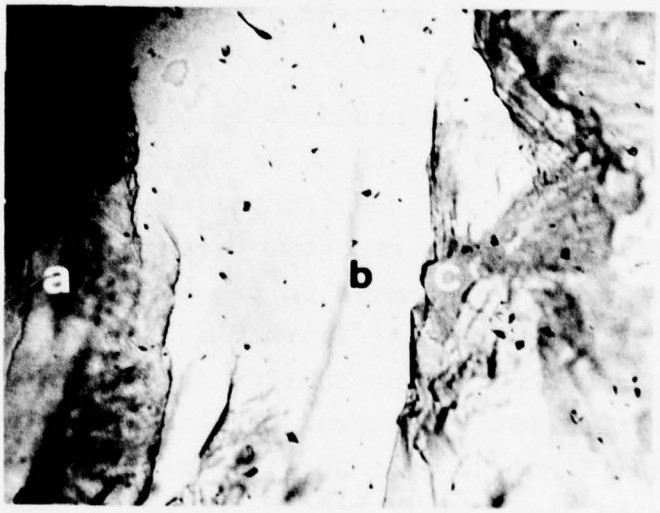

e. Area Outlined in Fig. b, Focused on
Zinc Selenide Substrate. Transmitted Light. 135X

Figure 33. Concluded.

The outer ring of cracks in Figures 33a and 33b appears to originate at the interface and penetrate into the zinc selenide substrate. This fact can be better seen in Figures 33d and 33e which show higher magnification micrographs of the area outlined in Figure 33b. By first focusing the microscope on the front surface of the zinc sulfide layer and then on the zinc selenide at the interface, it was possible to conclude that the cracks marked "a" extended through the zinc sulfide layer and stopped at the interface; crack "b" was a shallow crack on the outer surface of the zinc sulfide layer; and crack "c" initiated at the interface and extended down into the zinc selenide substrate. These conclusions were subsequently verified by examination of the back face of the zinc sulfide layer and the front face of the zinc selenide substrate after the layer was removed. Figure 34 shows the same impact site as Figure 33 after removal of the zinc sulfide layer.

The damage produced by a single drop impact on the specimen with the 0.020 in. (0.50 mm) thick layer is shown in Figure 35 as observed from the front surface of the specimen before the zinc sulfide layer was removed. Even at this increased thickness, the extent of damage on the zinc sulfide layer as revealed by reflected light (Figure 35a) was more extensive than that on homogeneous bulk zinc sulfide tested under similar conditions (Figure 10b). Figures 35c and 35d show that the cracks have just penetrated the zinc sulfide layer at the outer radius of the fractured area. This conclusion was subsequently verified by examination of the back face of the zinc sulfide layer and the front face of the zinc selenide substrate after the layer was removed. Figure 36 shows the same impact site as Figure 35 as viewed from the back face of the zinc sulfide layer. Examination of the front face of the zinc selenide substrate revealed no evidence of damage.

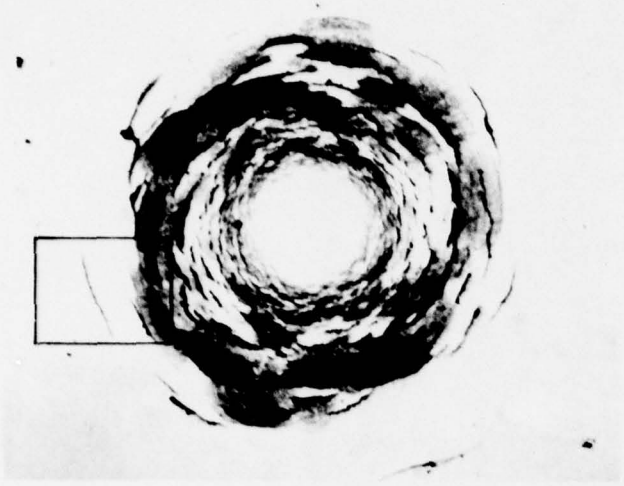

a. Fracture on ZnS as Viewed from Back Surface of Layer. Mirror Image of Figure 33b. Mag. 30X

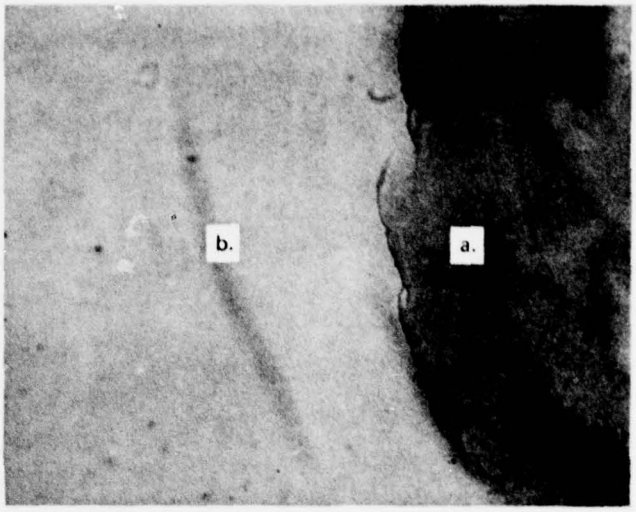

b. Area Outlined in Figure a. At Higher Magnification. Focused on Back Face. Mag. 135X

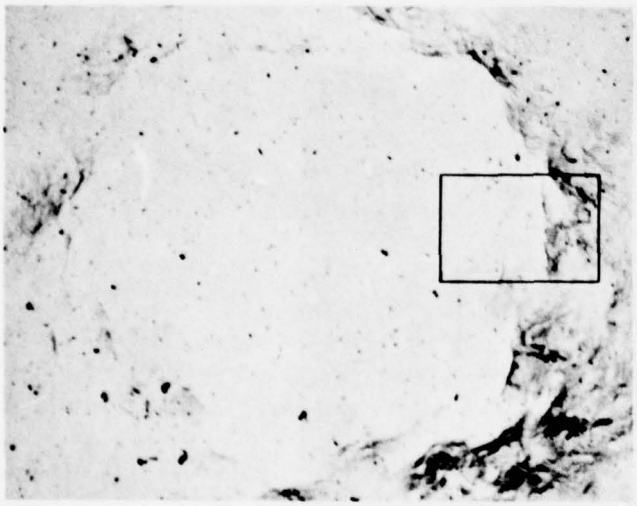

c. Fracture on ZnSe Substrate. Mag. 30X

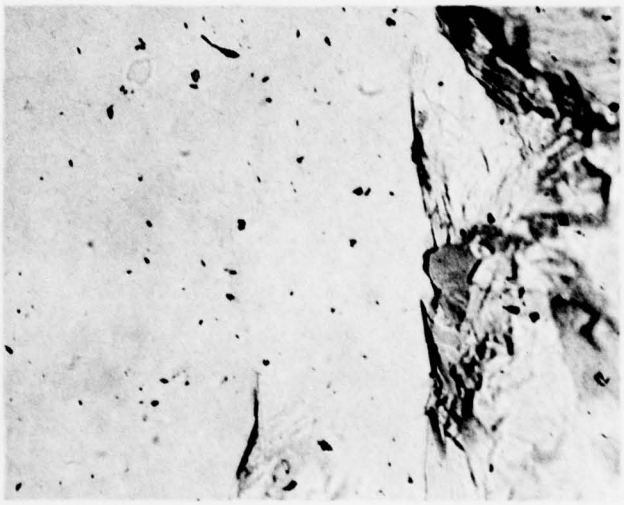

d. Area Outlined in Figure c. At Higher Magnification of 135X

Figure 34. Impact Site in Figure 33 as Observed after Removal of the Zinc Sulfide Layer. Transmitted Light.

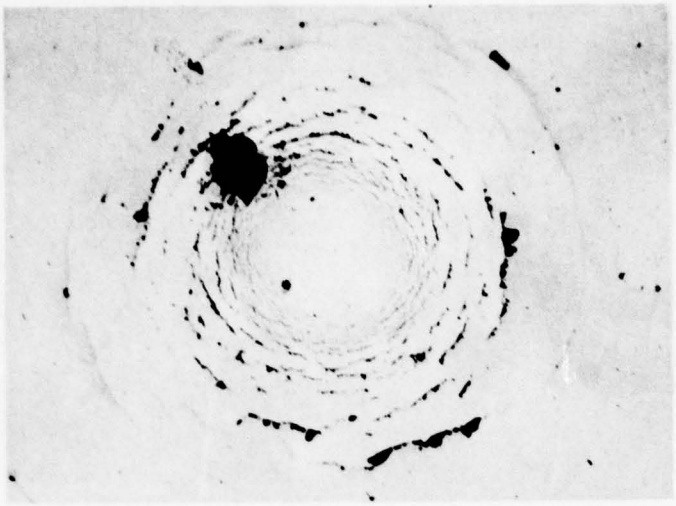

a. Reflected Light. Mag. 30X

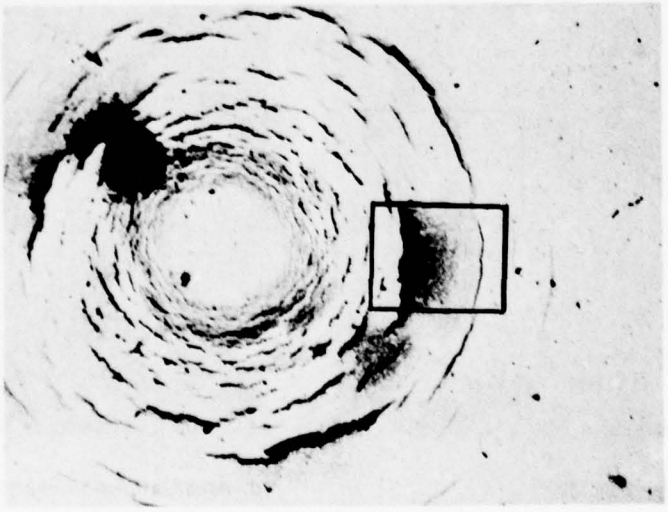

b. Transmitted Light. Mag. 30X

Figure 35. Impact Site on Front Surface of 0.020 in. (0.50 mm) Thick Layer of Zinc Sulfide Bonded to Zinc Selenide. Surface Impacted by 0.080 in. (2.0 mm) Diameter Water Drop at 1120 fps (342 m/s).

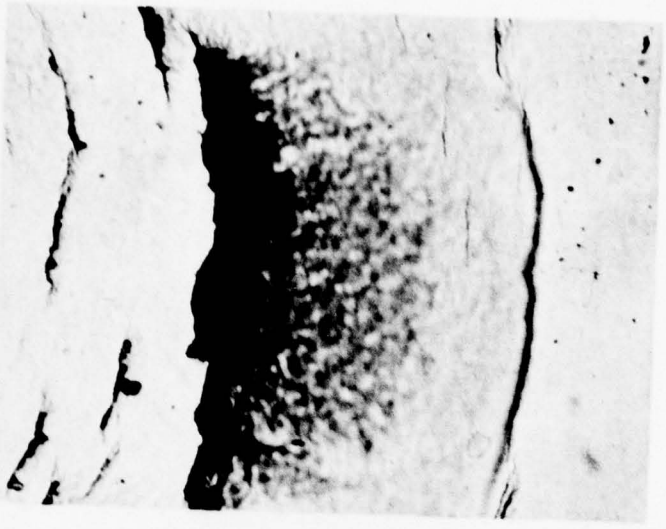

c. Area Outlined in Fig. b, Focused on
Front Surface. Transmitted Light. Mag. 135X

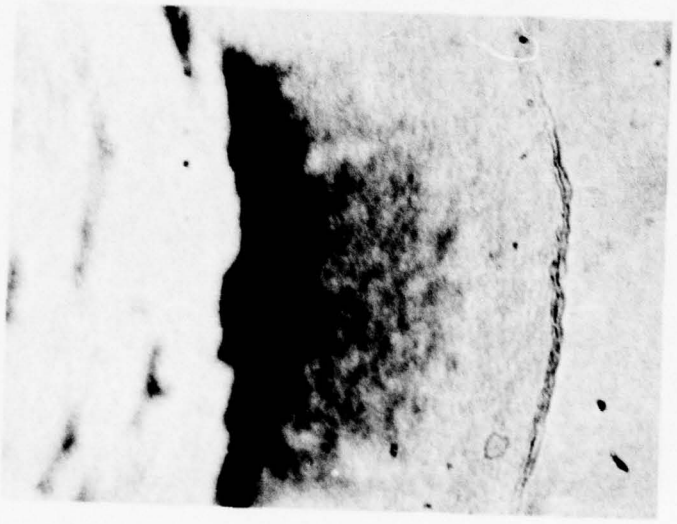

d. Area Outlined in Fig. b, Focused on
Zinc Selenide Substrate. Transmitted Light. Mag. 135X

Figure 35. Concluded.

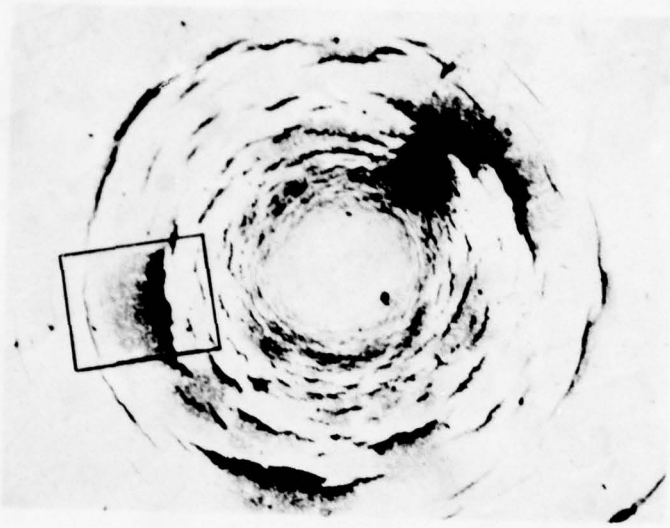

a. View from Back Face of ZnS. Transmitted Light. Mag. 30X

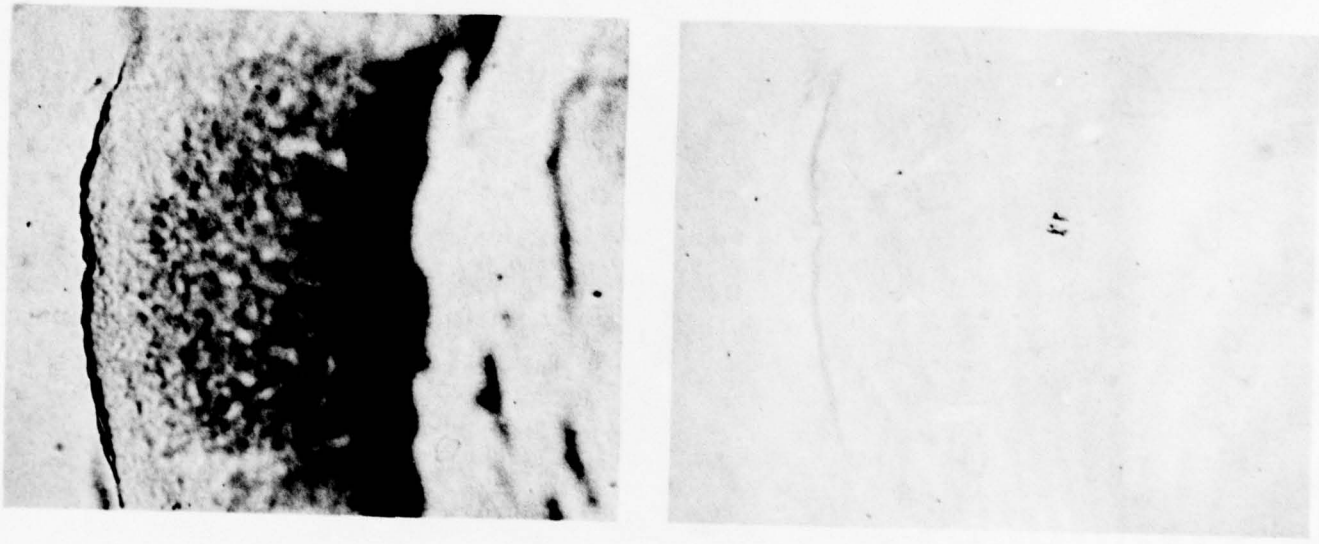

Transmitted Light

Reflected Light

b. Area Outlined in Figure a. At Higher Magnification Showing Cracks Penetrating to Back Face of ZnS. Mag. 135X

Figure 36. Impact Site in Figure 35 as Observed after Removal of the Zinc Sulfide Layer. Mirror Image of Figure 35.

The damage produced on the specimen with the 0.040 in. (1.00 mm) thick layer is shown in Figure 37. The fractures did not penetrate the zinc sulfide layer. In fact, the damage produced on this layer was similar to that produced on homogeneous bulk zinc sulfide tested under similar conditions (Figure 10b).

The zinc sulfide layers on the three bilayered specimens impacted at 1120 fps (340 m/s) and the 0.005 in. (0.12 mm) zinc sulfide layer on the specimen impacted at 730 fps (222 m/s) were etched in a heated solution of HCl and water (1:1 by volume) to reveal the grain structure. A range of structures was found as illustrated in Figure 38.

The 0.010 in. (0.25 mm) layer (Figure 38a) generally had uniform, small grains with a few scattered areas of elongated grains. The average grains had a diameter of approximately 0.0002 in. (5 μm) which was comparable to the grain size previously found on all the 0.375 in. (9.5 mm) thick zinc sulfide specimens previously tested.

The 0.020 in. (0.50 mm) layer (Figure 38b) had an unusual structure in which boundaries outlining large grains appeared to be superimposed on a structure of smaller grains. The large grains had diameters of up to 0.002 in. (50 μm). The 0.040 in. (1.00 mm) layer (Figure 38c) had a small grain size, although the grains were somewhat larger than those of the 0.010 in. (0.25 mm) layer. The 0.005 in. (0.12 mm) layer had uniform, small grains comparable to those in the left hand microphotograph of Figure 38a and so is not included in the figure.

Except for the specimen with the 0.020 in. (0.50 mm) layer, the grain size of the bilayered specimens tested as part of this program appeared to be normal. Thus, grain structure did not appear to contribute to the enhanced damage found on either the 0.005 in. (0.12 mm) layer impacted at 730 fps (222 m/s) or the 0.010 in. (0.25 mm) layer impacted at 1120 fps

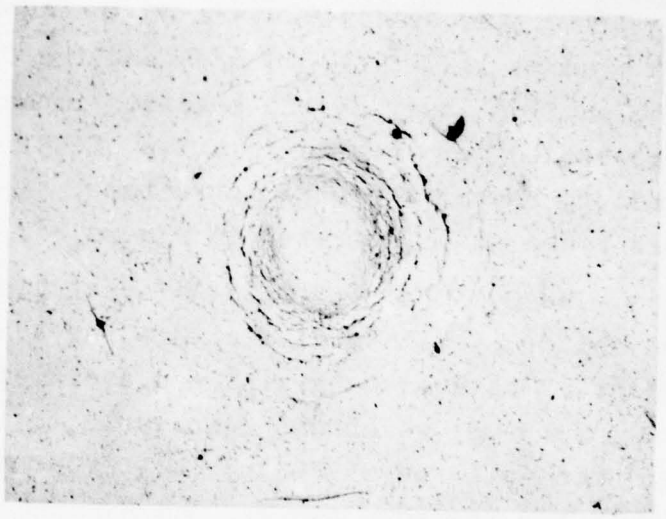

Figure 37. Impact Site on Front Face of 0.040 in. (1.00 mm) Thick Layer of Zinc Sulfide Bonded to Zinc Selenide. Surface Impacted by 0.080 in. (2.0 mm) Water Drop at 1120 fps (342 m/s). Transmitted Light. Mag. 30X

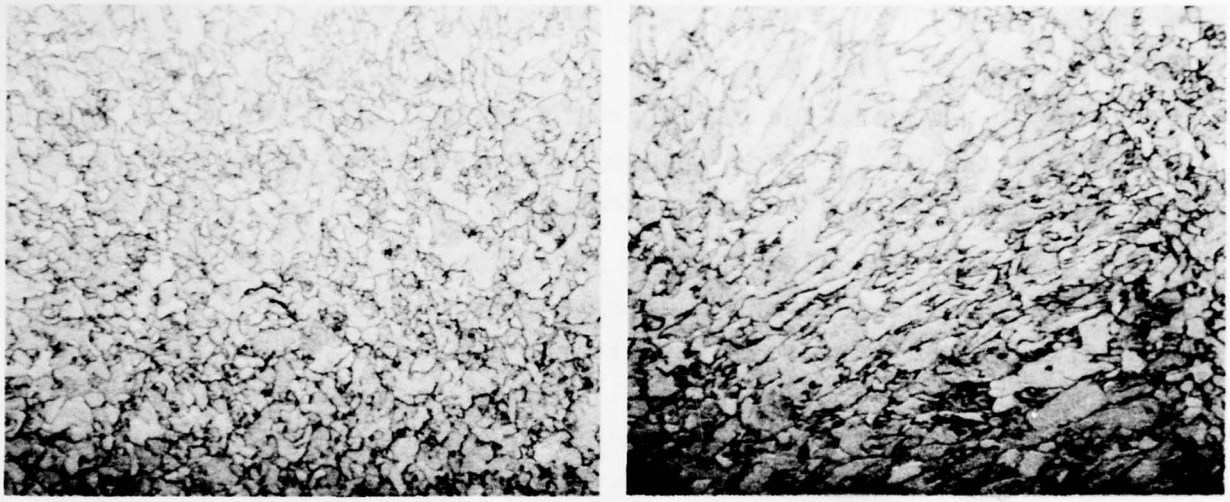

a. 0.010 in. (0.25 mm) Thick Layer. Layer Removed in Decementing Agent prior to Etching.

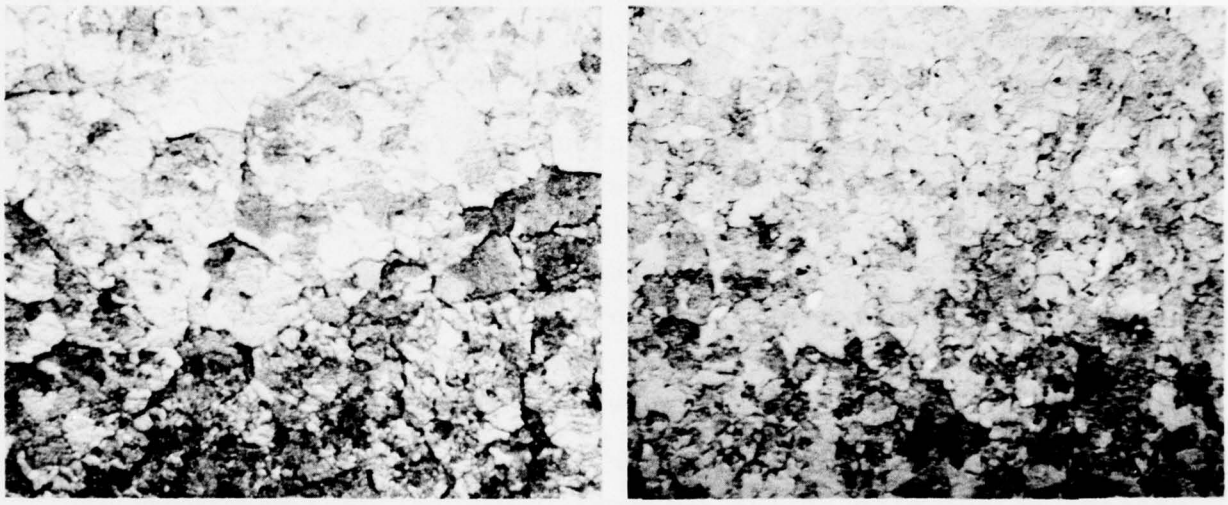

b. 0.020 in. (0.50 mm) Thick Layer. Layer Removed in Decementing Agent prior to Etching.

c. 0.040 in. (1.00 mm) Thick Layer. Layer Not Removed in Decementing Agent prior to Etching.

Figure 38. Grain Structure of Zinc Sulfide Layers on Bilayered Specimens Impacted with 0.080 in. (2.0 mm) Diameter Drops at 1120 fps (340 m/s). Mag. 470X.

(340 m/s). However, the large grains of the 0.020 in. (0.50 mm) layer impacted at 1120 fps (340 m/s) probably contributed to the enhanced damage found on this specimen.

The zinc sulfide layer of three bilayered specimens tested at 730 fps (222 m/s) during a previous program (Ref. 1) were also etched to reveal the grain structure. The 0.010 in. (0.25 mm) layer had uniform, small grains comparable to those in the left hand microphotograph of Figure 38a. Grain structure did not appear to contribute to the enhanced damage previously reported for this specimen. The 0.020 in. (0.50 mm) thick layer also had uniform, small grains with occasional rosettes composed of elongated grains. The 0.040 in. (1.0 mm) thick layer consisted of areas of large grains intermixed with area of small grains as illustrated in Figure 39. These two thicker layers had exhibited damage somewhat more extensive than that found on small grained, homogeneous zinc sulfide tested under similar conditions.

The large grain structure found on some of the bilayered specimens was not a result of heating in the decementing solution. Neither of the 0.040 in. (1.0 mm) layers was removed before etching: one layer had relatively small grains (Figure 38c) while the other had a mixed structure with large and small grains (Figure 39). Of the four layers removed before etching, only the 0.020 in. (0.50 mm) layer (Figure 38b) exhibited large grains.

The unusual grain structures must have been present on one side of the original 0.125 in. (3.2 mm) thick zinc sulfide plate from which the pieces were cut to prepare the outer layers for the bilayered specimens. Its random appearance in the etched specimens depended upon which side of the original layer was cemented to the zinc selenide and how much was ground off to obtain the final layer thickness.

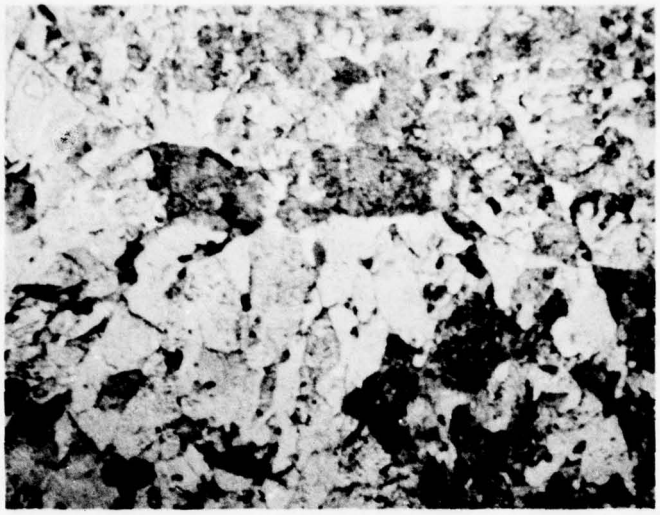

Figure 39. Grain Structure of 0.040 in. (1.00 mm) Thick Zinc Sulfide Layer on Bilayered Specimen Impacted with 0.080 in. (2.0 mm) Diameter Drops at 730 fps (222 m/s). Layer Not Removed prior to Etching. Mag. 470X.

Regardless of its origin, the unusual grain structure of some of the zinc sulfide layers did not affect the conclusions drawn from the results of this series of experiments. Zinc sulfide outer layers of 0.005 and 0.020 in. (0.12 and 0.50 mm) thickness prevented damage to zinc selenide substrates at impact velocities of 730 and 1120 fps (222 and 340 m/s), respectively. However, the fact that the ring fractures did completely penetrate the zinc sulfide layers at both of these conditions proved that the interface affected the response of the specimens to drop impact.

The maximum penetration depth of ring fractures formed on bulk, homogeneous zinc sulfide by the impact of a 0.080 in. (2.0 mm) diameter water drop at 730 fps (222 m/s) was previously estimated to be 0.0003 in. (8 μm) based on the projected image the cracks made with transmitted light. This is only 6% of the thickness of the layer which was penetrated under comparable conditions. The maximum depth of ring fractures formed on bulk, homogeneous zinc sulfide by impact of a similar drop at 1120 fps (340 m/s) was measured to be 0.008 in. (0.20 mm). This is only 40% of the thickness of the layer which was penetrated under comparable conditions. This experiment demonstrated the potential of the bonded layer approach; however, the outer layers must be sufficiently thick to eliminate effects of the interface.

10. Bimedia Window

As described above, the bilayered approach is a way to improve the erosion resistance of an otherwise desirable infrared window material. A variation of this bilayered approach is the bimedia window where the thin, erosion resistant outer layer is not cemented directly onto the substrate, but is separated from it by a layer of liquid. The purpose of the liquid is to modify the pressure which is transmitted to the outer layer during the impact of a water drop and, thus, reduce damage to this layer.

The feasibility of the bimedia window concept was investigated using a simulated bimedia specimen which had a soft, polyurethane elastomeric layer to simulate the liquid. The specimen consisted of a 0.040 in. (1.0 mm) thick zinc sulfide outer layer and a 0.375 in. (9.5 mm) thick zinc selenide substrate bonded together with a 0.080 in. (2.0 mm) thick layer of polyurethane rubber. The outer layer of zinc sulfide used for this bimedia specimen had been removed in decementing solution from one of the bilayered specimens which had not been tested. The bimedia specimen was prepared and tested before the zinc sulfide layers on the bilayered specimens were etched to reveal the unusual grain structure of some of the layers as described in the preceding section.

The simulated bimedia specimen was impacted with 0.080 in. (2.0 mm) diameter drops at 730 fps (222 m/s). Figure 40 compares a typical ring fracture formed on the outer layer of the bimedia specimen with one formed on a 0.375 in. (9.5 mm) thick, homogeneous zinc sulfide specimen. The annular area encompassing the ring fractures was smaller on the bimedia window specimen. The ring fractures on the bimedia window specimen were quite similar in size and appearance to those formed previously on the thin specimen of zinc sulfide which was backed with PMMA during the test (Figure 19c).

Etching the bimedia specimen in a heated solution of HCl and water (1:1 by volume) revealed that the zinc sulfide layer had grains with diameters as large as 0.0016 to 0.0019 in. (40 to 50 μm) as shown in Figure 41a. The grain size of the 0.375 in. (9.5 mm) thick sulfide specimens had previously been found to be generally smaller in diameter than 0.0004 in. (10 μm). The bimedia specimen would be expected to suffer less damage (fewer and less extensive cracks) than shown in Figure 40a if the grain size of the zinc sulfide outer layer were smaller. The bimedia approach demonstrated sufficient promise that it should be investigated further.

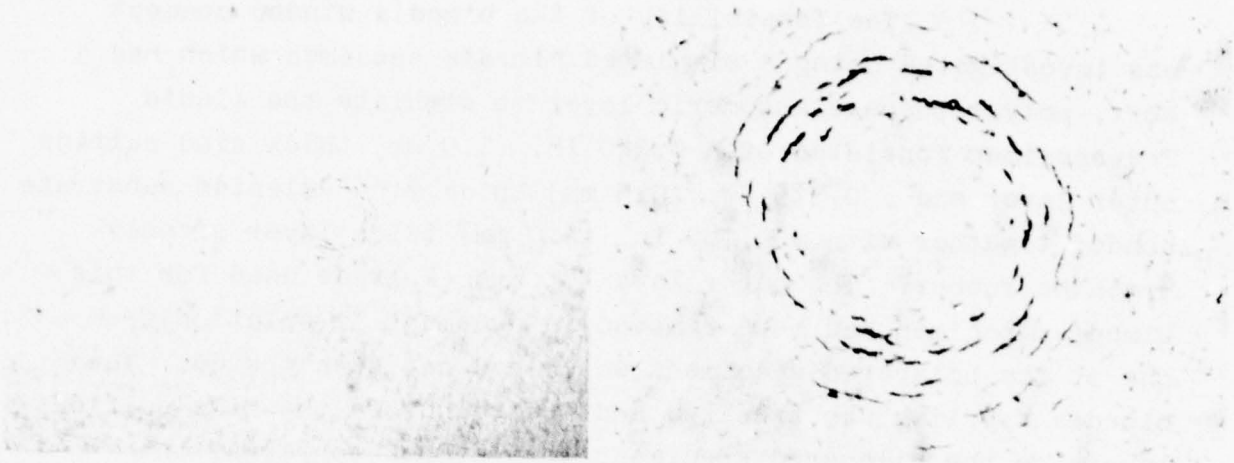

Mag. 30X

a. Simulated Bimedia Window Specimen

Mag. 135X

Mag. 30X

b. Homogeneous Zinc Sulfide

Mag. 135X

Figure 40. Comparison of Single Drop Impact Damage on Simulated Bimedia Window Specimen and Homogeneous Zinc Sulfide. 0.080 in. (2.0 mm) Diameter Drop Impacting at 730 fps (222 m/s). Transmitted Light.

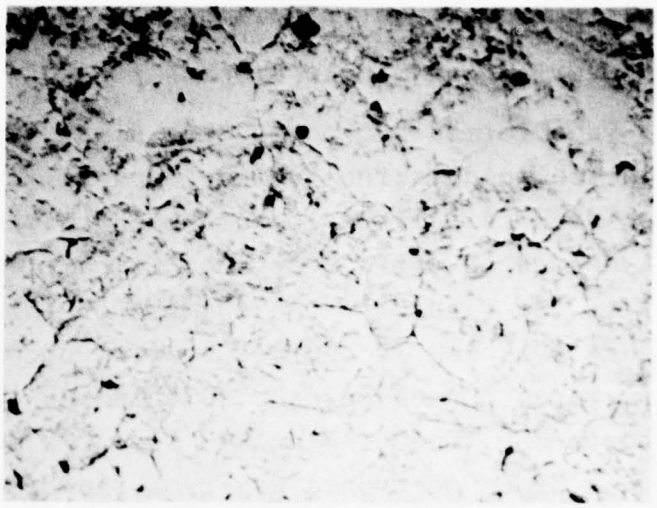

a. Zinc Sulfide Layer on Simulated Bimedia Window Specimen.

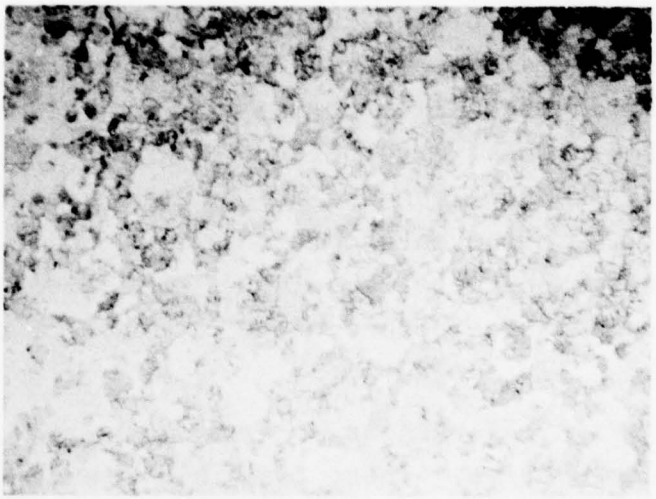

b. Homogenous Zinc Sulfide. Same Specimen as Figure 40 b.

Figure 41. Comparison of Grain Structure of Zinc Sulfide Layer on Simulated Bimedia Window Specimen and Homogeneous Zinc Sulfide Specimen. Mag. 470X.

C. Multiple Drop Impact Experiments

1. Overlapping Single Drops

Once formed by impact of a single drop, ring fractures on zinc selenide, zinc sulfide, and gallium arsenide were found to be surprisingly resistant to additional damage from the impact of a second or third drop whose ring fractured area overlapped that of the first.[1] An example of this resistance is shown in Figure 42 which is a cross section of overlapping doublet ring fractures formed on zinc selenide by two 0.100 in. (2.5 mm) diameter drops impacting at 730 fps (222 m/s). The specimen which was cross sectioned was from the prior work described in Reference 1. It is not known which impact occurred first; however, as can be seen, the cracks in the region of overlap are not appreciably deeper than those at the opposite sides.

As part of the current program, an experiment was performed to investigate in more detail the progress of damage to zinc selenide as additional 0.080 in. (2.0 mm) diameter drops impacted the same area at a velocity of 730 fps (222 m/s). For this experiment, the specimen was exposed for a sequence of long increments of time to the environment created by the single drop generator. Photographs were taken of several preselected areas after each increment of exposure. The progress of damage at one such area is shown in Figure 43.

Figure 43b shows an area where ring fractures from four drop impacts overlap. These fractures are numbered in the micrograph made with transmitted light. No ejection of material to form a surface pit had occurred where the four ring fractures overlap. Figure 43c shows the same area after a fifth drop had impacted the same location: still no ejection of material had occurred. As the number of exposures to the single drop environment increased, new impact sites could be seen to form in areas where previously there were none; however, it was impossible to

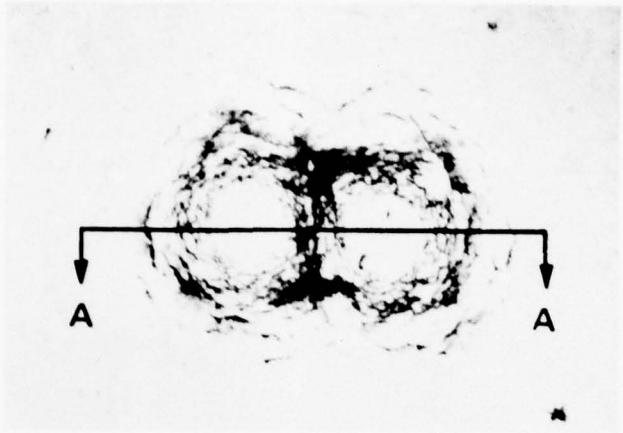

a. Plan View. Mag 30X

b. Section A-A. Mag 55X

Figure 42. Overlapping Doublet Ring Fractures on Zinc Selenide Formed by 0.100 in. (2.5 mm) Diameter Water Drops Impacting at 730 fps (222 m/s).

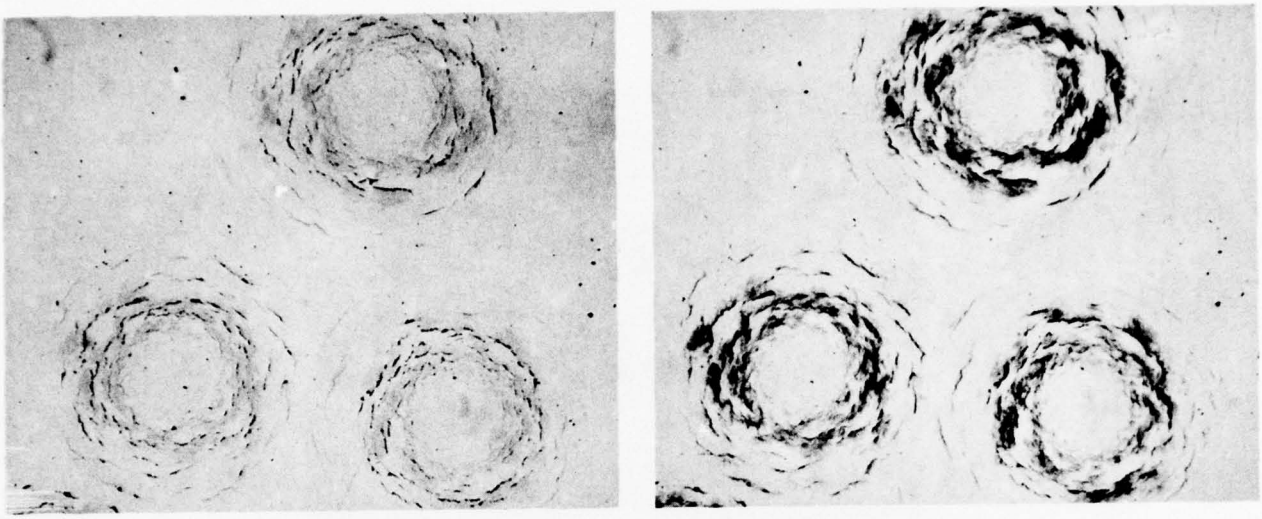

Reflected Light

Transmitted Light

a. 35 Min., Exposure

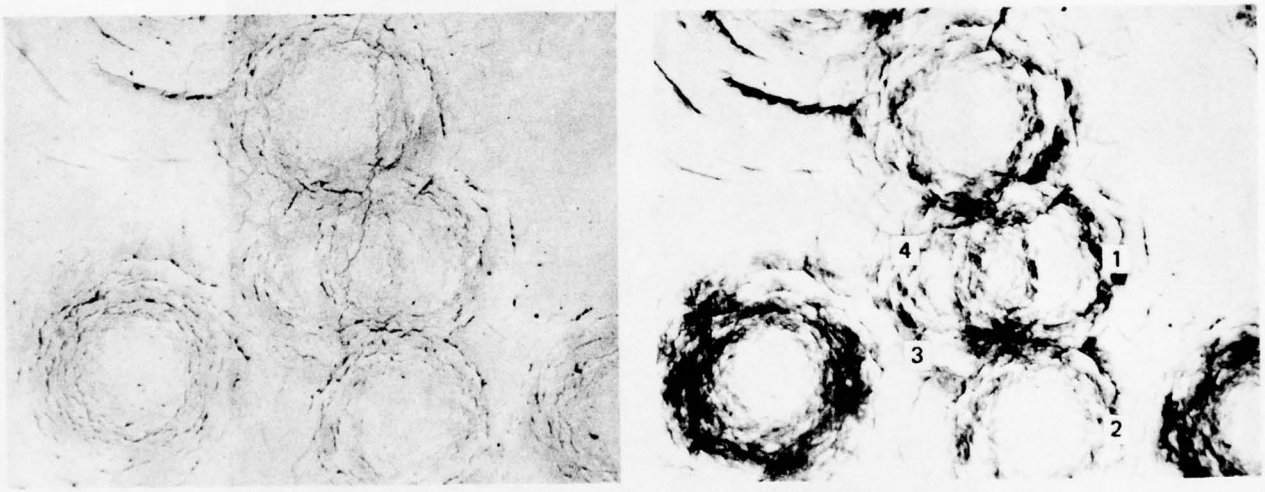

Reflected Light

Transmitted Light

b. 50 Min. Exposure.

Figure 43. Effect of Multiple Drop Impact on Area A of Zinc Selenide Specimen. 0.080 in. (2.0 mm) Diameter Drops Impacting at 730 fps (222 m/s). Mag. 30X. Continued.

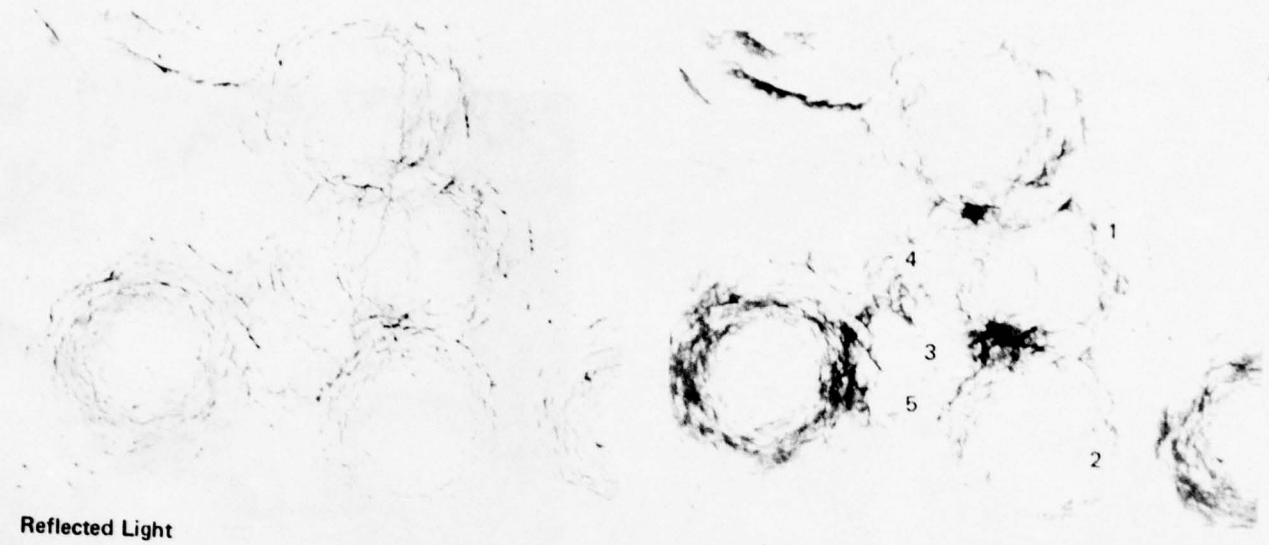

Reflected Light

Transmitted Light

c. 65 Min. Exposure

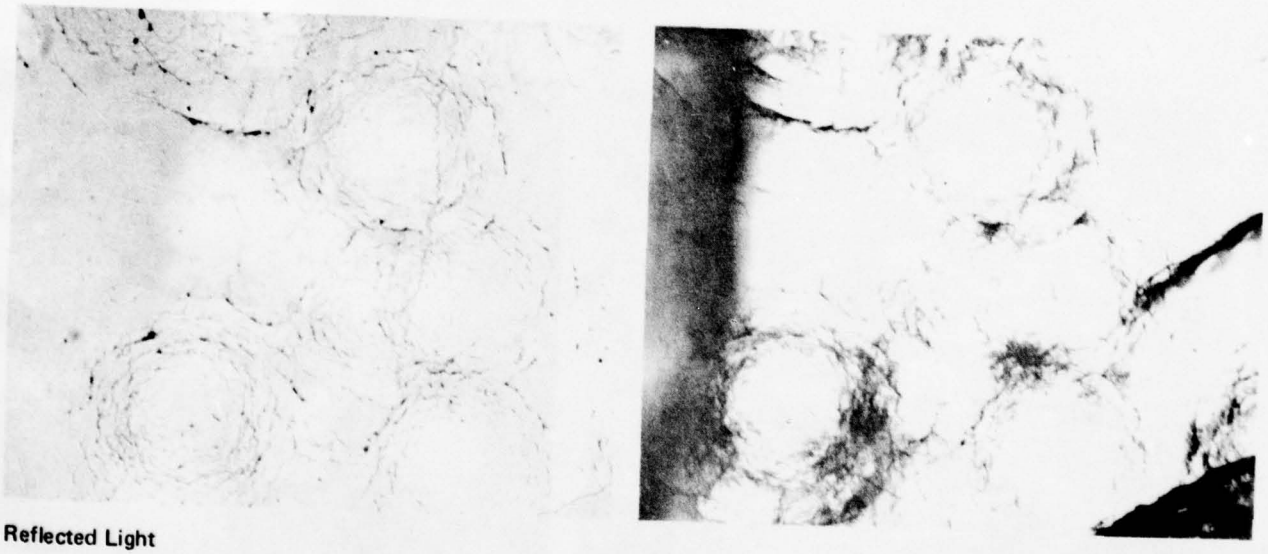

Reflected Light

Transmitted Light

d. 80 Min. Exposure

Figure 43. Continued.

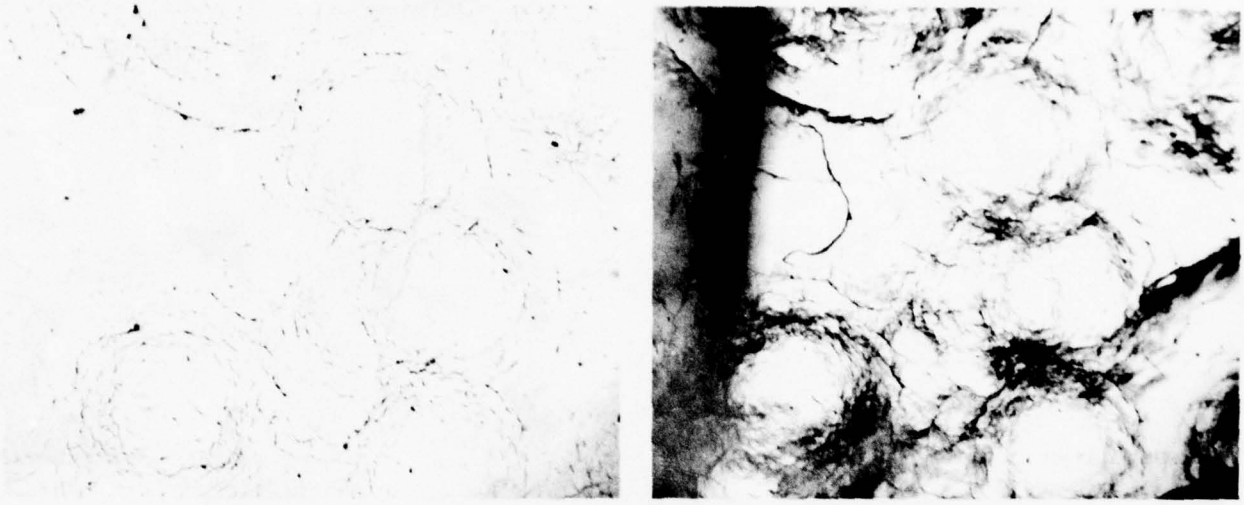

Reflected Light

Transmitted Light

e. 110 Min. Exposure

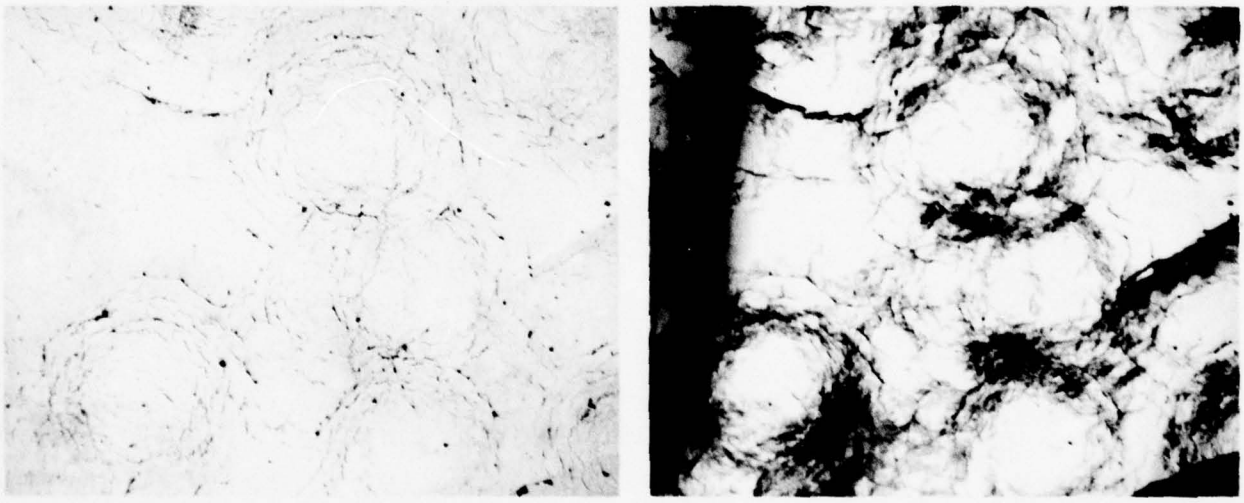

Reflected Light

Transmitted Light

f. 140 Min. Exposure

Figure 43. Continued.

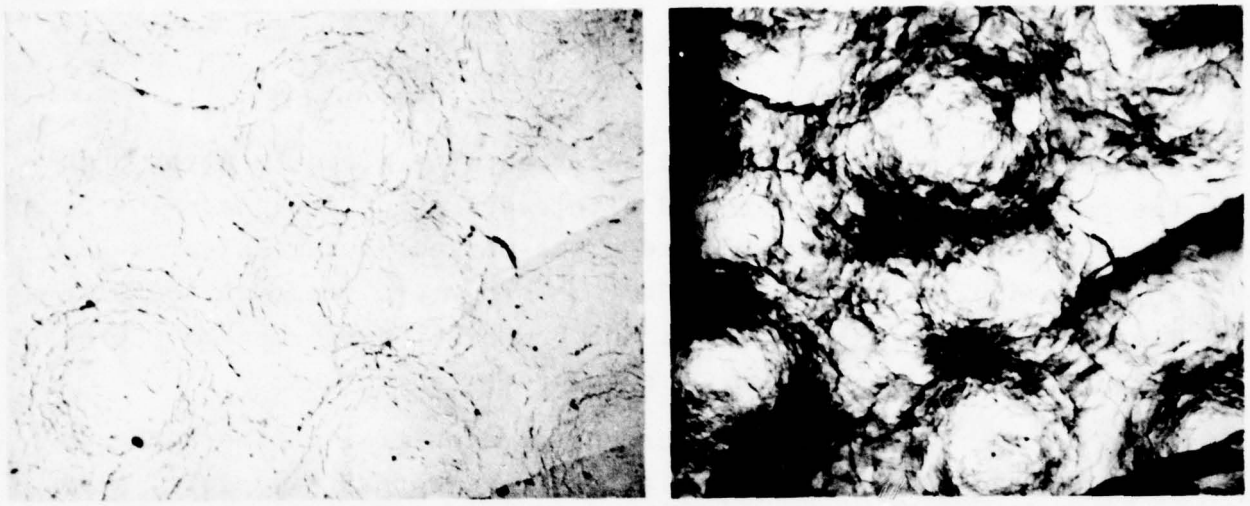

Reflected Light

Transmitted Light

g. 200 Min. Exposure

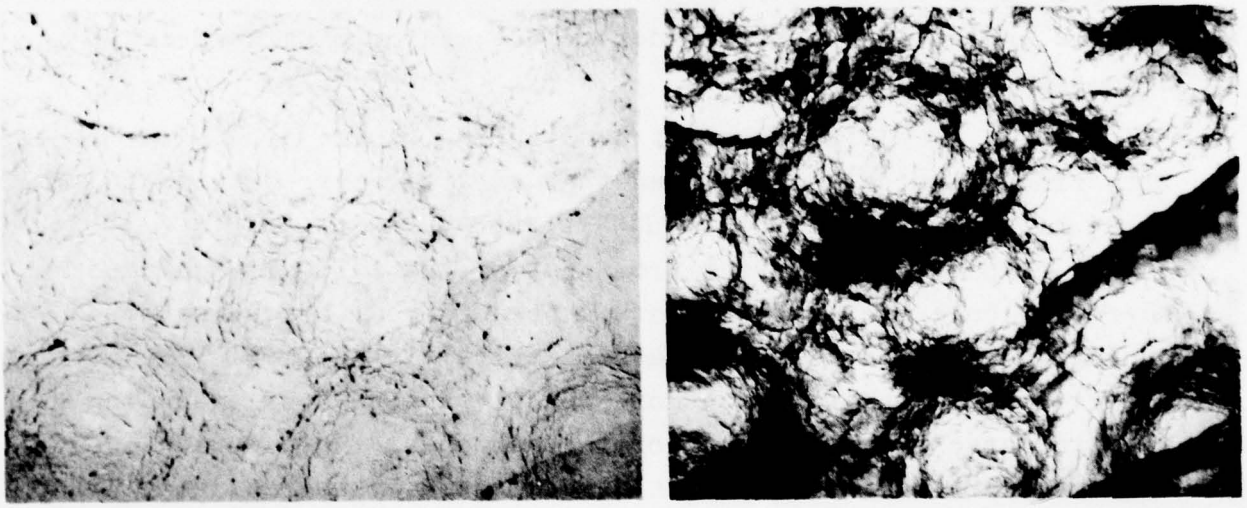

Reflected Light

Transmitted Light

h. 290 Min. Exposure

Figure 43. Concluded.

determine how many impacts had occurred at a given location once the entire area became covered with overlapping impacts. The ring fractures formed an approximate close-packed, hexagonal array which is apparent in Figure 43g. This pattern predominated with little change in appearance as the number of drop impacts increased during the final increment of exposure (Figure 43h).

Figure 44, microphotographs from another area on the specimen taken after the latter increments of exposure, also shows the formation of an approximate close-packed, hexagonal arrange of ring fractures. From an exposure of 140 minutes (Figure 44b) to an exposure of 290 minutes (Figure 44d), the only change in this pattern appears to be an increase in subsurface damage. This is evidenced by the general decrease in transmittance visible in the lower left corner of the microphotographs taken with transmitted light.

This series of overlapping single drop experiments with zinc selenide demonstrated that an area covered by an initial array of ring fractures responds to subsequent drop impact in a manner completely different from that of the initial undamaged surface. Once a crack pattern has been formed, stress wave propagation in the material becomes extremely complex. Then, impact energy appears to be more readily absorbed by extending existing cracks rather than forming new ones. This would account for the increase in subsurface damage shown by the sequence of microphotographs taken with transmitted light in Figures 44b, c, and d. The microphotographs taken with reflected light show only the intersection of the ring fractures with the specimen surface. It is difficult to detect any increase in the surface damage of the area shown in the lower left corner of the reflected light microphotographs in the sequence of Figures 44b, c, and d.

AD-A070 004 BELL AEROSPACE TEXTRON BUFFALO N Y F/G 17/5
BEHAVIOR OF INFRARED WINDOW MATERIALS EXPOSED TO RAIN DROP ENVI--ETC(U)
SEP 78 J V HACKWORTH, L H KOCHER F33615-77-C-5069
UNCLASSIFIED AFML-TR-78-184 NL

2 OF 2
AD A070004

END
DATE FILMED
7-79
DDC

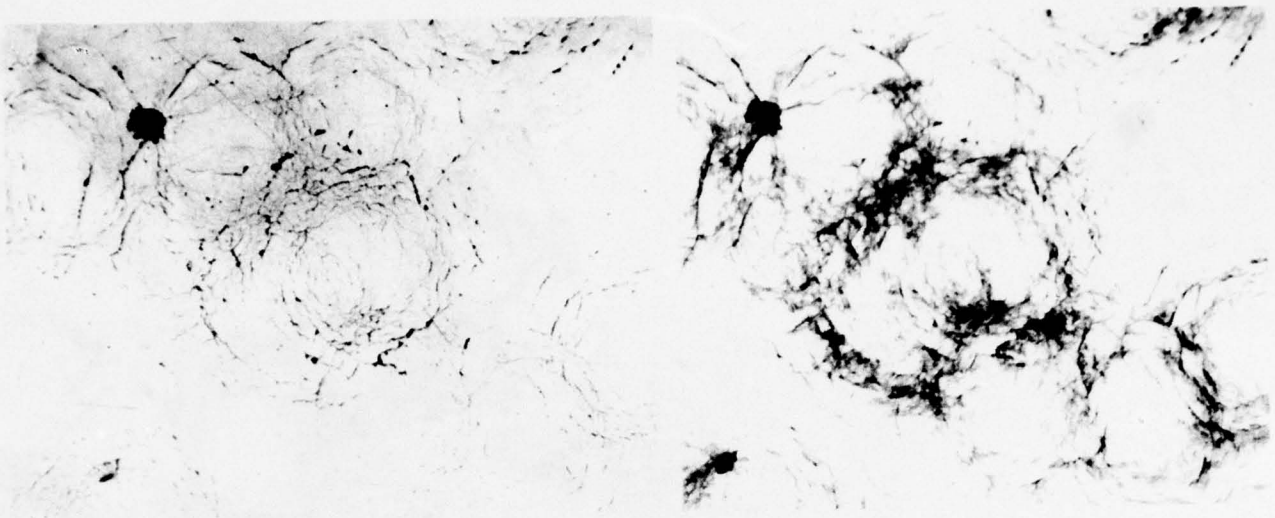

Reflected Light

Transmitted Light

a. 80 Min. Exposure

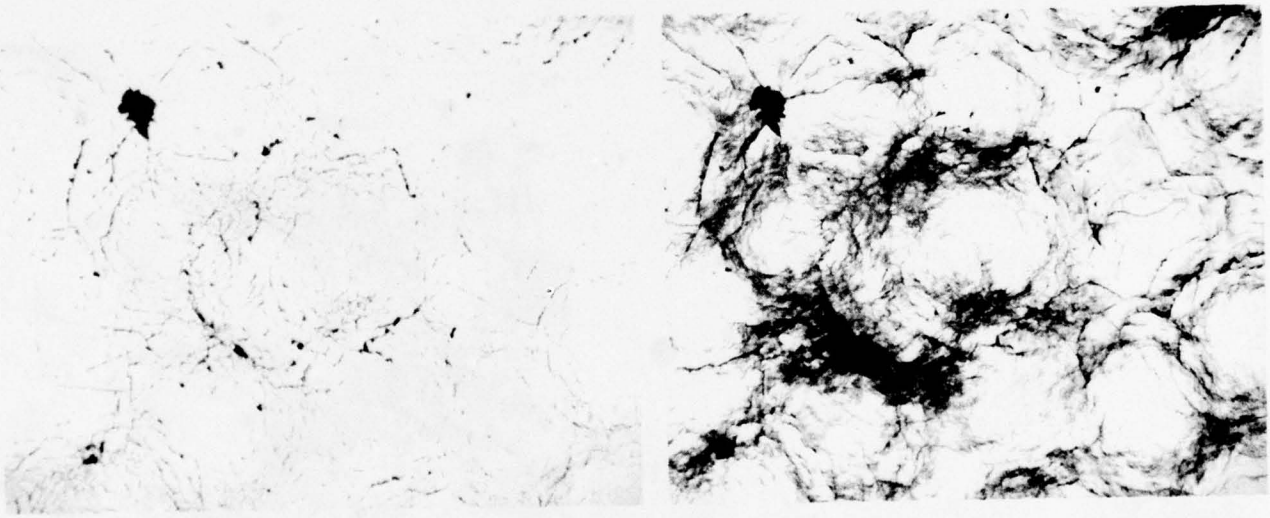

Reflected Light

Transmitted Light

b. 140 Min. Exposure

Figure 44. Effect of Multiple Drop Impacts on Area B of Zinc Selenide Specimen. 0.080 in. (2.0 mm) Diameter Drops Impacting at 730 fps (222 m/s). Mag. 30X. Continued.

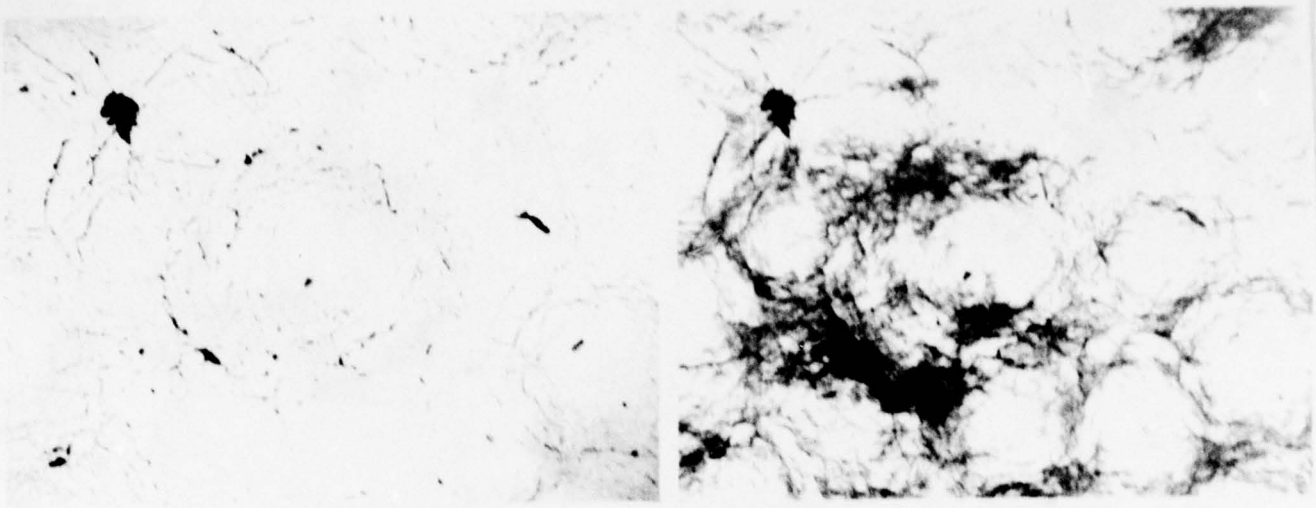

Reflected Light

Transmitted Light

c. 200 Min. Exposure

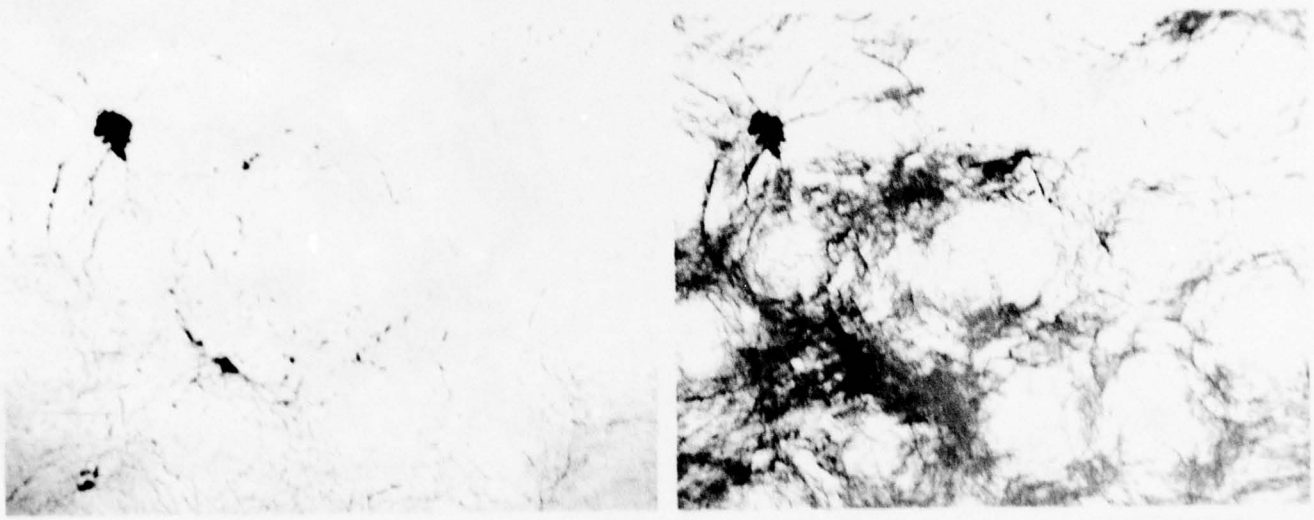

Reflected Light

Transmitted Light

d. 290 Min. Exposure

Figure 44. Concluded.

2. Small Drop Rainfield

a. Calibration

Plumbing was installed to produce a small drop rainfield in the AFML/Bell erosion facility. Up to this time, the rainfield in the facility had a mean drop diameter of 0.070 in. (1.8 mm) and a rainfall rate of 1.0 in/hr (2.5 cm/hr). This rainfield, hereafter referred to as the standard rainfield, is produced by four nozzles mounted in the center of the chamber so as to spray up and out in a radial direction toward the wall of the chamber. The small drop rainfield, on the other hand, is produced by eight nozzles equally spaced around a circular manifold which is attached to the wall of the chamber. Each nozzle has a solenoid on-off valve. Simultaneous actuation of these valves permits the rapid build-up and termination of the rainfield that is required to follow the progress of erosion during a sequence of short exposure times.

The small drop rainfield was calibrated for drop size by measuring the diameters of drops captured in petri dishes distributed throughout the rainfield in the path of specimen rotation. These dishes contained two layers of oil: the bottom layer had a specific gravity greater than 1.0 and the top layer had a specific gravity less than 1.0. Water drops trapped between these two layers retained their spherical shape and the diameters could be readily measured. The distribution of drop size produced by this rainfield is shown in Figure 45. The drop diameters had an almost normal distribution with a mean diameter of 0.030 in. (0.75 mm). The rainfall rate at the flow settings used to produce this drop size was 0.4 in/hr (1.0 cm/hr).

b. Erosion of Zinc Selenide and Zinc Sulfide

Specimens of zinc selenide and zinc sulfide were exposed to the small-drop rainfield for several increments of time at 730 fps (222 m/s) to characterize the progress of damage. Cumulative exposure times for the zinc selenide specimen

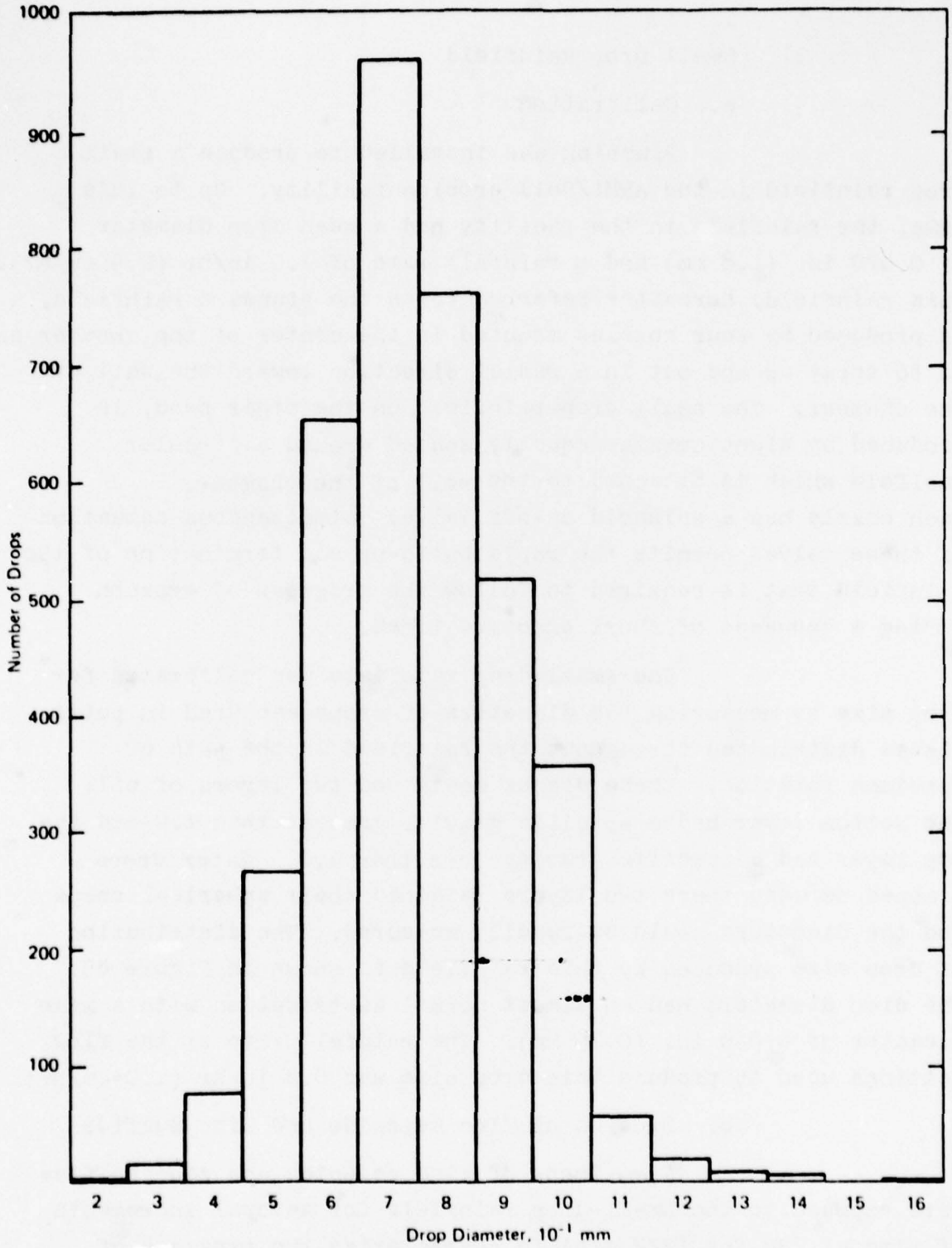

Figure 45. Drop Size Distribution of Small Drop Rainfield at Rainfall Rate of 0.4 in./hr (1.0 cm/hr)

were 25, 60, 120, 150, and 180 seconds. Cumulative exposure times for the more erosion resistant zinc sulfide were 6, 12, 15, and 18 minutes. Before the tests, and after each increment of exposure, transmittance of the specimens was measured over the wavelength range of 0.5 to 2.1 μm with a Cary Model 14 spectrophotometer and over the wavelength range of 2.5 to 20 μm with a Perkin-Elmer Model 621 spectrophotometer. Photomicrographs were also obtained after each increment of exposure. The tests were terminated when the transmittance at the longer wavelengths dropped to below 50 percent.

The effects of rain erosion on transmittance between 0.5 and 2.1 μm for the two materials are shown by the curves in Figures 46 and 47. Loss of transmittance at the shorter wavelengths, e.g., 2.0 μm, appears to start off at one rate and then change to a greater rate as cumulative exposure time increases. Of course, the rates are different for the two materials, but both show the same trend. The change in slope is particularly apparent for zinc selenide (Figure 46) between cumulative exposure times of 60 and 120 seconds. Unfortunately, a cumulation exposure time of 90 seconds was eliminated because the transmittance had not decreased very much after the first two increments of exposure. A similar change in slope is apparent for zinc sulfide (Figure 47) between cumulative exposure times of 6 and 12 minutes.

The effects of rain erosion on transmittance between 2.5 and 20 μm for the two materials are shown by the curves in Figures 48 and 49. Examination of the curves in Figure 48 discloses that zinc selenide lost transmittance at a slower rate at wavelengths between 10 and 15 μm than at wavelengths between 2.5 and 9 μm. A distinct hump in the transmittance curve had developed between 10 and 15 μm after a cumulative exposure of 120 seconds. Zinc sulfide (Figure 49) did not exhibit this phenomenon. There is also evidence of an incubation period

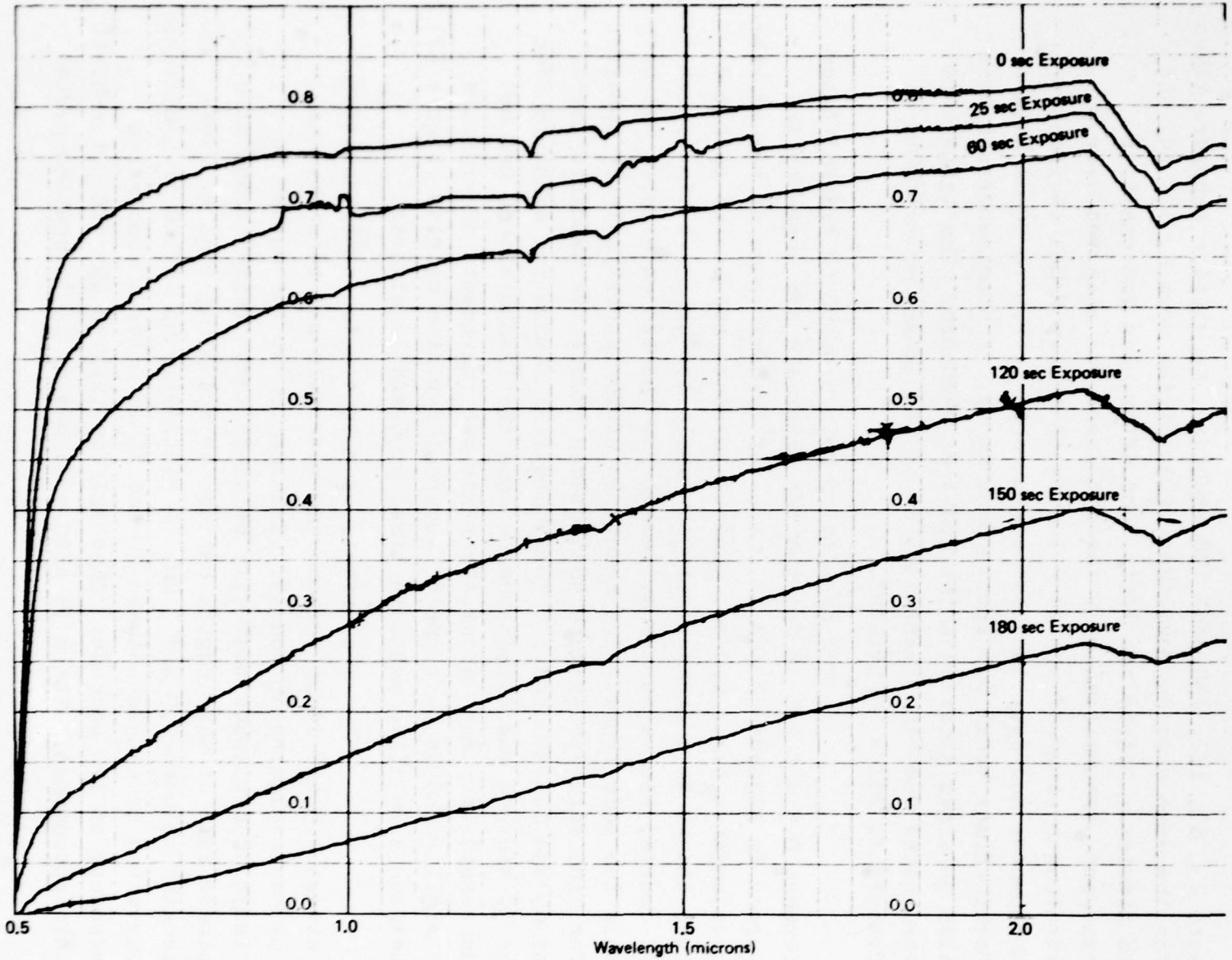

Figure 46. Effects of Exposure Time at 730 fps (222 m/s) in Small Drop Rainfield on Spectral Transmittance of Zinc Selenide between 0.5 and 2.1 Microns.

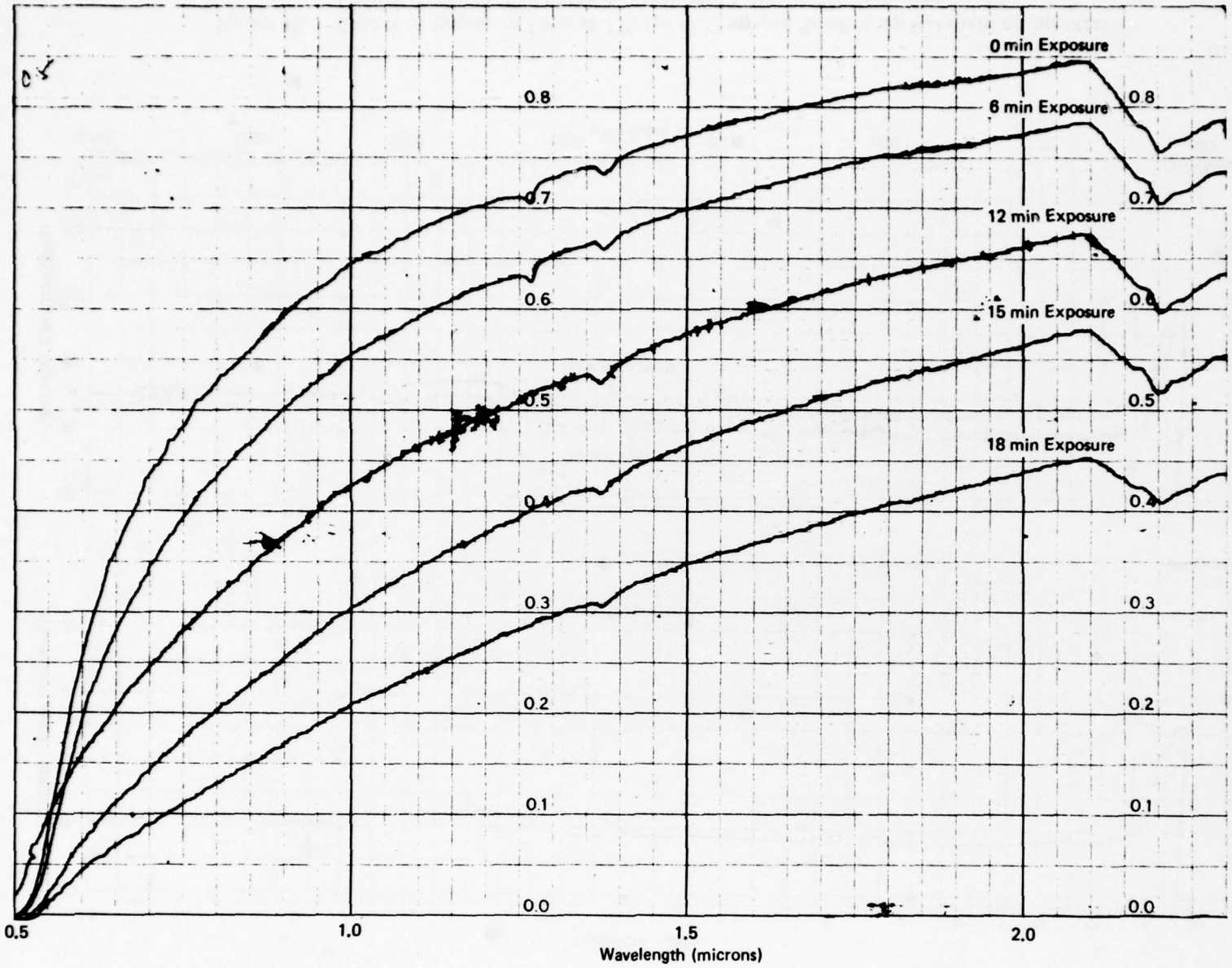

Figure 47. Effects of Exposure Time at 730 fps (222 m/s) in Small Drop Rainfield on Spectral Transmittance of Zine Sulfide between 0.5 and 2.1 Microns.

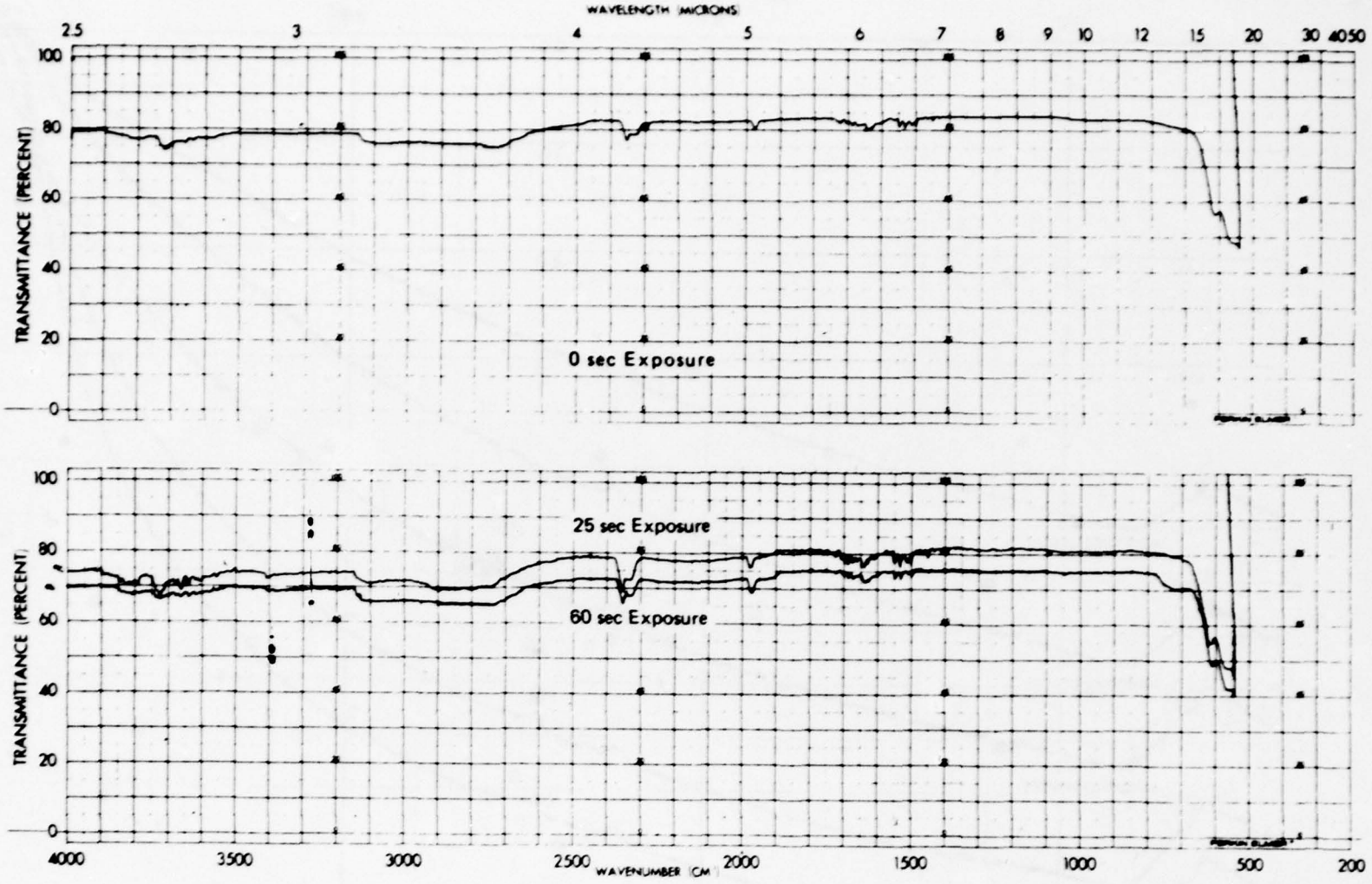

Figure 48. Effects of Exposure Time at 730 fps (222 m/s) in Small Drop Rainfield on Spectral Transmittance of Zinc Selenide between 2.5 and 25 Microns. Continued.

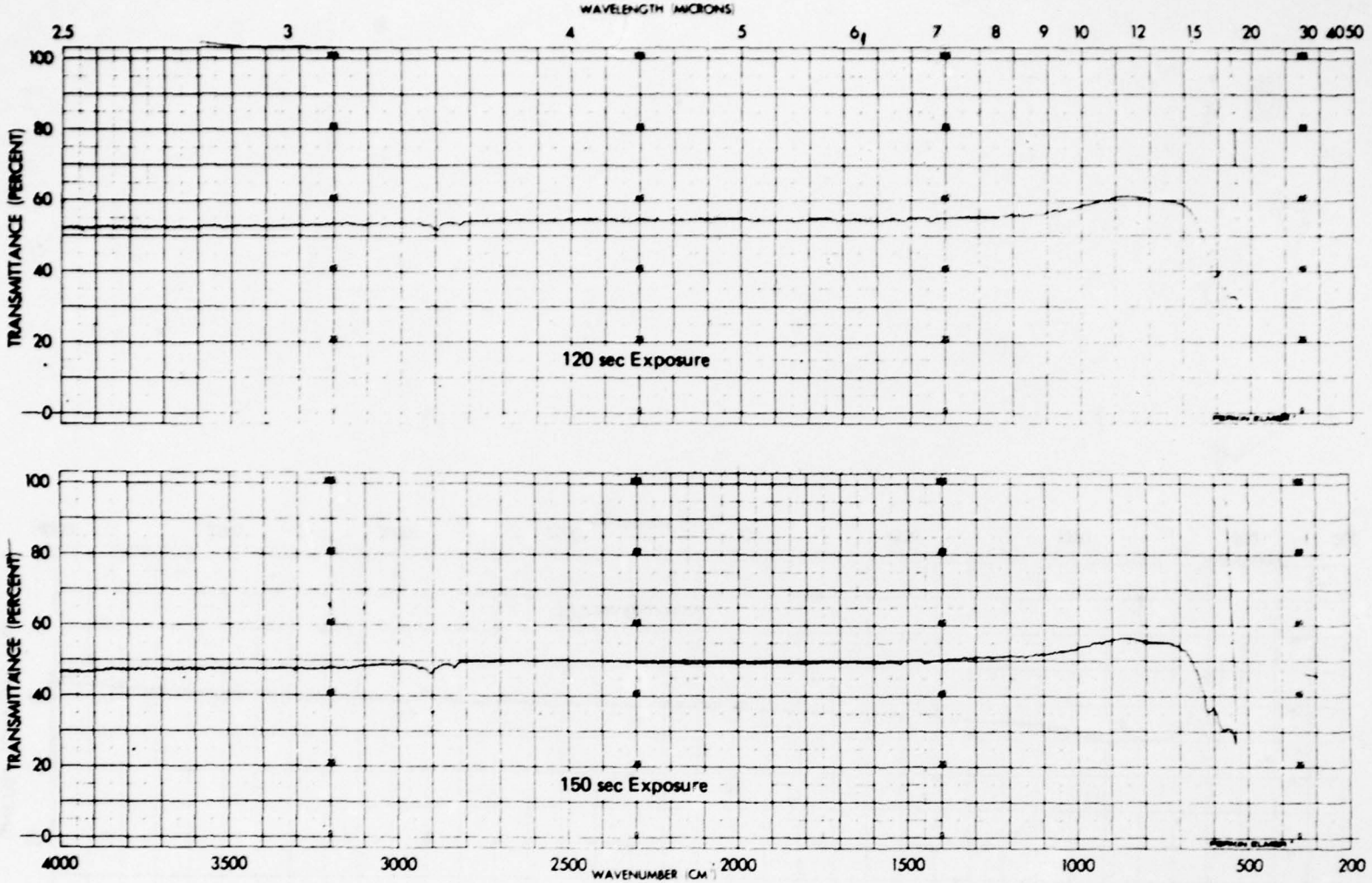

Figure 48. Continued

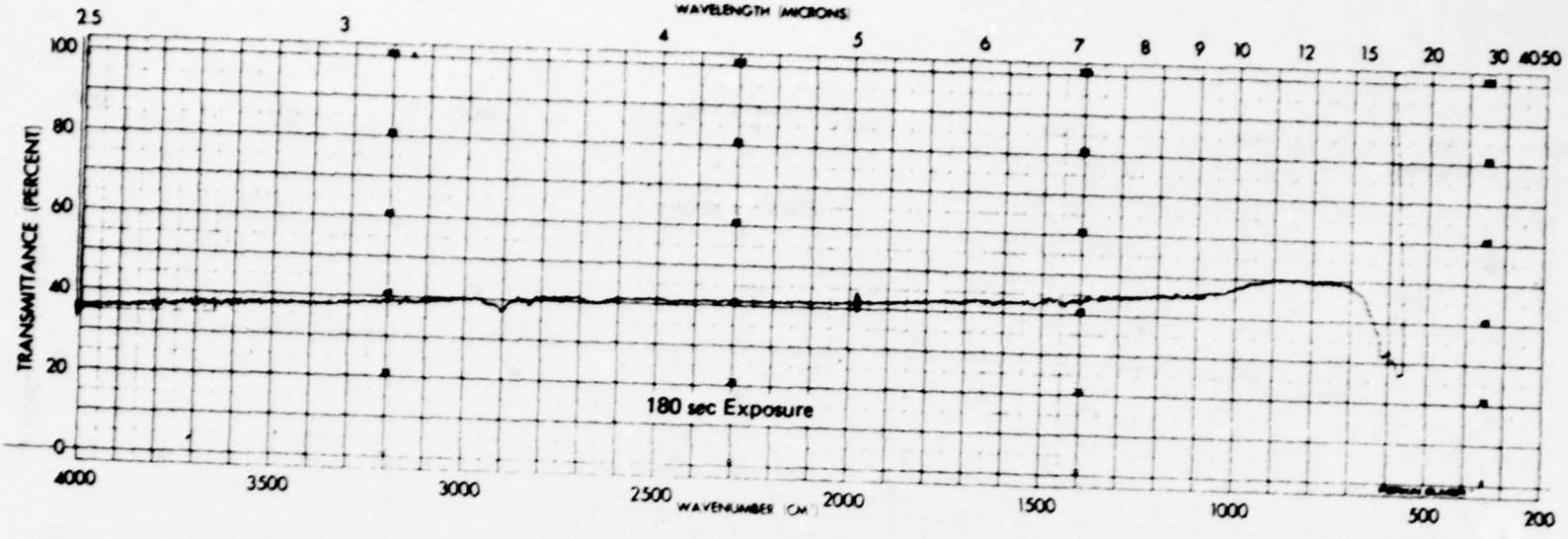

Figure 48. Concluded

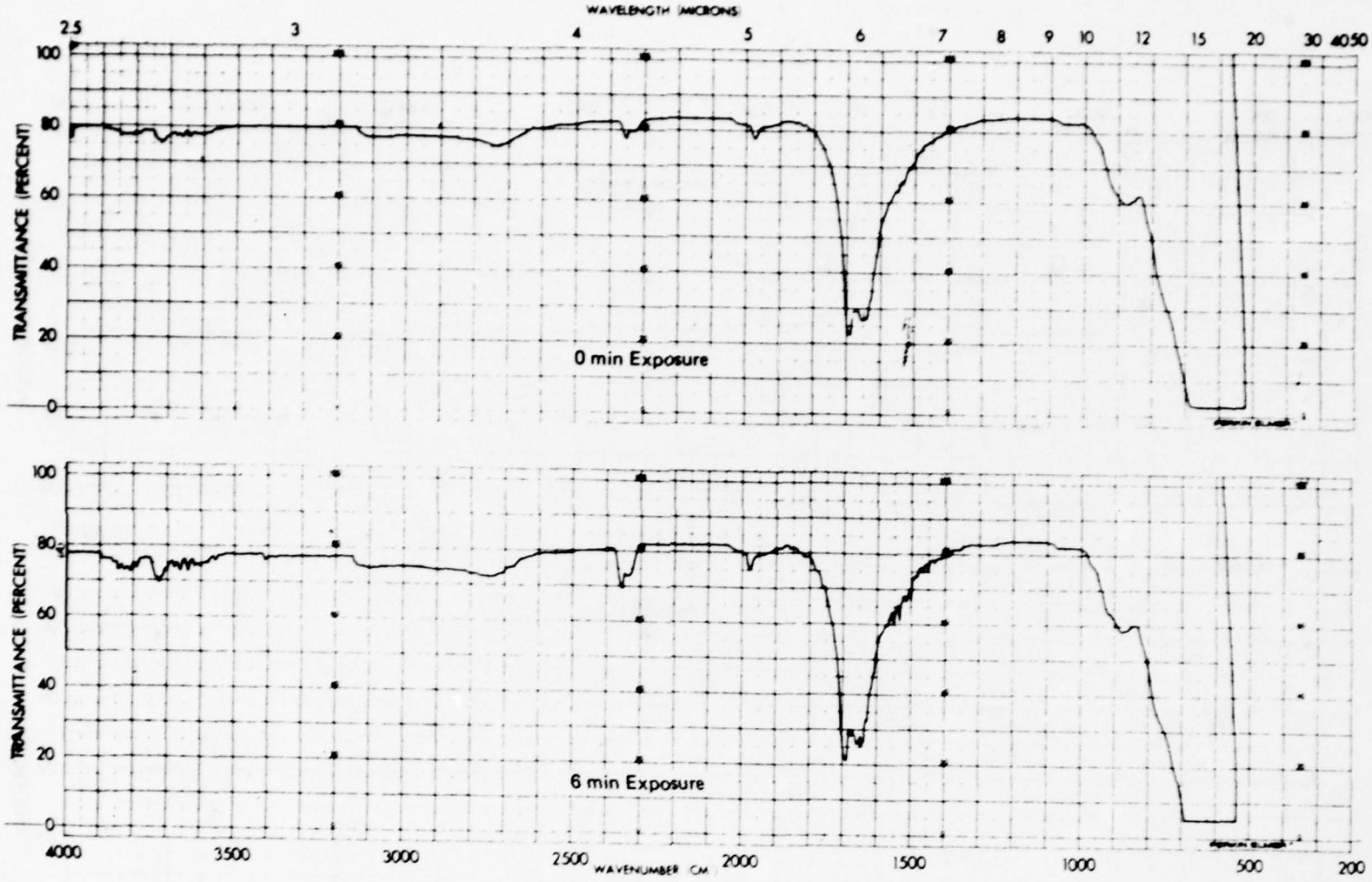

Figure 49. Effects of Exposure Time at 730 fps (222 m/s) in Small Drop Rainfield on Spectral Transmittance of Zinc Sulfide between 2.5 and 25 Microns. Continued.

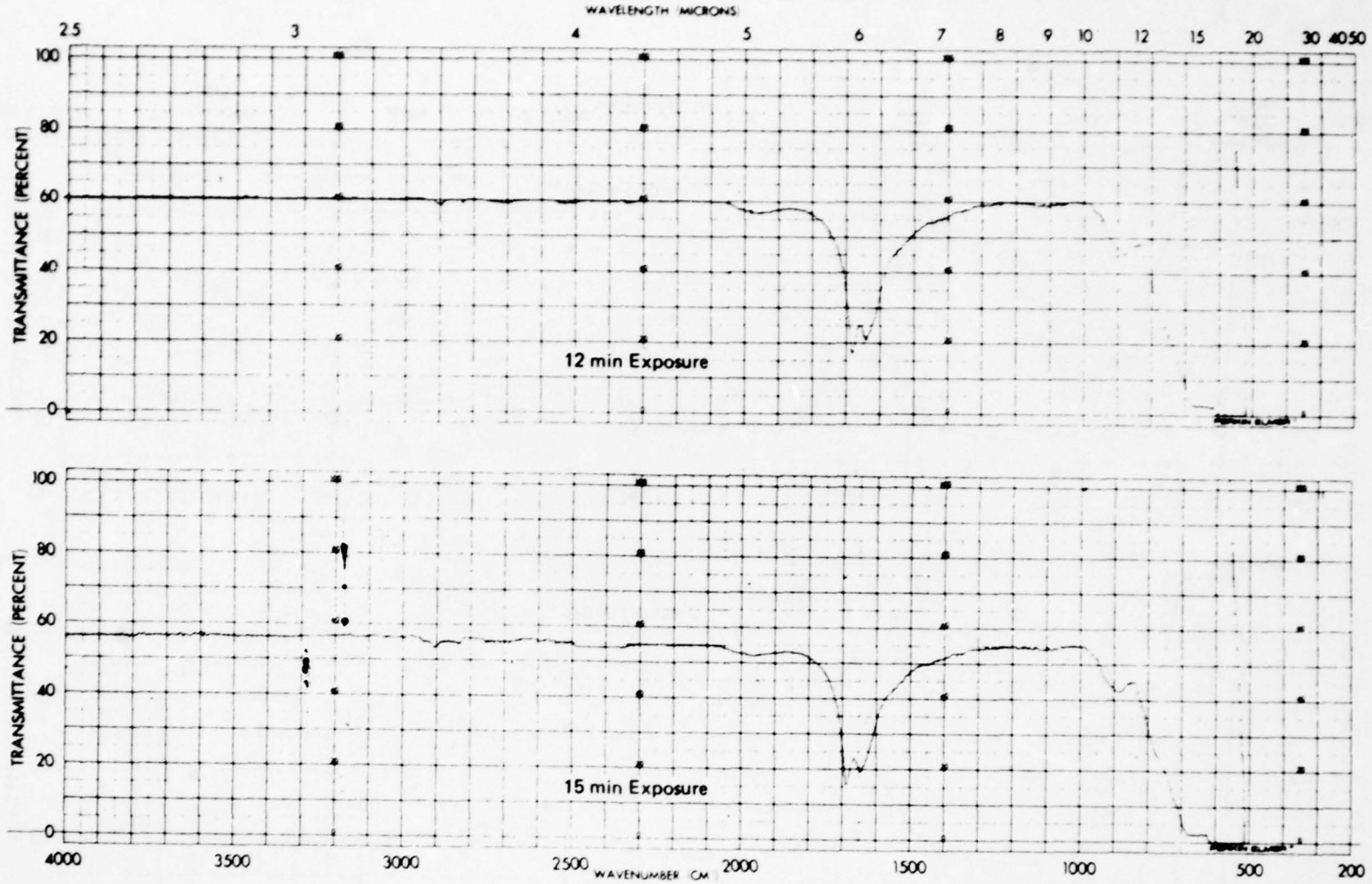

Figure 49. Continued

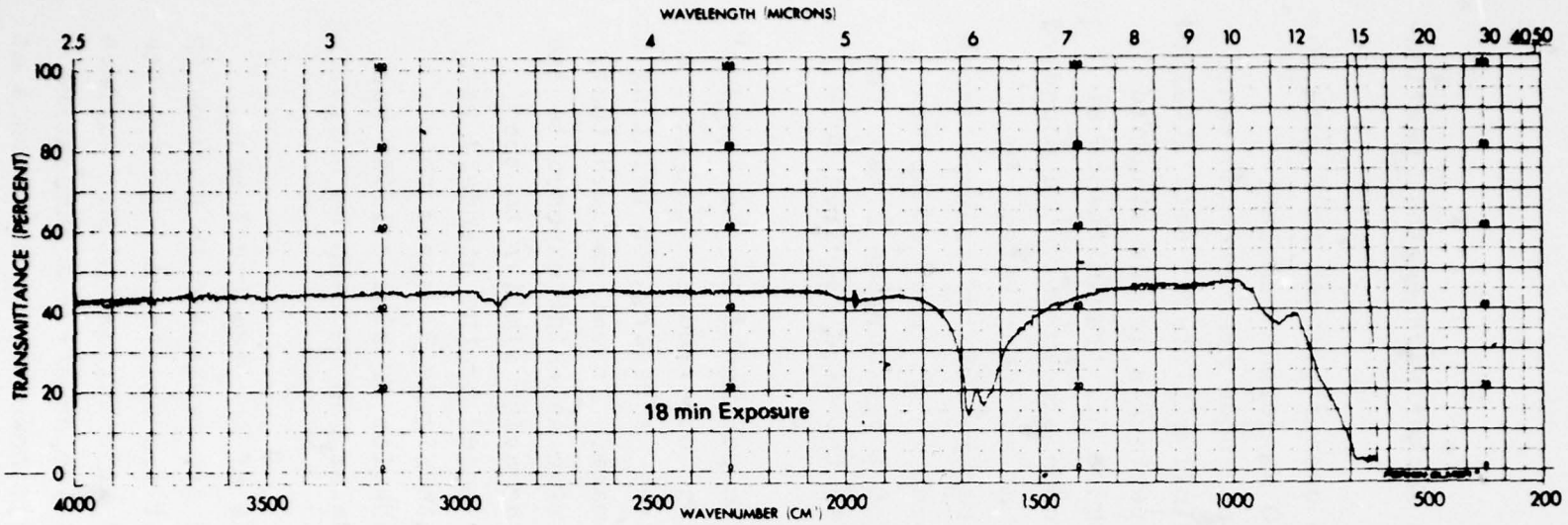

Figure 49. Concluded

before loss of transmittance at the longer wavelengths, particularly for zinc sulfide.

The curves have been replotted in Figure 50 to show transmittance at 2 μm and 10 μm versus cumulative exposure time so the trends discussed above are more apparent. Figure 51 presents for comparison similar plots of data obtained for zinc sulfide during previous experiments in the standard rainfield.[1] As can be seen in Figure 51, transmittance at 2 μm began to decrease immediately upon exposure to the standard rainfield and continued to decrease at a linear rate. An extended incubation period existed before loss of transmittance began at 10 μm. Transmittance loss at 10 μm appeared to be caused by the formation and growth of large surface pits: the incubation period was associated with the time required to nucleate these pits.[1]

In the previous experiments in the standard rainfield, damage to zinc selenide had occurred at too great a rate to obtain the number of exposures necessary for relating loss of transmittance to erosion damage. It was assumed that, except for a different time scale, zinc selenide exposed to the small drop rainfield would exhibit behavior similar to that found previously for zinc sulfide exposed to the standard rainfield. Comparison of Figure 50a with Figure 51 shows this obviously was not the case. The behavior of zinc sulfide was even different in the two rainfields as can be seen by comparing Figure 50b with Figure 51.

Photomicrographs of the two specimens exposed to the small drop rainfield are presented in Figures 52 and 53. These micrographs show that transmittance loss for the long wavelengths was not associated with surface pits. Surface pits were not significant on zinc selenide after a cumulative exposure of 120 seconds (Figure 52c); however, transmittance at

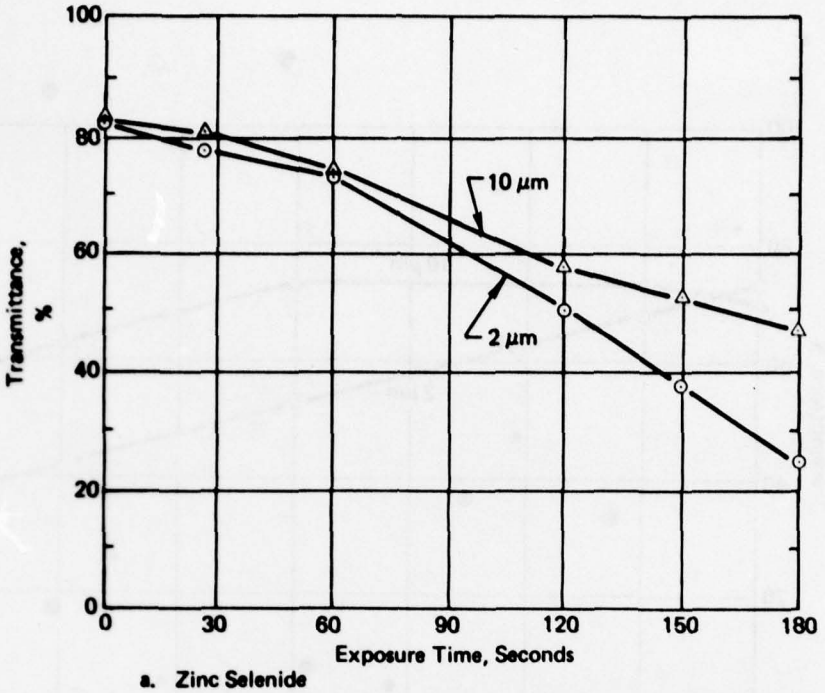

a. Zinc Selenide

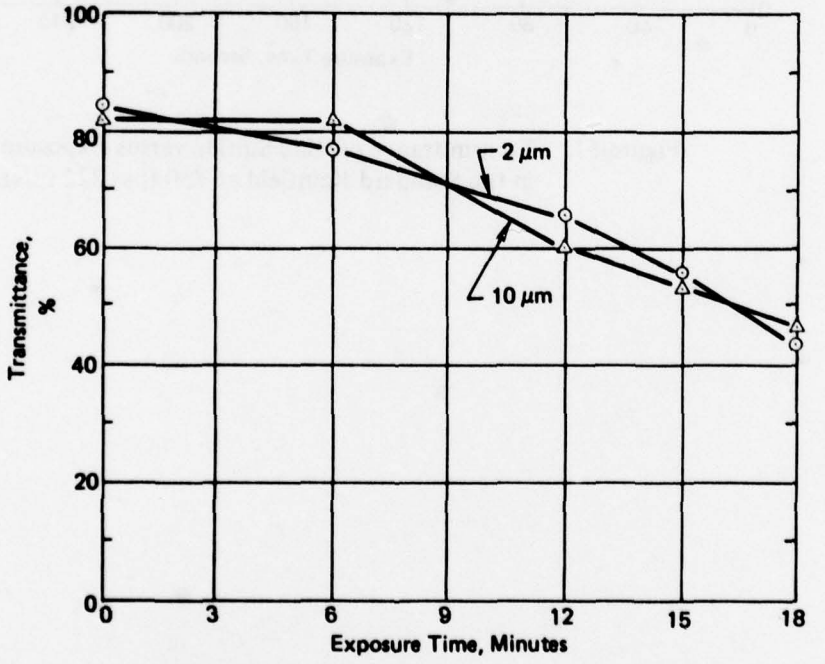

b. Zinc Sulfide

Figure 50. Transmittance of Zinc Selenide and Zinc Sulfide Vs Exposure Time in the Small Drop Rainfield at 730 fps (222 m/s).

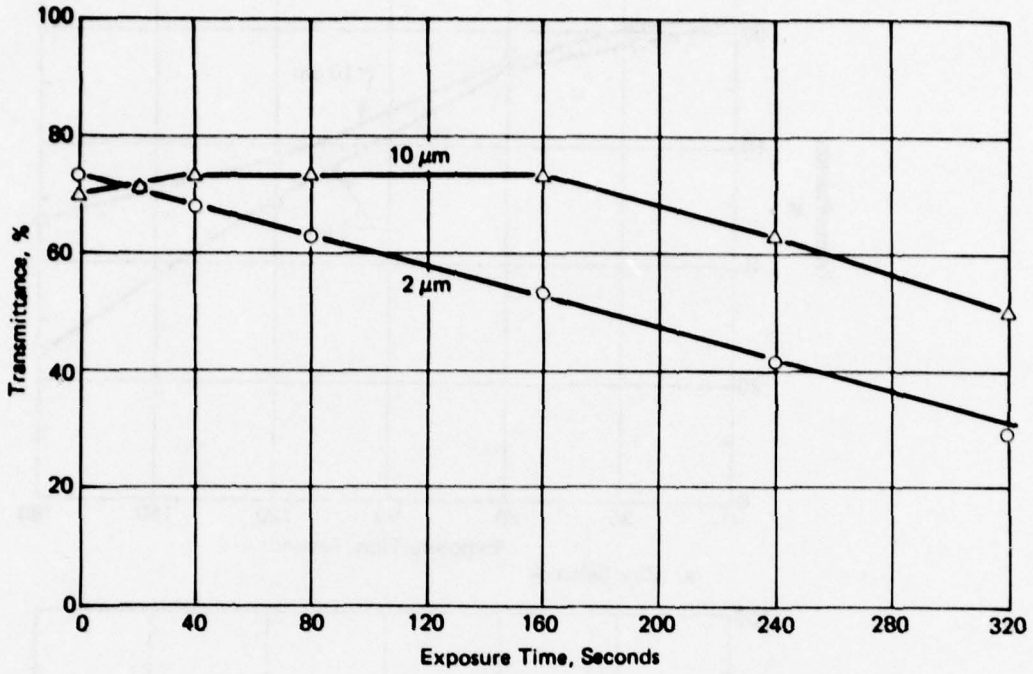

Figure 51. Transmittance of Zinc Sulfide versus Exposure Time in the Standard Rainfield at 730 fps (222 m/s).

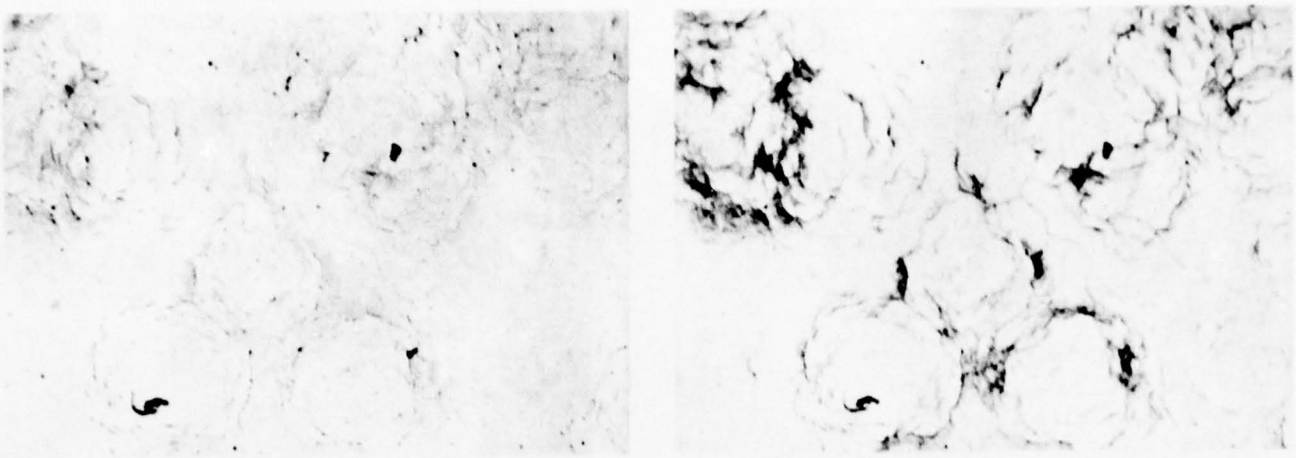

Reflected Light

Transmitted Light

a. 25 Seconds Exposure

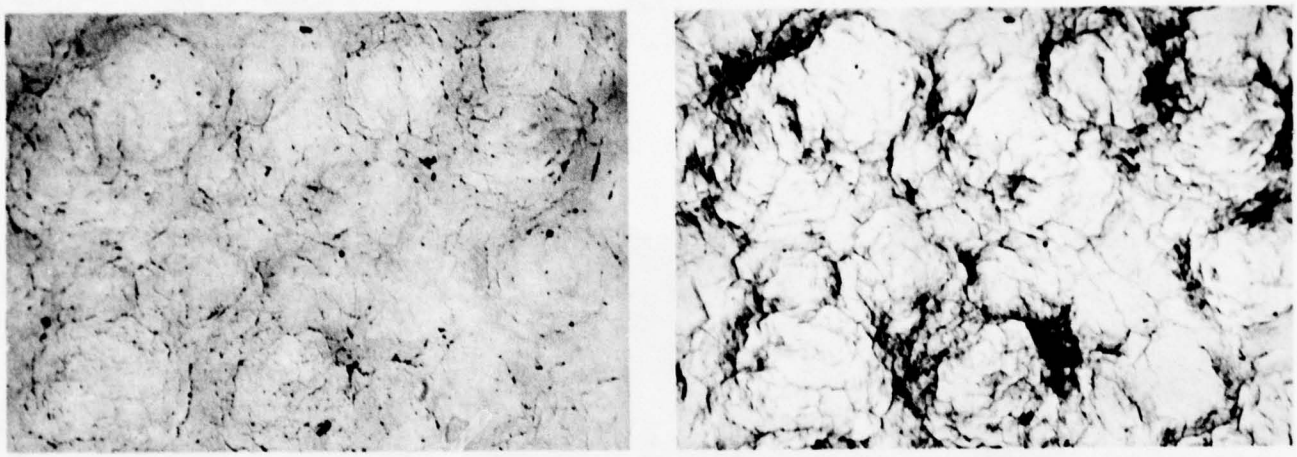

Reflected Light

Transmitted Light

b. 60 Seconds Exposure

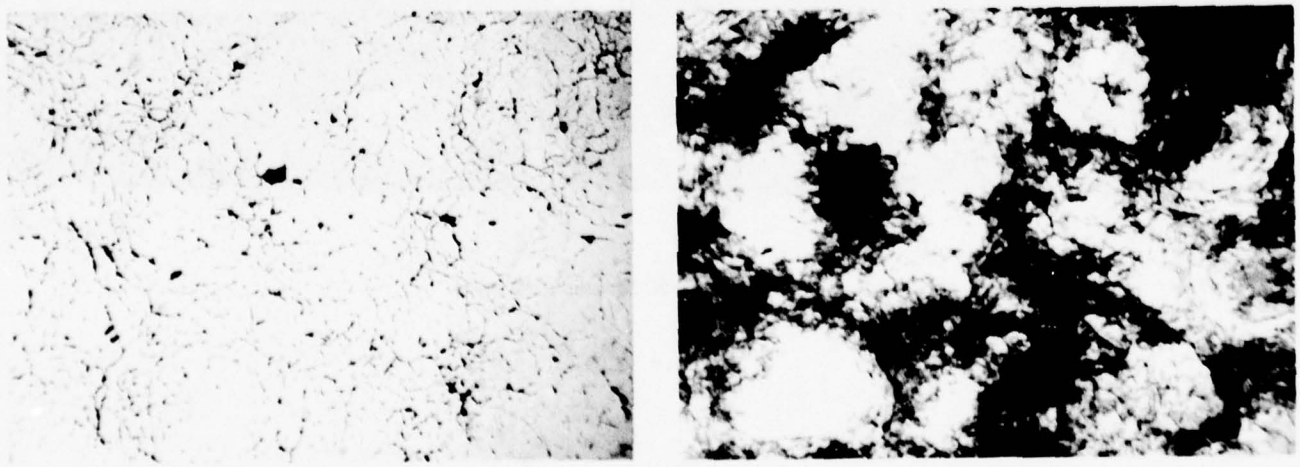

Reflected Light

Transmitted light

c. 120 Seconds Exposure

Figure 52. Progress of Erosion Damage on Zinc Selenide Exposed at 730 fps (222 m/s) to Small Drop Rainfield. Mag. 30X. Continued.

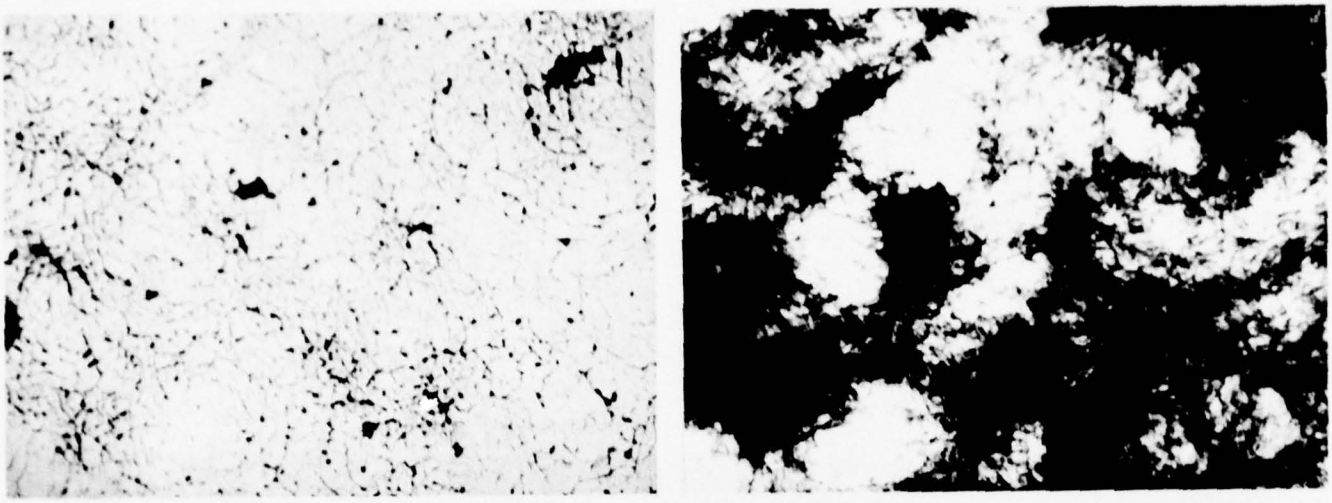

Reflected Light

Transmitted Light

d. 150 Seconds Exposure

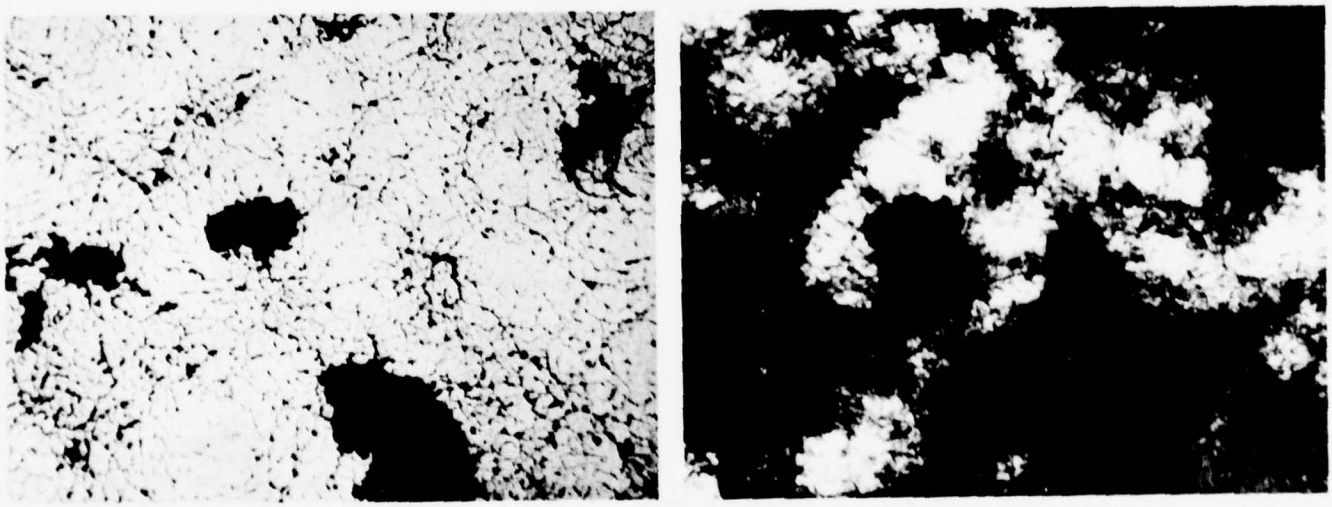

Reflected Light

Transmitted Light

e. 180 Seconds Exposure

Figure 52. Concluded.

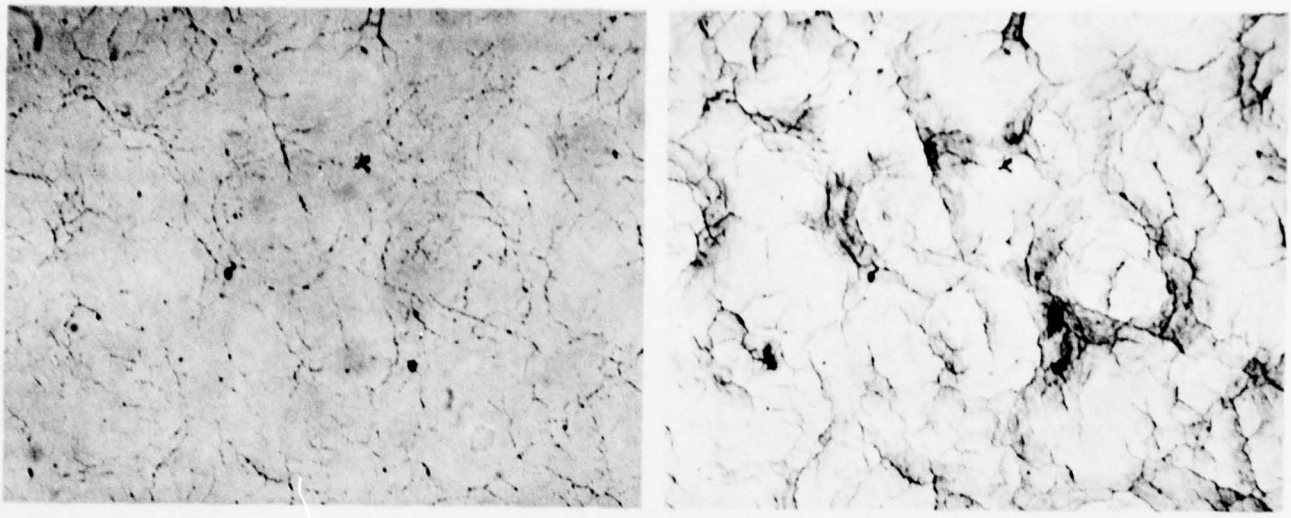

Reflected Light

Transmitted Light

a. 6 Min. Exposure

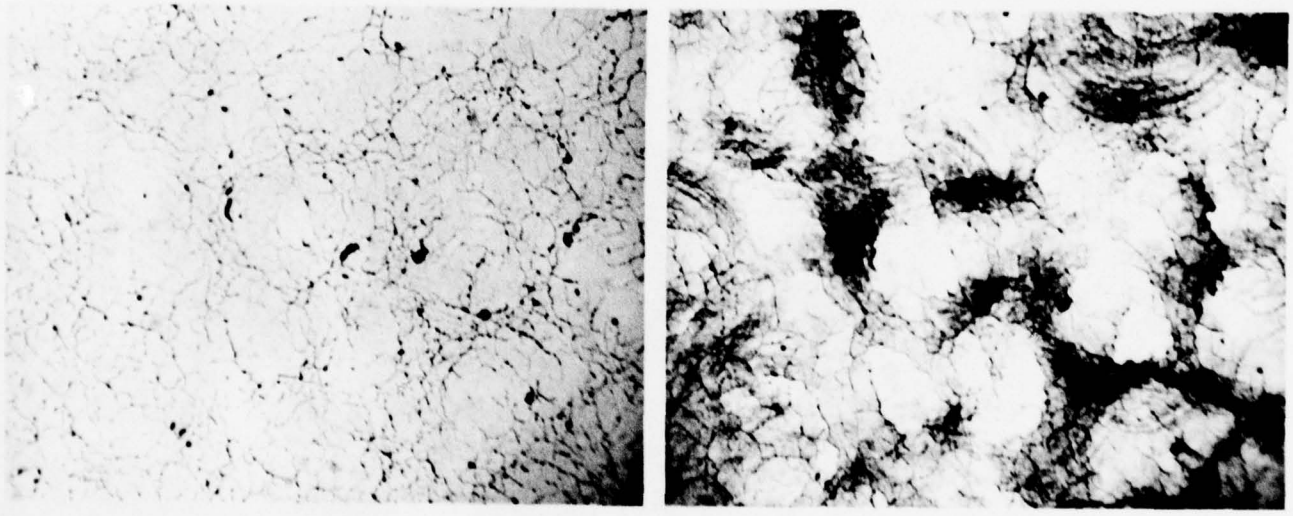

Reflected Light

Transmitted Light

b. 12 Min. Exposure.

Figure 53. Progress of Erosion Damage on Zinc Sulfide Exposed at 730 fps (222 m/s) to Small Drop Rainfield. Mag. 30X. Continued.

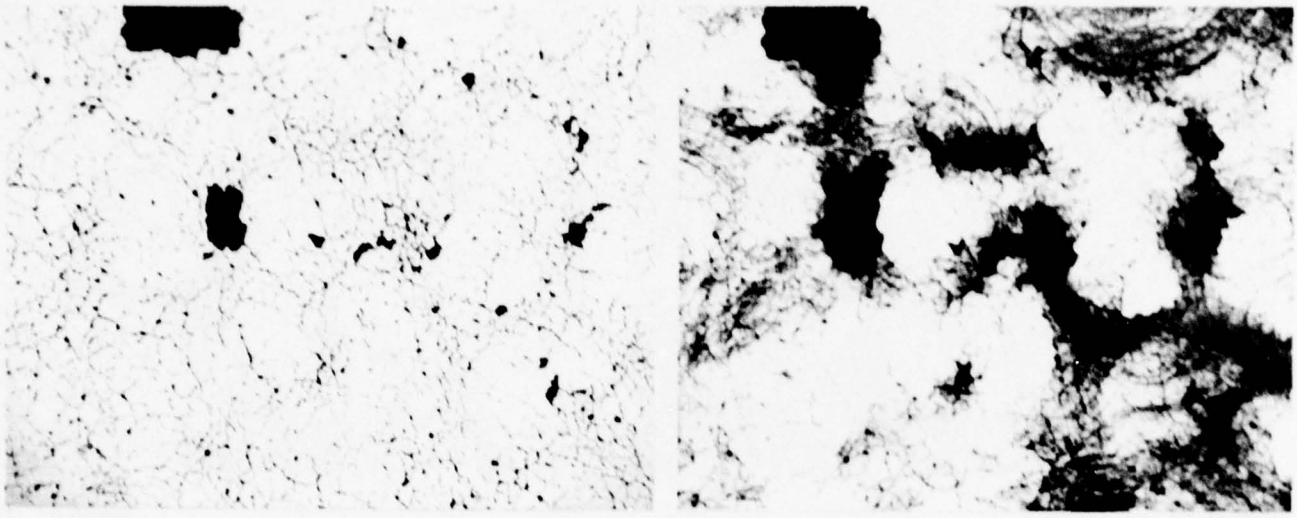

Reflected Light

Transmitted Light

c. 15 Minutes Exposure

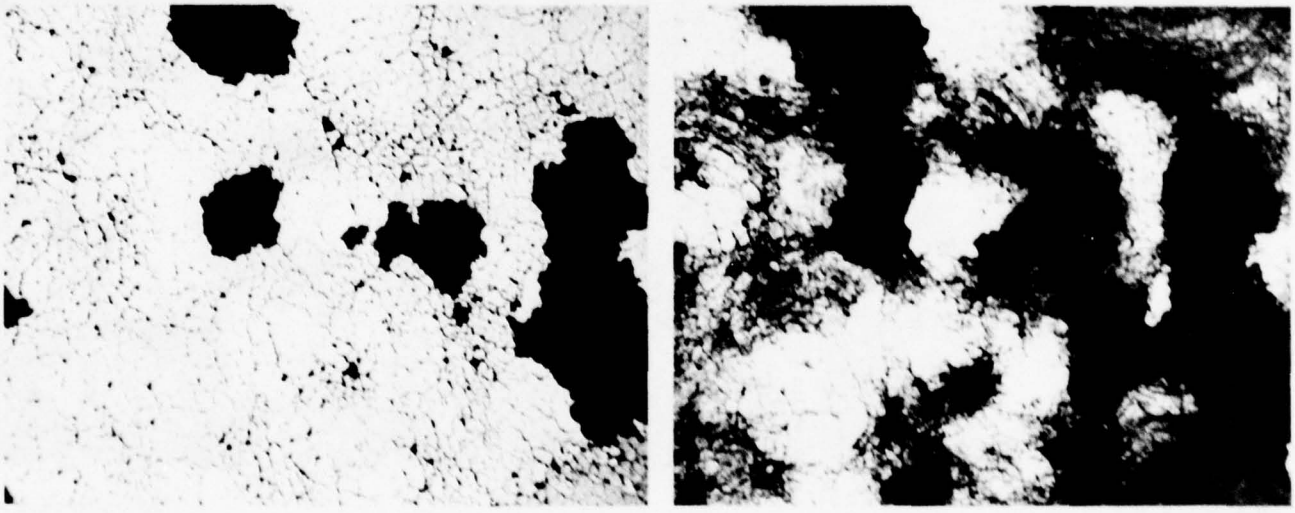

Reflected Light

Transmitted Light

d. 18 Minutes Exposure

Figure 53. Concluded

10 μm had decreased by 30 percent. Likewise, zinc sulfide had no significant surface pitting after a cumulative exposure of 12 minutes (Figure 53b) even though transmittance at 10 μm had decreased by 27 percent.

The sequence of photomicrographs in Figures 52 and 53 reveal similarities in the progress of damage of the two materials. Both materials tended to form close-packed hexagonal arrays of ring fractures during the initial increments of exposure. Drop impacts during subsequent exposures increased the extent of subsurface damage at the initial impact site rather than form new ones. This is similar to the phenomenon discussed earlier which was found during the experiments with overlapping 0.080 in. (2.0 mm) diameter single drop impacts on zinc selenide (Figures 43 and 44).

The sequence of micrographs in Figure 52 and 53 also reveal distinct differences in the progress of damage of the two materials exposed to the small drop rainfield. Zinc sulfide exhibited what appeared to be growth of prior ring fractures by a stepwise process as subsequent drops impacted the same site. This phenomenon was evidenced by the concentric rings which can first be seen in the photomicrograph made with transmitted light in Figure 53b. Sites with these concentric rings became numerous as the cumulative time of exposure to the rainfield increased. These unique ring fractures were not found on the zinc selenide specimen exposed to the small drop rainfield. A re-examination of the zinc sulfide specimen previously exposed to the standard rainfield also failed to reveal any sites with concentric rings.

Evidence of the differences in response of the two materials to the two different drop size rainfields can be seen in the photomicrographs of the surfaces of the specimens in Figures 54 and 55. Figure 54 compares the zinc selenide specimen exposed for 180 seconds in the small drop rainfield with

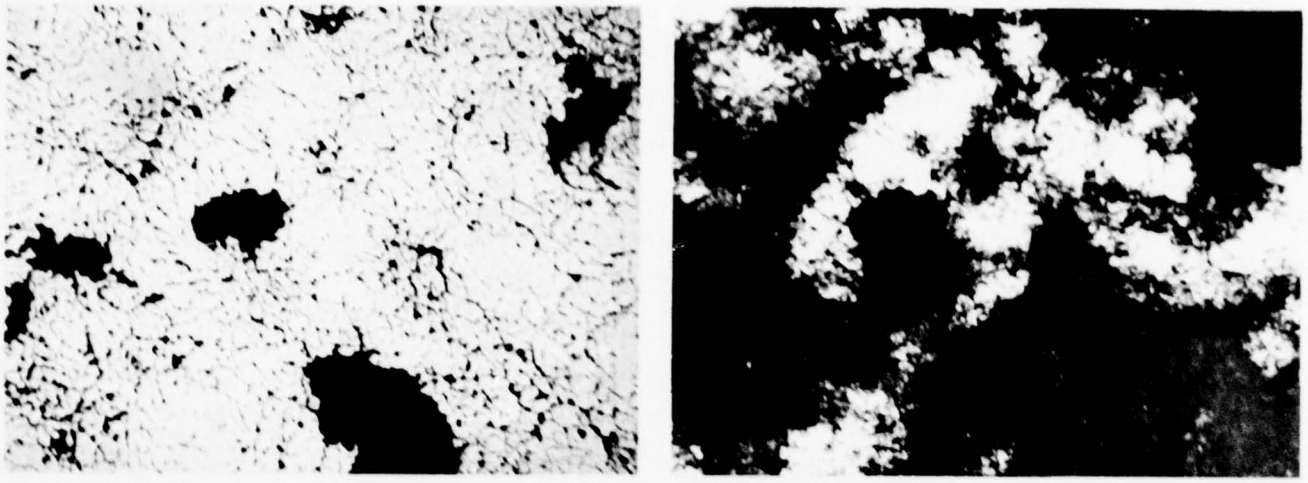

Reflected Light

Transmitted Light

a. Small Drop Rainfield (180 Sec Exposure)

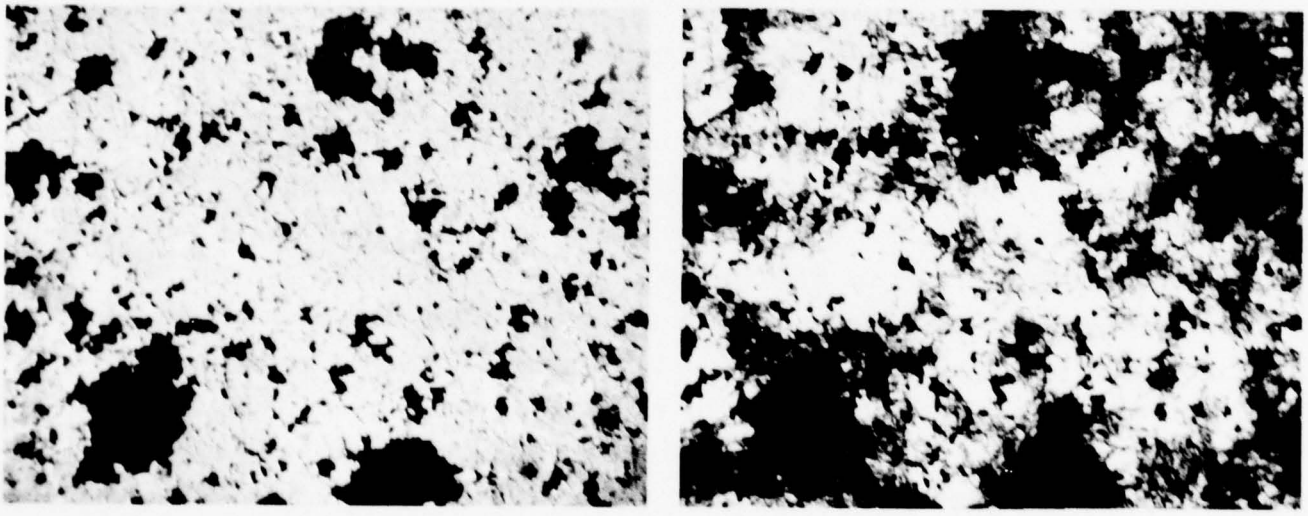

Reflected Light

Transmitted Light

b. Standard Rainfield (30 Sec. Exposure)

Figure 54. Comparison of Damage Produced on Zinc Selenide by Small Drop Rainfield and Standard Rainfield. Mag. 30X.

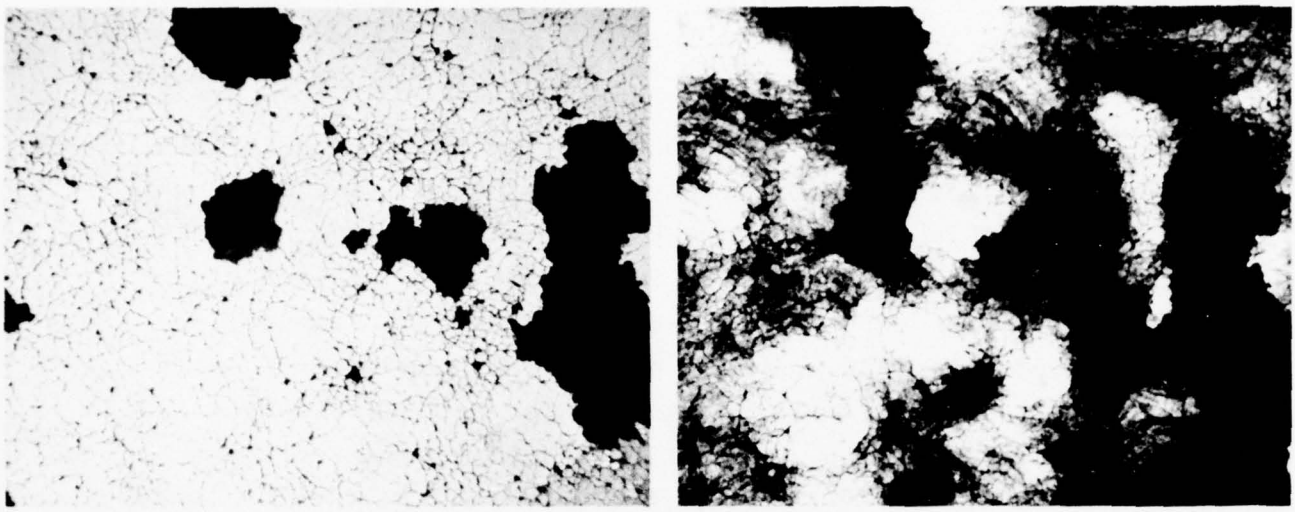

Reflected Light

Transmitted Light

a. Small Drop Rainfield (18 Min. Exposure)

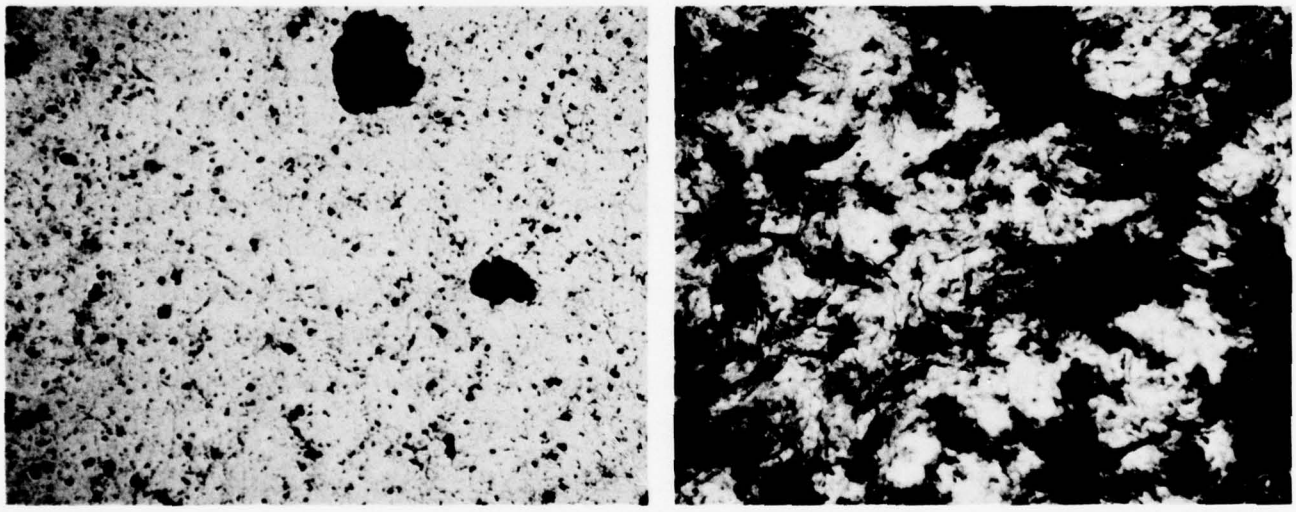

Reflected Light

Transmitted Light

b. Standard Rainfield (320 Sec. Exposure)

Figure 55. Comparison of Damage Produced on Zinc Sulfide by Small Drop Rainfield and Standard Rainfield. Mag. 30X.

the specimen exposed for 30 seconds in the standard rainfield. Transmittance loss was comparable for both specimens as shown by the data in Table 2. Figure 55 compares the zinc sulfide specimen exposed for 18 minutes in the small drop rainfield with the specimen exposed for 5-1/3 minutes (320 seconds) in the standard rainfield. Again, as shown by the data in Table 2, the transmittance loss was comparable for both specimens. In general, the small drop rainfield produced more extensive subsurface damage than did the larger drop standard rainfield. The tendency to retain the initially formed close-packed hexagonal array of ring fractures was also stronger in the small drop rainfield.

Cross sections of the specimens exposed to the two rainfields were also prepared to characterize further the differences in damage mechanisms produced by the two rainfields. The depth and structure of the subsurface cracks were then readily revealed with optical microscopy using polarized light. The cross section of the zinc selenide specimen exposed for 180 seconds in the small drop rainfield (Figure 56) showed evidence of deeper and more extensive subsurface damage than the zinc selenide specimen exposed for 30 seconds in the standard rainfield (Figure 57). The surfaces of the cracks formed in zinc selenide in the small drop rainfield also displayed more distinct facets of cleavage planes as can be seen by comparing the higher magnification photomicrographs in Figures 56 and 57.

The cross section of the zinc sulfide specimen exposed for 18 minutes in the small drop rainfield (Figure 58) also showed evidence of more extensive subsurface damage than the specimen exposed for 5-1/3 minutes (320 seconds) in the standard rainfield (Figure 59). The stepwise crack growth of the ring fractures on the zinc sulfide specimen exposed to the small drop rainfield are evident in the higher magnification photomicrograph in Figure 58.

TABLE 2

COMPARISON OF BEHAVIOR IN SMALL DROP RAINFIELD AND STANDARD RAINFIELD FOR ZINC SELENIDE AND ZINC SULFIDE

Material	Rainfield	Cumulative Exposure	Percent Transmittance At 2 μm	10 μm
ZnSe	Small Drop	0 Sec.	82	83
		180 Sec.	25 (70% loss)	48 (42% loss)
ZnSe	Standard[a]	0 Sec.	74	75
		30 Sec.	14 (81% loss)	34 (55% loss)
ZnS	Small Drop	0 Min.	84	82
		18 Min.	44 (48% loss)	47 (43% loss)
ZnS	Standard[a]	0 Sec.	74	70
		320 Sec.	29 (51% loss)	50 (29% loss)

[a] Data for standard rainfield taken from Reference 1.

Mag. 40X

Mag. 250X

Figure 56. Cross Section of Zine Selenide Specimen Exposed for 180 Seconds to Small Drop Rainfield at 730 fps (222 m/s).

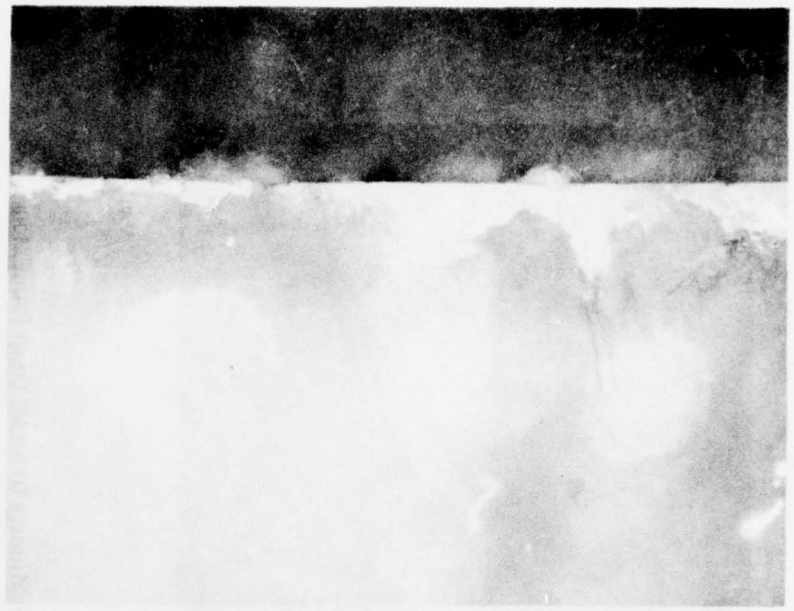

Mag. 40X

Mag. 250X

Figure 57. Cross Section of Zinc Selenide Specimen Exposed for 30 Seconds to Standard Rainfield at 730 fps (222 m/s).

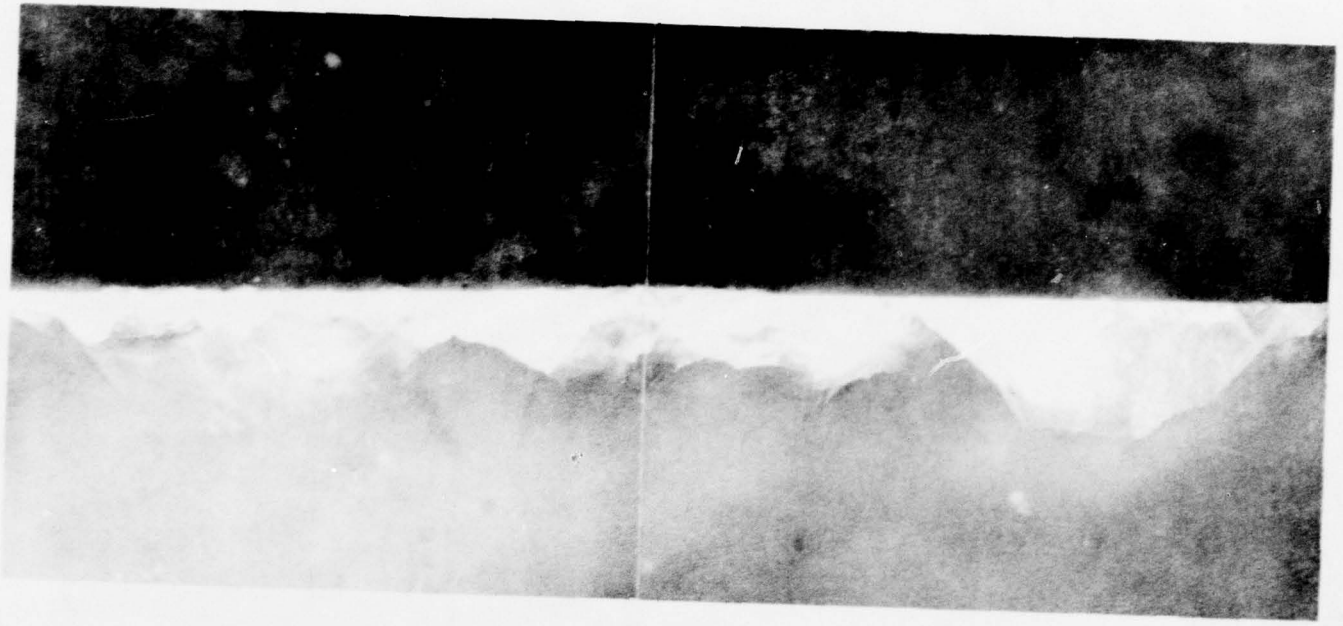

Mag. 40X

Figure 58. Cross Section of Zinc Sulfide Specimen Exposed for 18 Minutes to Small Drop Rainfield at 730 fps (222 m/s). Continued.

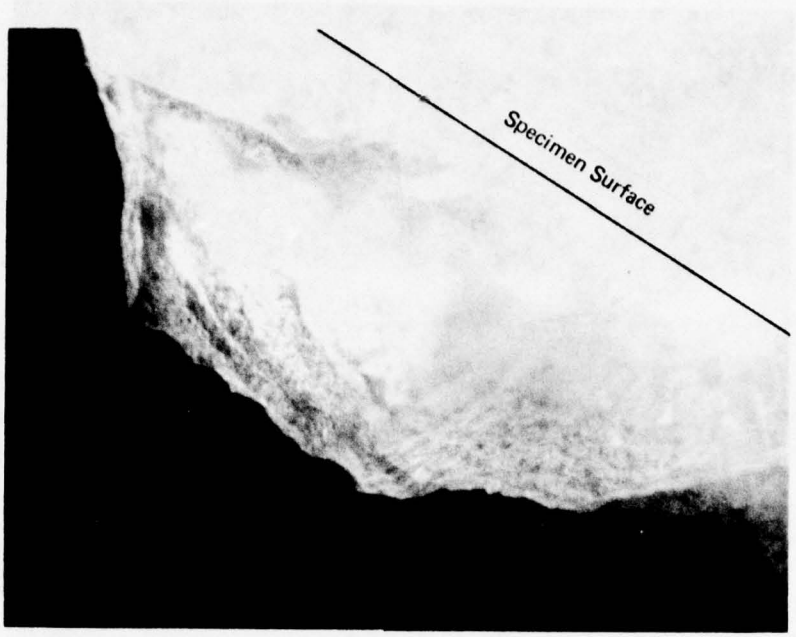

Mag. 100X

Figure 58. Concluded

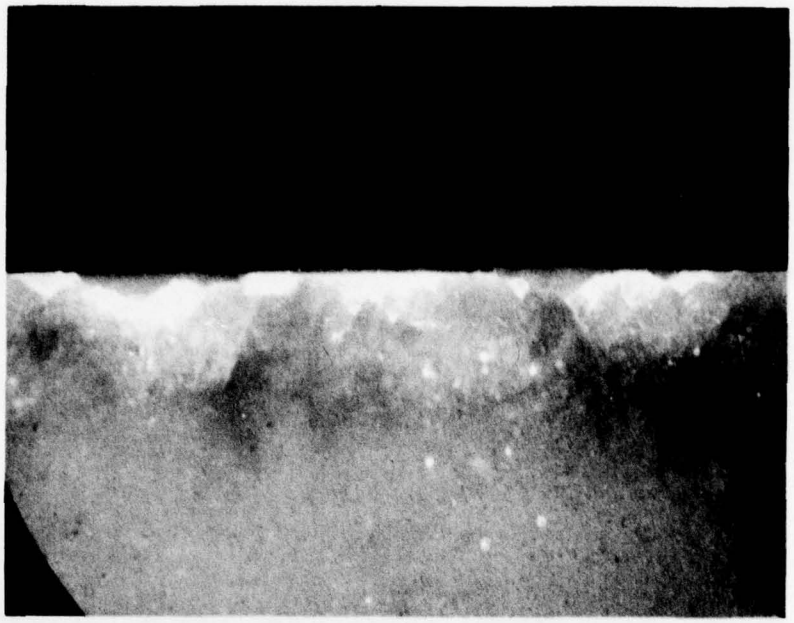

Figure 59. Cross Section of Zinc Sulfide Specimen Exposed for 320 Seconds to Standard Rainfield at 730 fps (222 m/s). Mag. 40X.

The number of drops impacting a unit area of a specimen per unit exposure time at a given velocity in a rainfield in the AFML/Bell erosion facility can be calculated by the equation below.

$$N = \frac{j \ (r_2^2 - r_1^2) \ d \ (0.0178 \ V)}{57{,}600 \ \sqrt{2gh} \ r^3}$$

where:

- N is the number of drop impacts/inch^2/sec.
- j is rainfall rate in inches/hr.
- r_2 and r_1 are radial distance in inches to the outboard and inboard locations of the unit area of interest.
- d is the height of the specimen in inches.
- V is the rotational velocity in ft/sec.
- g is the gravitational constant in ft/sec^2.
- h is the distance of drop fall in feet.
- r is the radius of the drops in inches.

The approach used to derive this equation has been previously described.(3) This equation provides an approximate value since it assumes that all drops have diameters equal to the mean.

A specimen rotated at 730 fps (222 m/s) will impact approximately 56 drops/inch^2/sec (8.7 drops/cm^2/sec) in the standard rainfield and approximately 370 drops/inch^2/sec (57 drops/cm^2/sec) in the small drop rainfield. Thus, a unit area of specimen is impacted by 6.6 times as many drops per second in the small drop rainfield as in the standard rainfield. However, the mass of the mean drop in the small drop rainfield is only 0.072 times that of the mean drop in the standard rainfield. The small drop rainfield therefore imparts 0.48 times the mass of water per unit area per unit time than does the standard rainfield.

Based on the assumption that damage (loss of transmittance) at a given impact velocity is directly proportional to total mass of water impacted per unit area, a specimen would have to be exposed close to twice as long in the small drop rainfield as in the standard rainfield for an equivalent amount of damage. However, the data in Table 2 show that for equivalent loss of transmittance, the ratio of exposure time in the small drop rainfield to exposure time in the standard rainfield was somewhat greater than 6 for zinc selenide and about 3.4 for zinc sulfide. A simple mass equivalency does not appear to be adequate to correlate damage rates with rainfield drop diameters.

As demonstrated by the results of these experiments, the relationship of damage rate and drop size also depends on the material. The relative erosion resistance of zinc sulfide compared to zinc selenide proved to be less in the small drop rainfield than in the standard rainfield. The relationships among environmental parameters, material properties, erosion damage, and transmittance loss are complex. Additional experimentation will be required to formulate a damage prediction model.

c. Erosion of a LaF_3 Antireflection Coating on Zinc Sulfide

The zinc sulfide specimen with the lanthanum fluoride antireflection coating was exposed for 12 minutes in the small drop rainfield at a velocity of 730 fps (222 m/s). This specimen had previously appeared to suffer no damage during two different exposures to impact by single drops as discussed in Section II, A, 8. For a comparative standard, an uncoated zinc sulfide specimen was also exposed to the rainfield for 12 minutes at a velocity of 730 fps (222 m/s) immediately following the exposure of the coated specimen. Transmittance of each of the specimens was measured between 2.1 and 20 μm before and after exposure to the rainfield.

Figure 60 presents curves of transmittance versus wavelength for the coated and uncoated specimens. The initial improvement in transmittance between 8 and 10 μm imparted by the antireflection coating is evident when the before exposure curves in Figures 60a and 60b are compared. The coating also increased transmittance between 3 and 4 μm. Following the 12 minutes exposures, the transmittance of the coated specimen was comparable at all wavelengths to that of the uncoated standard.

Microscopic examination revealed no trace of the lanthanum fluoride coating on the area of the surface exposed to the environment. Comparable types and magnitudes of damage were present on the coated and uncoated specimens as illustrated by the photomicrographs in Figure 61.

The single drop impact experiments discussed earlier, demonstrated that antireflection coatings can have a significant influence on the response of the material to drop impact, seeming to reduce or eliminate ring fractures in many cases. However, the initial presence of the lanthanum fluoride coating did not affect the overall behavior of the zinc sulfide exposed to the rainfield. The rainfield test verified the general problem of poor adhesion of antireflection coatings on zinc sulfide which became apparent during the single drop impact experiments.

d. Erosion of a ZnS/ZnSe Bilayered Specimen

A bilayered specimen having a 0.020 in. (0.50 mm) thick outer layer of zinc sulfide bonded with Loctite adhesive to a 0.375 in. (9.5 mm) thick zinc selenide substrate was exposed to the small drop rainfield for 12 minutes at a velocity of 730 fps (222 m/s). Figure 62 shows the transmittance between 2.1 and 20 μm for this specimen before and after the rainfield exposure. The strong adsorption bands of the adhesive make it difficult to compare directly the behavior of the

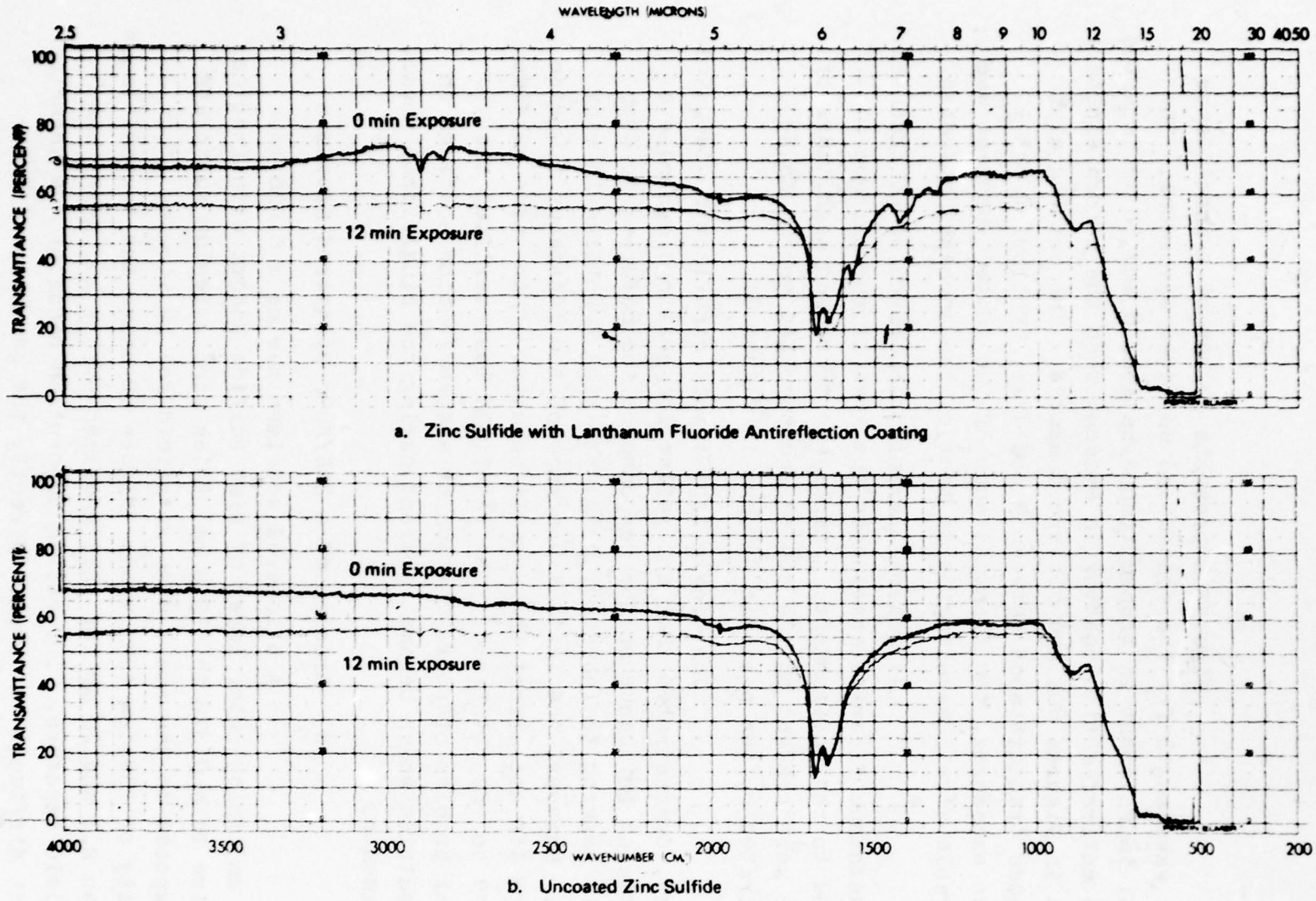

Figure 60. Effect of Lanthanum Fluoride Antireflection Coating upon Loss of Transmittance of Zinc Sulfide Exposed at 730 fps (222 m/s) to Small Drop Rainfield.

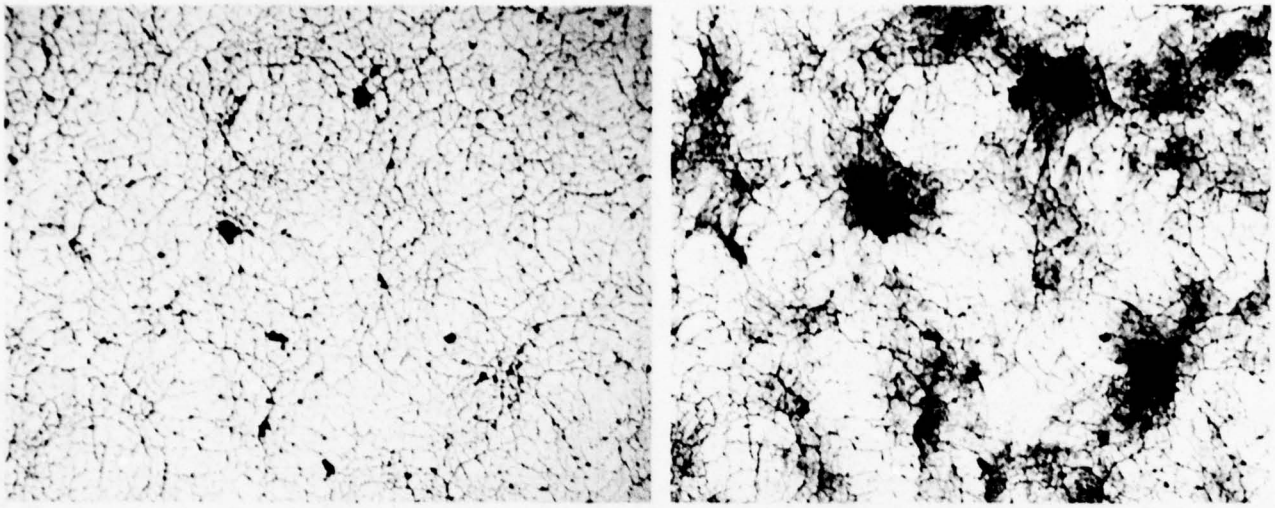

Reflected Light

Transmitted Light

a. Zinc Sulfide with Lanthanum Fluoride Antireflection Coating

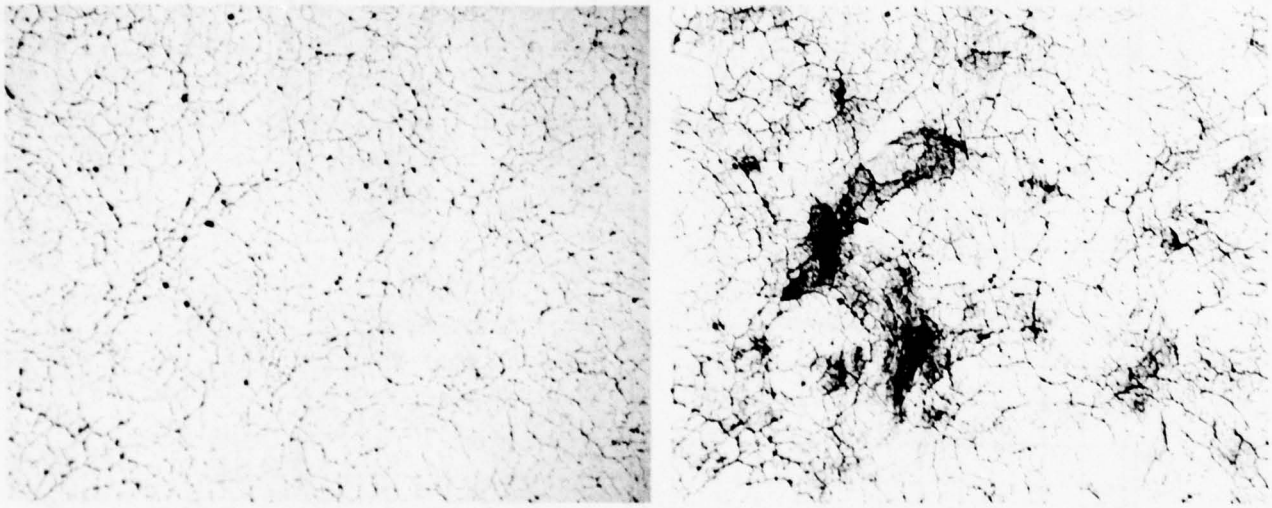

Reflected Light

Transmitted Light

b. Uncoated Zinc Sulfide

Figure 61. Effect of Lanthanum Fluoride Coating on Damage of Zinc Sulfide Exposed at 730 fps (222 m/s) to Small Drop Rainfield. Mag. 30X.

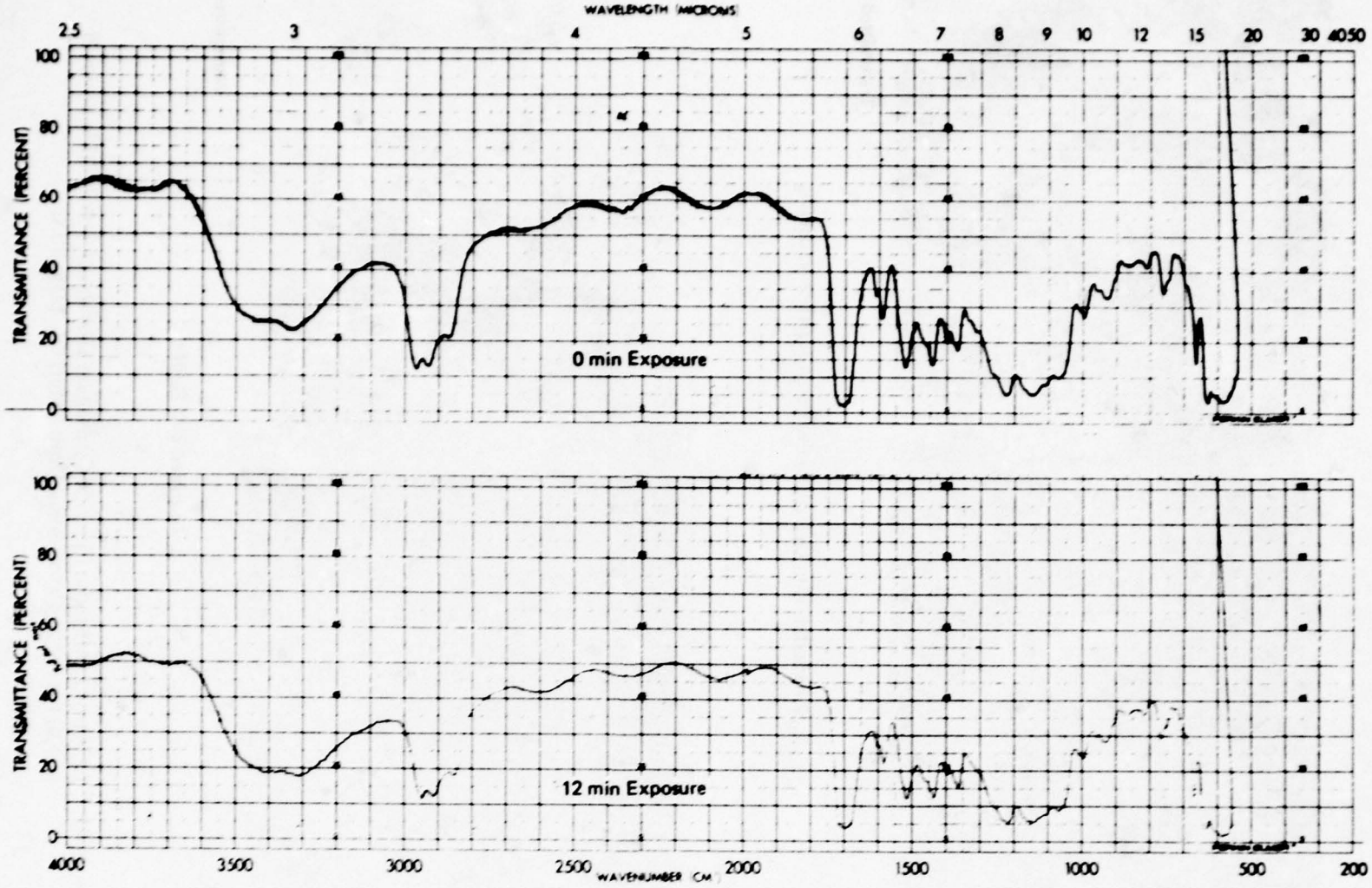

Figure 62. Transmittance Loss of Bilayered Specimen Exposed at 730 fps (222 m/s) to Small Drop Rainfield. Specimen had 0.020 in. (0.50 mm) Thick Outer Layer of Zinc Sulfide Bonded with Loctite Adhesive to Zinc Selenide Substrate

bilayered specimen with that of the zinc sulfide standard (Figure 60b). However, the differences in before and after transmittance of 14, 13, and 4% for the bilayered specimen at wavelengths of 2.5, 4, and 10 μm are comparable to the differences of 13, 8, and 3% for the standard specimen at the same wavelengths. The 0.020 in. (0.50 mm) thick layer of zinc sulfide appeared to behave in a manner similar to the thicker, homogeneous standard.

Microscopic examination of the bilayered specimen showed that damage on the zinc sulfide layer was comparable to that on the zinc sulfide standard. This can be seen by comparing Figure 63a with Figure 61b. The ring fractures had penetrated to the back face of the zinc sulfide layer as illustrated in Figure 63b. No evidence of damage to the zinc selenide substrate was detected. Etching the specimen in a heated solution of HCl in water (1:1, by volume) revealed the small, uniform grain size illustrated in Figure 64.

The cross section of the zinc sulfide specimen exposed to the small drop rainfield for 18 minutes (Figure 58) showed cracks that had penetrated to a depth slightly greater than 0.020 in. (0.50 mm). Only 12 minutes was required for a crack to penetrate the 0.020 in. (0.50 mm) thick zinc sulfide layer on the bilayered specimen. The presence of the interface affected somewhat the response of the zinc sulfide layer. Increasing the layer thickness to 0.040 in. (1.00 mm) should provide bilayered performance equivalent to that of homogeneous zinc sulfide.

e. Erosion of Spinel

A specimen of single crystal spinel was exposed to the small drop rainfield at a velocity of 1750 fps (533 m/s) for a period of 5 minutes. At the end of the run, the specimen was found to be broken with three pieces still remaining in the fixture. The surface of these pieces showed significant damage in the form of large pits. The pieces were not suitable for measurement of transmittance.

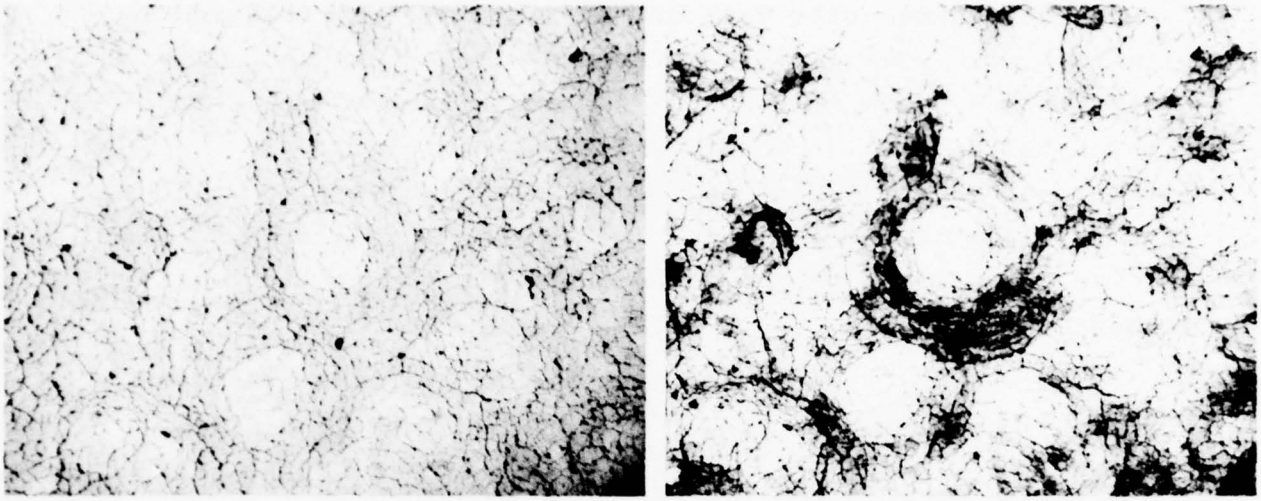

Reflected Light

Transmitted Light

a. Focused on Front Surface. Mag. 30X

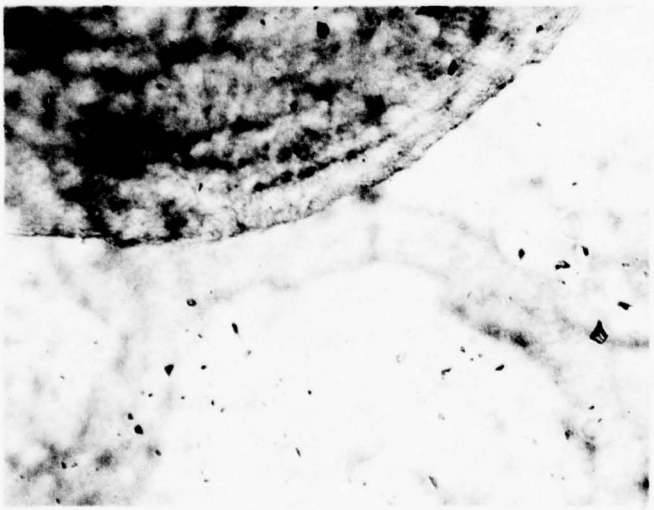

b. Focused on Back Surface. Transmitted Light. Mag. 135X.

Figure 63. Damage on Bilayered Specimen Exposed for 12 Min. at 730 fps (222 m/s) to Small Drop Rainfield. Specimen Had 0.020 in. (0.50 mm) Thick Outer Layer of Zinc Sulfide Bonded with Loctite Adhesive to Zinc Selenide Substrate.

Figure 64. Grain Structure of 0.020 in. (0.50 mm) Thick Zinc Sulfide Layer on Bilayered Specimen Exposed to Small Drop Rainfield. Mag. 470X.

A specimen of fusion-cast spinel was then exposed for 2-1/2 minutes to the small drop rainfield at the same velocity of 1750 fps (533 m/s). The appearance of the eroded surface of this specimen is shown in Figure 65. Transmittance before and after the exposure is shown in Figure 66. The transmittance between 2.5 and 4 μm decreased by about 5% of the initial value. This decrease was less than the percent of total surface which was pitted. It was not possible to draw any conclusion on the comparative erosion resistance of the two different forms of spinel based on these first rainfield tests with these materials.

Figure 65. Damage on Fusion Cast Spinel Specimen Exposed for 2½ Minutes at 1750 fps (533 m/s) to Small Drop Rainfield. Mag. 6X.

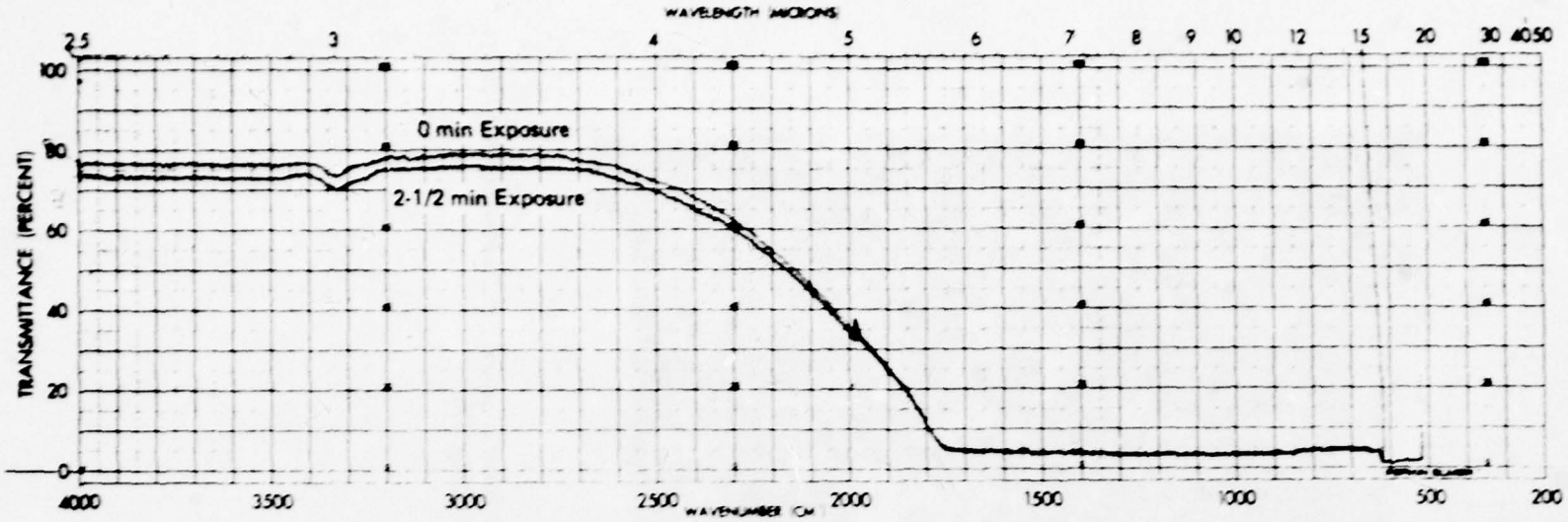

Figure 66. Transmittance Loss of Fusion Cast Spinel Exposed at 1750 fps (533 m/s) to Small Drop Rainfield.

SECTION III

THEORETICAL PREDICTION OF STRESSES GENERATED BY DROP IMPACT

In previous work, an analytical model was used to compute, as a function of time and location, the stresses induced by a single water drop impact on zinc selenide, zinc sulfide, gallium arsenide, and polymethylmethacrylate.[1] The predicted locations of the inner radii of the ring fracture annuli agreed with the experimental results indicating that the analytical model provided a reasonable representation of the drop impact process.

The model was based on a method developed by Blowers to calculate the transient stress distribution within an elastic half-space subjected to a uniform pressure loading distributed over an expanding circular region.[4] A perfectly compressible, spherical water drop colliding with a rigid surface was assumed for the caluclation of the radius of the loaded region as a function of time. The perfectly compressible water drop impact is illustrated by the sketch in Figure 67. The radius of the loaded region is labeled a(t). A one-dimensional shock wave relationship for a water drop striking a deformable solid was then used to compute the magnitude of the pressure loading.

The assumption that the pressure on the expanding loaded area remained constant with time was felt to be a major compromise incorporated into the model. Modifications of the model to incorporate a first order, time dependent pressure function.

A. Modification of the Pressure Function

The time dependent pressure chosen, presented in Figure 68, was derived from work by Rosenblatt et al.[5, 6]. The pressure function assumes that at the instant of impact the pressure is the water hammer pressure $P_o = \rho_o V_o C_o$. The pressure then increases to a peak value P_k at $t = t_c$ where t_c is the time at which the velocity of the moving boundary becomes subsonic with respect to the speed of sound in the impacting water drop. This effect has been demonstrated by detailed short time analysis of liquid drop impacts using the WAVE-L program.[5,6]

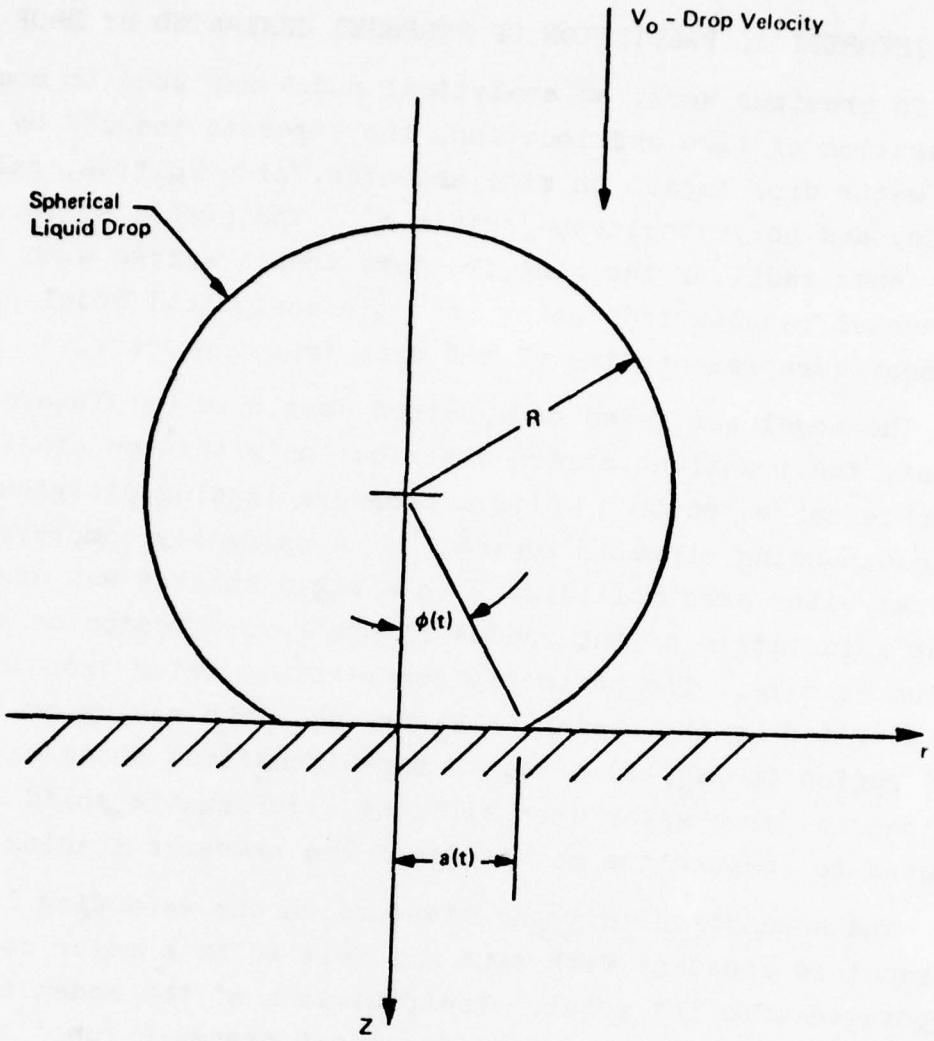

Figure 67. Perfectly Compressible Liquid Drop Impacting a Solid Surface

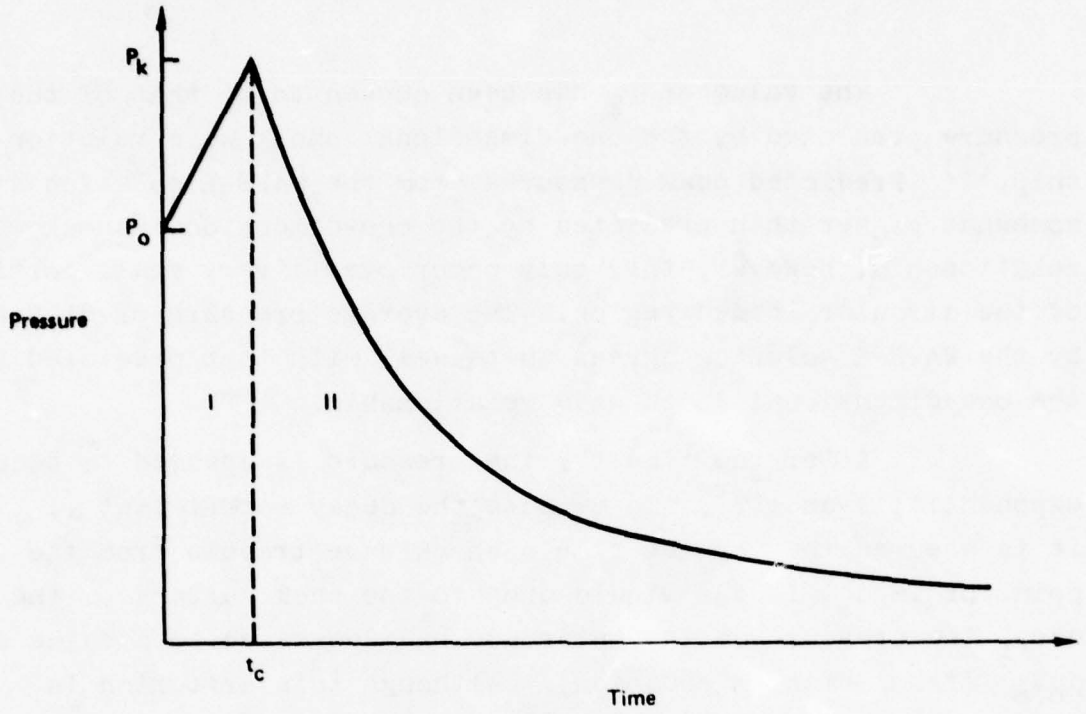

Region I

$$P = P_o + \frac{P_o (k - 1) t}{t_c}$$

Region II

$$P = k P_o e^{-\alpha \sqrt{t - t_c}}$$

where

$$k = \frac{P_k}{P_o}$$

$$P_o = \rho_o V_o C_o$$

$$t_c = \frac{R V_o}{2 C_o^2}$$

α = Decay Constant

Figure 68. Modified Pressure Function for Turban Program

The value of P_k has been chosen to be that of the pressure predicted by the one-dimensional shock wave relationship.[1] Predicted peak pressures from the WAVE-L solution are somewhat higher than predicted by the one-dimensional shock wave relationship; however, they only occur over a very small portion of the circular loaded region. The average pressure predicted by the WAVE-L solution agrees quite well with that predicted by the one-dimensional shock wave relationship.

After the time t_c, the pressure is assumed to decay exponentially as $t^{1/2}$. To compute the decay coefficient α, it is assumed that by the time a shock wave travels from the point of impact in the liquid drop to the back surface of the drop, the pressure on the interface has decreased to a value of $\rho_o V_o^2$ (from momentum equation). Although this criterion is arbitrary, the resulting pressure function agrees reasonably well with the WAVE-L predictions as shown in Figure 69.

The computation of stresses for the time dependent pressure distribution is approximated by the equation below.

$$\sigma(r,z,t) = P(o)\sigma_o(r,z,t) + \int_o^t \sigma_o\,(r,z,t,-\tau)P'(\tau)d\tau$$

where $P(t)$ = assumed pressure function

$P'(t) = \frac{dP(t)}{dt}$

$\sigma_o(r,z,t)$ = any stress component computed for a constant pressure loading

$\sigma(r,z,t)$ = new stress

The above equation is exact when the original pressure loading function is truly independent of time. In the original Blowers' formulation, the pressure was assumed constant; however, the area over which it was applied was a function of time. Thus, the above equation does not provide a rigorous solution for the time dependent pressure loading, but rather a first order approximation. This approximation assumes the pressure magnitude and

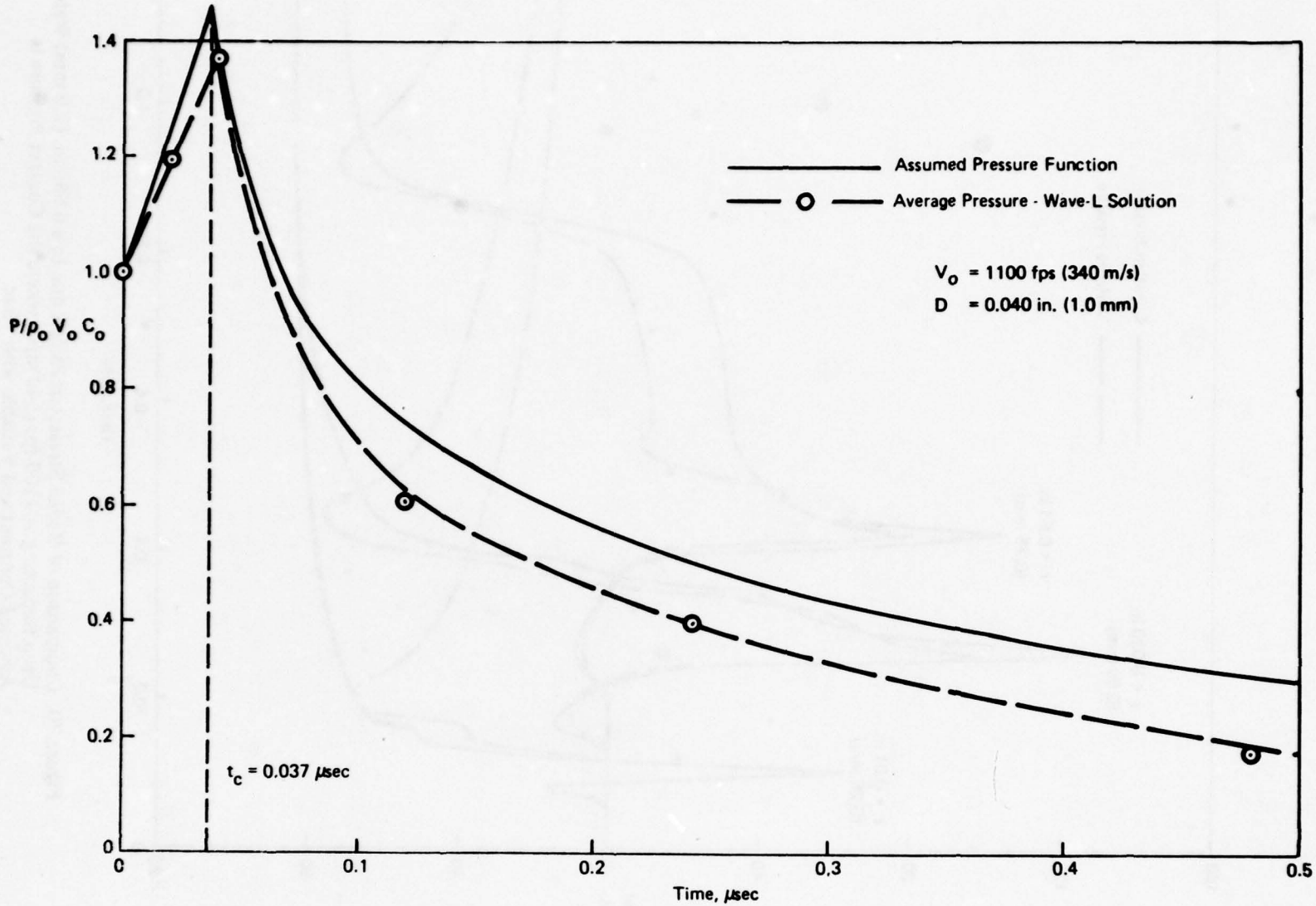

Figure 69. Comparison of Assumed Pressure Function with Wave – L Predictions

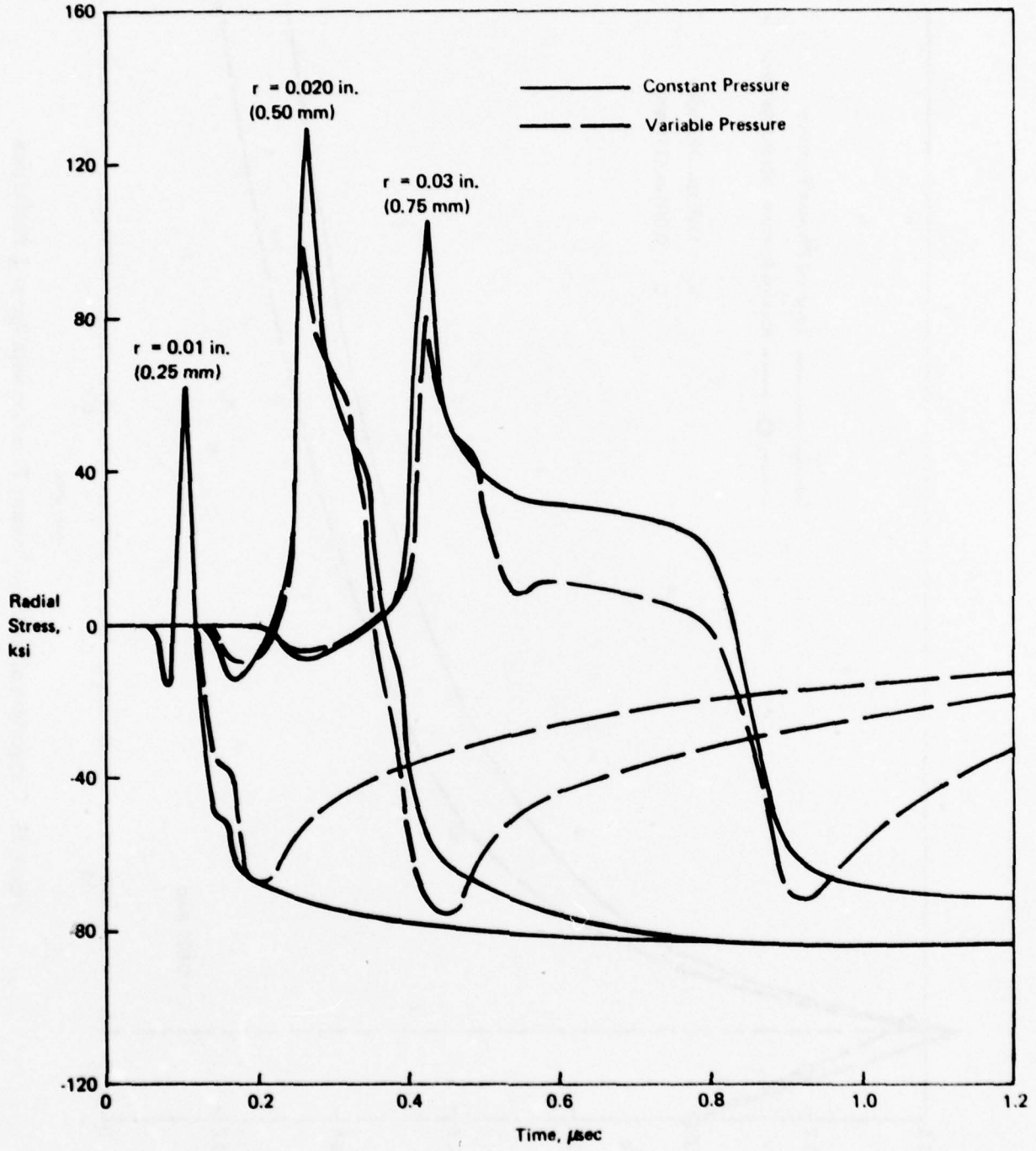

Figure 70. Comparison of Radial Stresses in PMMA due to a 0.080 in. (2.0 mm) Water Drop Impacting at 1100 fps (340 m/s), where the Contact Pressure is Assumed Constant and Variable with Time

area over which it acts are separable with the above equation being applied to account for a time dependency in the pressure magnitude.

Figure 70 compares the radial tensile stress in polymethlmethacrylate (PMMA) due to a 0.080 in. (2.0 mm) water drop impacting at 1120 fps (340 m/s), when the contact pressure is assumed to be constant and when it is assumed to be time dependent. The stresses were calculated at a depth of 0.0002 in. (5 μm) at three radial distances from the center of impact. For the constant pressure case, the magnitude of the pressure computed from the one-dimensional shock relationship was 106 ksi (731 MPa). For the variable pressure case, the pressure was assumed to equal the water hammer value $\rho_o V_o C_o$ = 72.5 ksi (500 MPa) at t = 0; increase linearly to the one-dimensional shock value of 106 ksi (731 MPa) at $t = t_c$ = 0.074 μ sec; and then decay exponentially to zero.

For constant pressure, the stress curves are characterized by an initial tensile spike which becomes compressive, asymptotically approaching a value of -84 ksi (-580 MPa). For variable pressure, the initial part of the stress curve at each radial position is similar to that for constant pressure, with the exception that the predicted peak tensile values are about 25% lower. The stresses then become compressive, reach a maximum negative value, and finally decay expontentially to zero. Of particular interest are the predictions at r = 0.03 in. (0.75 mm). At this radial position, tensile stresses exist for a relatively long time for both cases, approximately 0.6μ sec; however, the magnitude is significantly lower for stresses based on variable pressure.

It is felt that the stress/time curves computed using the time dependent contact pressure are much more realistic than those computed by the original analytical model. The modified model retains the relative computational simplicity of the original program. No significant increase in computer time is required.

B. Predicted Stresses in Zinc Selenide

Single 0.080 in. (2.0 mm) diameter water drops impacting zinc selenide were analyzed for impact velocities of 500, 730, and 1120 fps (152, 222, and 340 m/s) using the modified program. Predicted pressures and related parameters necessary to define the time dependent pressure function for the three velocities considered are presented in Table 3. Stresses resulting from the drop impact were calculated at a depth of 0.4 mil (10 μm) for radial positions encompassing regions where experiments had shown fractures to occur. The depth was increased from that used for the test case with PMMA. This reduced the problems inherent in the numerical evaluation of the integrals used in the computation, particularly in the vicinity of the Rayleigh wave front.

Figure 71 presents the predicted temporal distribution of radial tensile stress at various radial locations for an impact velocity of 500 fps (152 m/s). Significant tensile stresses are produced at radial locations equal to or greater than 0.008 in. (0.20 mm). This case is near the damage threshold velocity which was found experimentally to be somewhat less than 500 fps (152 m/s). A few ring fractures were formed by drop impact at 500 fps (152 m/s), but none could be detected after drop impact at 450 fps (137 m/s). The fact that the predicted tensile stresses for drop impact at 500 fps (152 m/s) are close to the measured ultimate strength of 8.5 ksi (58.6 MPa) for zinc selenide agrees with the experimentally determined threshold velocity. This agreement demonstrates the validity of the modified analytical model.

Based on quasistatic fracture strength as the failure criterion, ring fracture would be predicted to occur at radial locations ranging from somewhat less than 0.008 in. (0.20 mm) to somewhat greater than 0.020 in. (0.50 mm). Experimentally, fractures were found between radial locations of r = 0.008 to 0.0125 in. (0.20 to 0.32 mm). Agreement between predicted and experiment results is good for the location of the inner radius

TABLE 3

PREDICTED PRESSURE FUNCTION PARAMETERS FOR

2.0 mm WATER DROP IMPACTS

Vo		Po				
fps	(m/s)	ksi	(MPa)	$k = \frac{Pk}{Po}$	t_c, sec.	α, $sec^{-1/2}$
500	(152)	33.0	(228)	1.18	.0342	2.146
730	(222)	48.1	(332)	1.29	.0499	1.903
1120	(341)	73.9	(510)	1.47	.0765	1.657

V_o = Drop velocity

$P_o = \rho_o V_o C_o$ (water hammer pressure)

P_k = Pressure from 1-D shock relationship (peak pressure)

t_c = Critical time where $P = P_k$

α = Decay constant

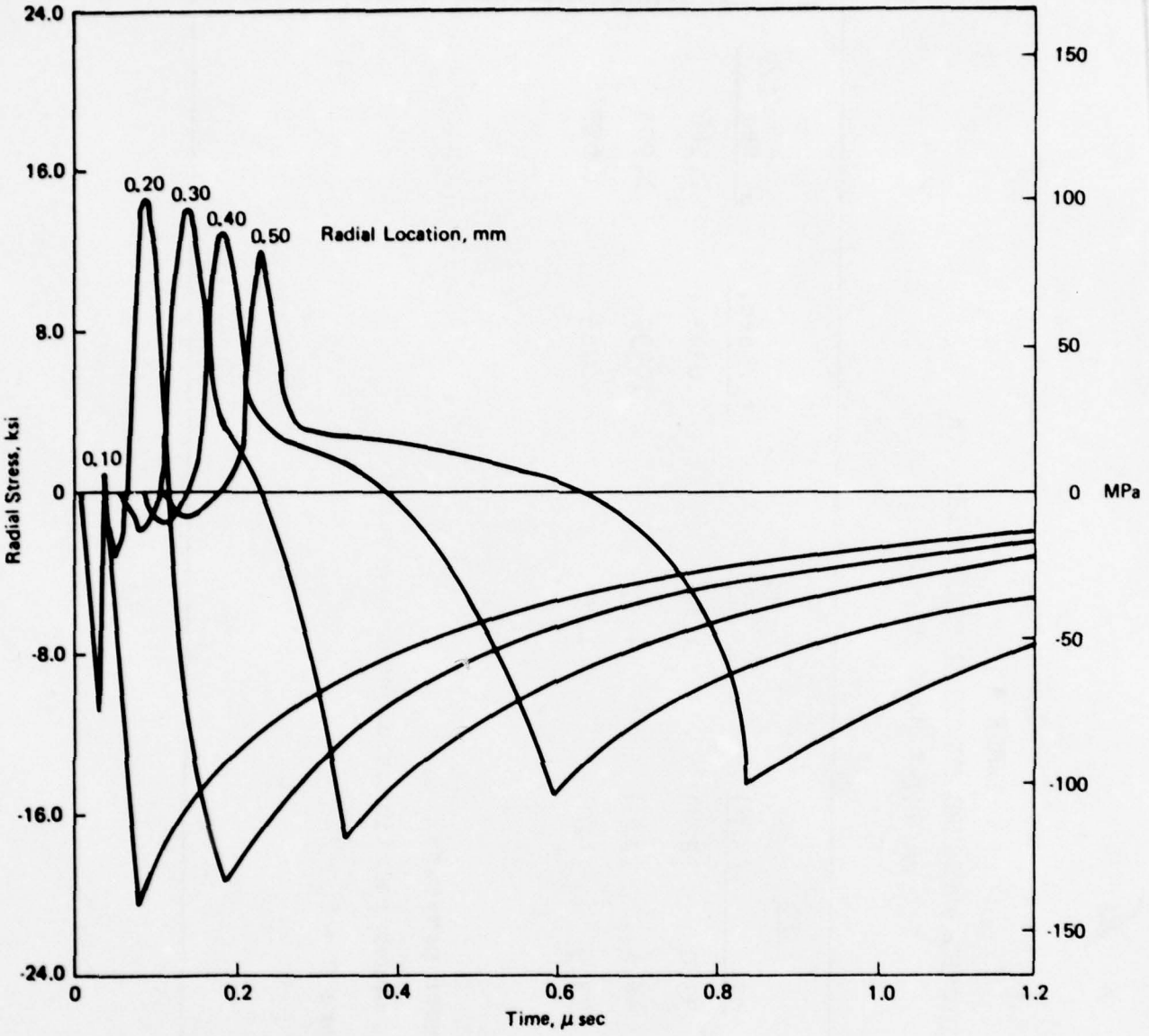

Figure 71. Temporal Distribution of Radial Stress at Depth z = 0.0004 in. (10 μm) for an 0.080 in. (2.0 mm) Water Drop Impacting ZnSe at 500 fps (152 m/s)

of the annulus of ring fractures. However, the predicted outer radius is greater than was found experimentally.

Similar plots of radial tensile stress versus time for impact velocities of 730 and 1120 fps (222 and 340 m/s) are presented in Figures 72 and 73. Predicted tensile stresses for both of these velocities are several times the fracture strength of zinc selenide and they exist over a much larger annular region as compared to the 500 fps (152 m/s) case.

At 730 fps (222 m/s), the measured annular fracture zone was between r = 0.007 and 0.028 in. (0.18 and 0.71 mm). The inner radius of the measured fracture zone agrees well with the prediction, but as in the 500 fps case, the analysis indicates fractures should occur well outside the measured fracture zone. The predicted tensile stress is still twice the fracture strength at a radial distance of 0.060 in. (1.5 mm).

At 1120 fps (340 m/s), the measured annular fracture zone was between r = 0.014 and 0.056 in. (0.35 and 1.41 mm). Based on quasistatic fracture strength for the failure criterion, fracture would be predicted over a larger area ranging from radial locations r < 0.008 in. (0.20 mm) to r > 0.069 in. (1.75 mm). Quasistatic fracture strength becomes a less suitable failure criterion as the impact velocity increases.

A first order improvement of the failure criterion was investigated. This work was based on a method proposed by Taler and Butcher[7] and used by Rosenblatt et al.[5] where time is introduced into the failure criterion. Current analytical methods often predict tensile stresses in excess of the static ultimate strength of the material in regions where fractures are not observed. It was felt that the time duration where stress exceeds some critical stress may be an important parameter. The criterion is stated as follows where K_T is the stress failure parameter:

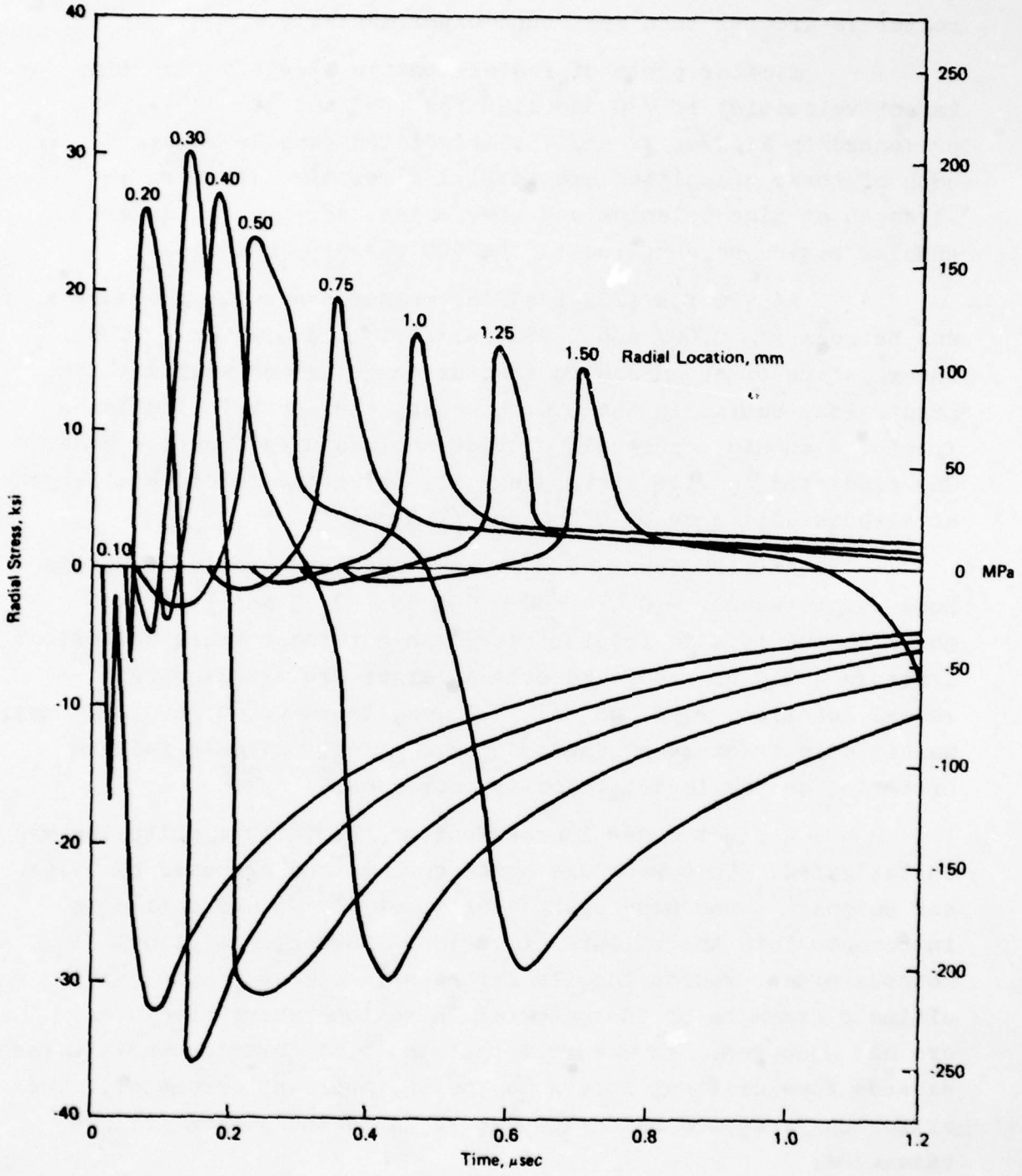

Figure 72. Temporal Distribution of Radial Stress at Depth z = 0.0004 (10 μm) for an 0.080 in. 2.0 mm) Water Drop Impacting ZnSe at 730 fps (222 m/s)

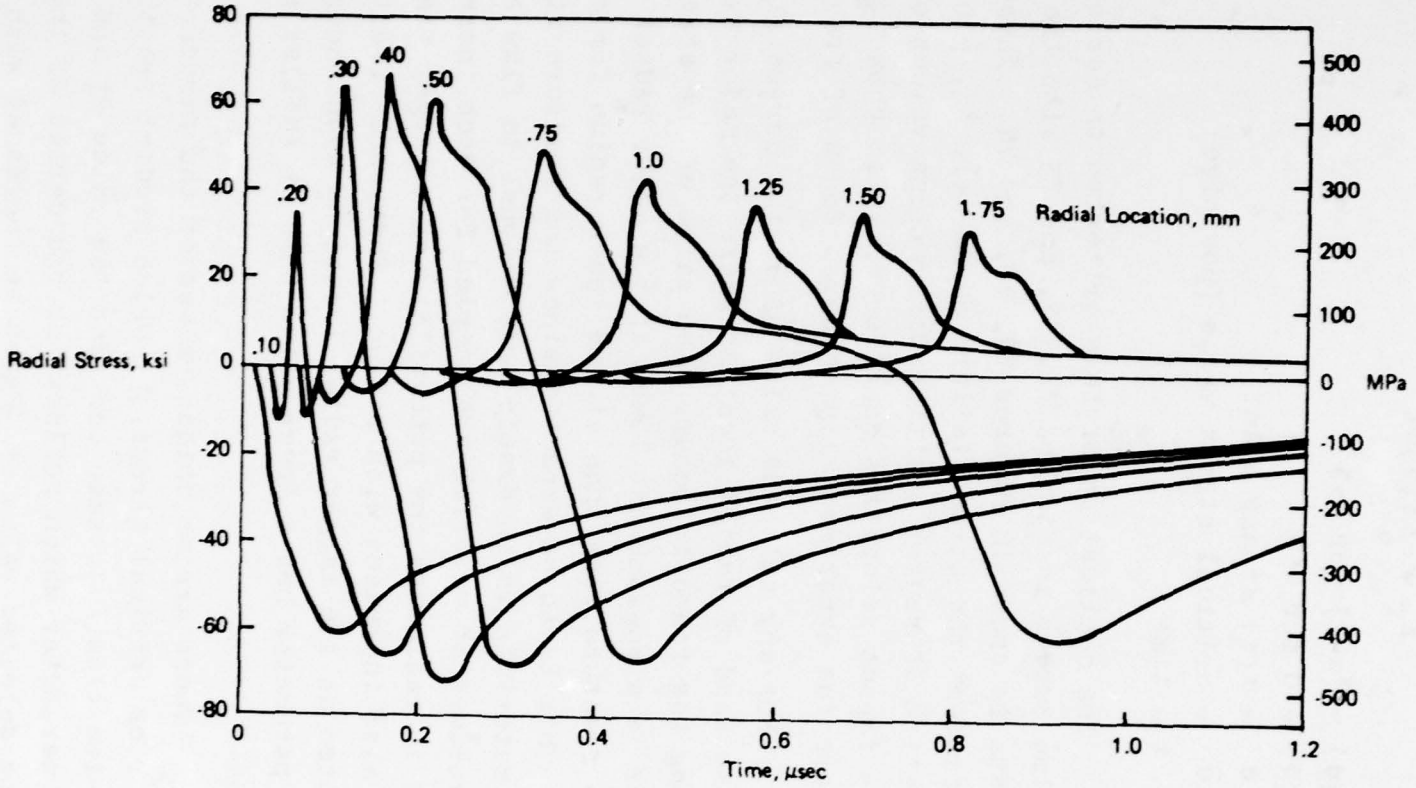

Figure 73. *Temporal Distribution of Radial Stress at Depth z = 0.0004 (10 μm)* for an 0.080 in. (2.0 mm) Water Drop Impacting ZnSe at 1120 fps (341 m/s)

$$K_T = \int_0^\infty f(\sigma)dt$$

where $f(\sigma) = (\sigma-\bar{\sigma})$ for $\sigma>\bar{\sigma}$

$f(\sigma) = 0$ for $\sigma<\bar{\sigma}$

$\sigma = \sigma(t)$ at any point

$\bar{\sigma}$ = critical stress value (positive)

t = time

The application of this criterion to correlate the stress-time curves in Figures 71, 72, and 73 with the experimental data is shown in Figures 74, 75, and 76. These latter figures present the stress failure parameter, K_T, plotted as a function of radial position for various values of $\bar{\sigma}$ at the three impact velocities considered. Also shown on the figures are the experimentally measured zones of fracture

For any selected value of $\bar{\sigma}$, the curves all peak within the band of radial location where the major extent of fracturing was found to occur. The value of the stress failure parameter is also somewhat lower at the outer radius of the measured fracture zone than at the inner radius for each critical stress. This is to be expected since the fracture strength of brittle materials is inversely proportional to flaw size. Larger volumes of material are sampled for each incremental increase in radius so the probability of a larger flaw being present also increases with radius. Thus, some fracturing would be expected at the larger radial locations even though the stress failure parameter has a lower value than at smaller radial locations.

There are no unique values of the stress failure parameter or critical stress, $\bar{\sigma}$, which predict fracture at all three velocities. To keep constant the value of the stress failure parameter which defines the boundaries of the fractured zone, the selected value of $\bar{\sigma}$ must be increased with an increase

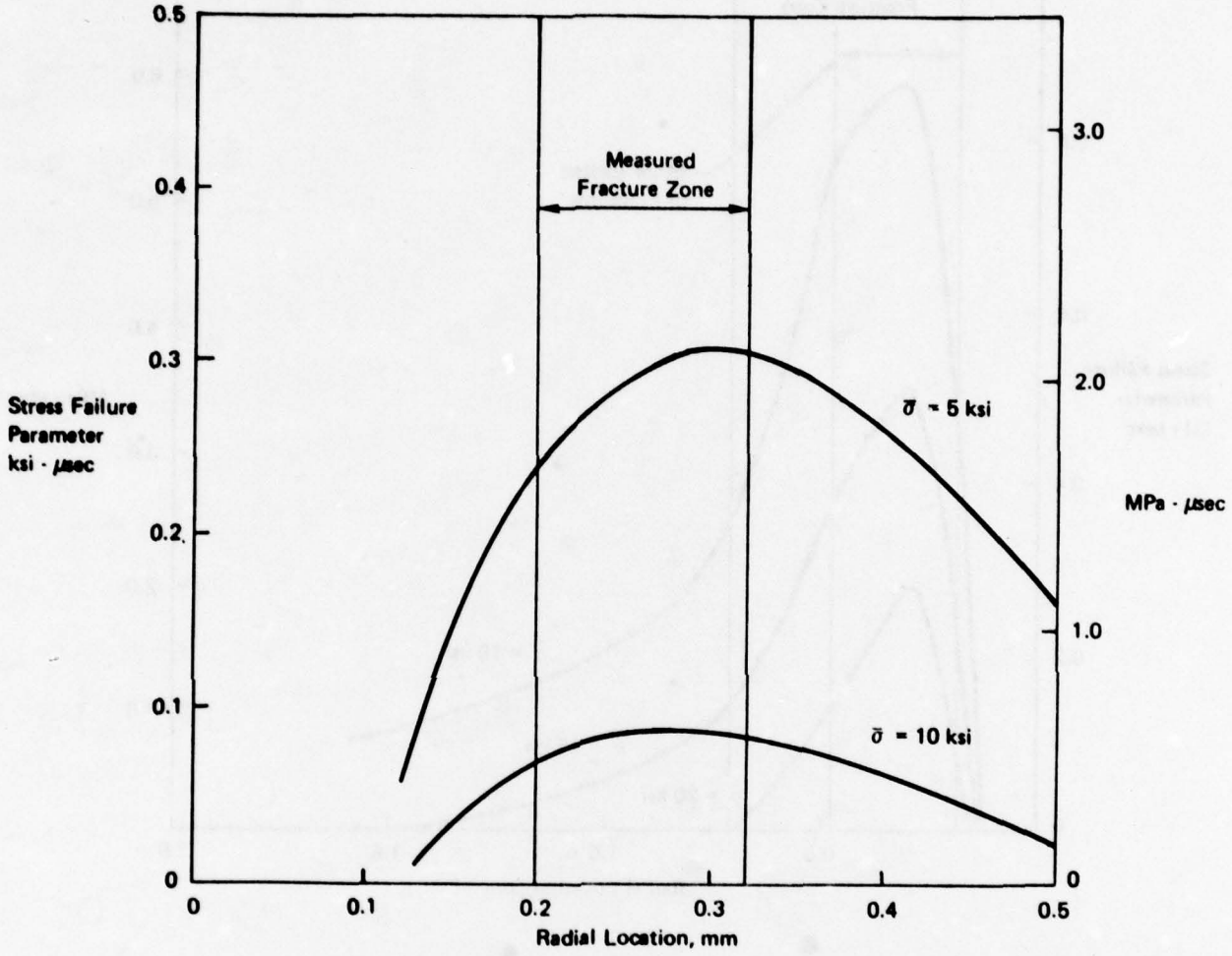

Figure 74. Stress Failure Parameter versus Lower Limit Stress $\bar{\sigma}$ and Radial Position for a 0.080 in. (2.0 mm) Drop Impacting ZnSe at 500 fps (152 m/s)

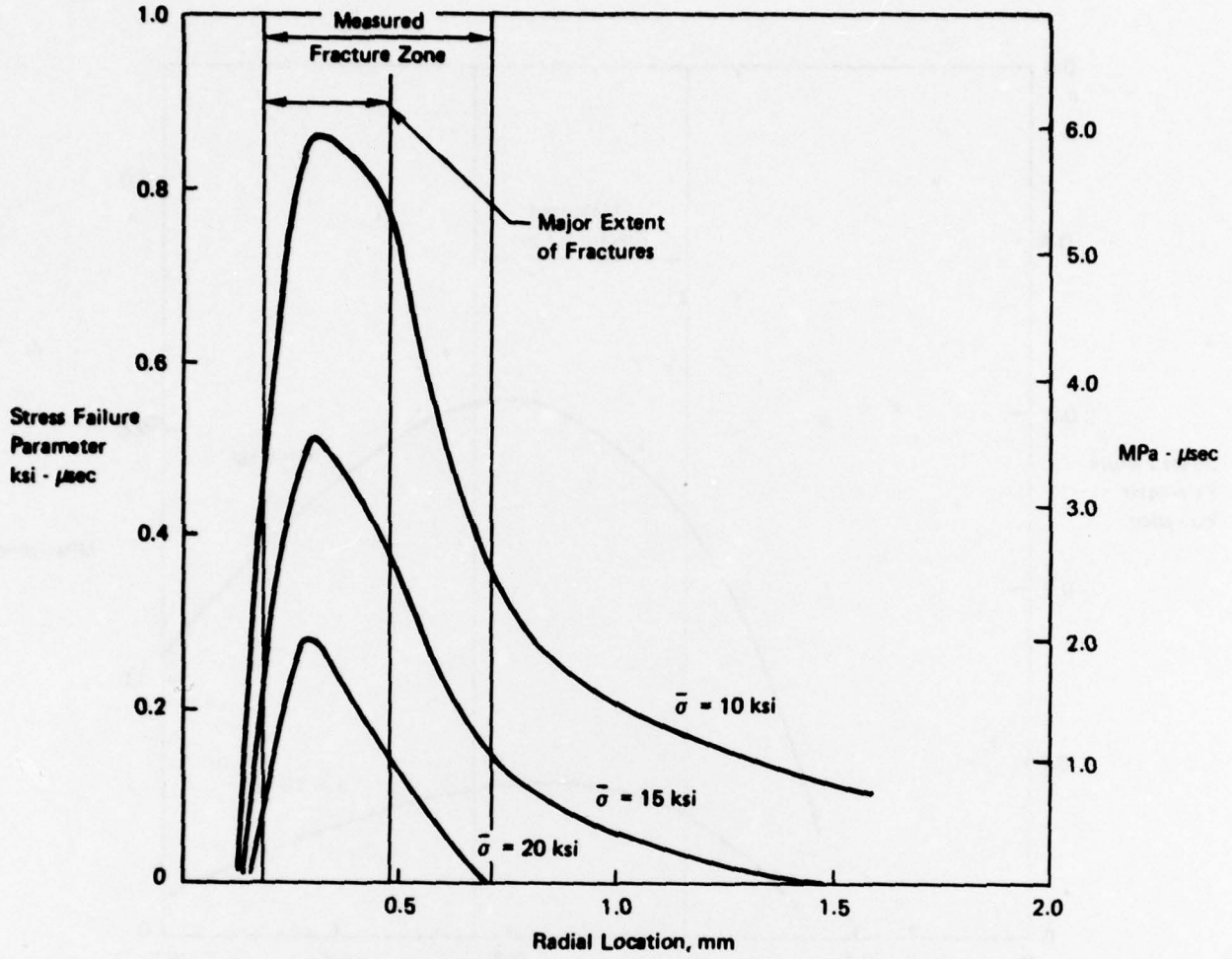

Figure 75. Stress Failure Parameter versus Lower Limit Stress $\bar{\sigma}$ and Radial Position for a 0.080 in. (2.0 mm) Drop Impacting ZnSe at 730 fps (222 m/s)

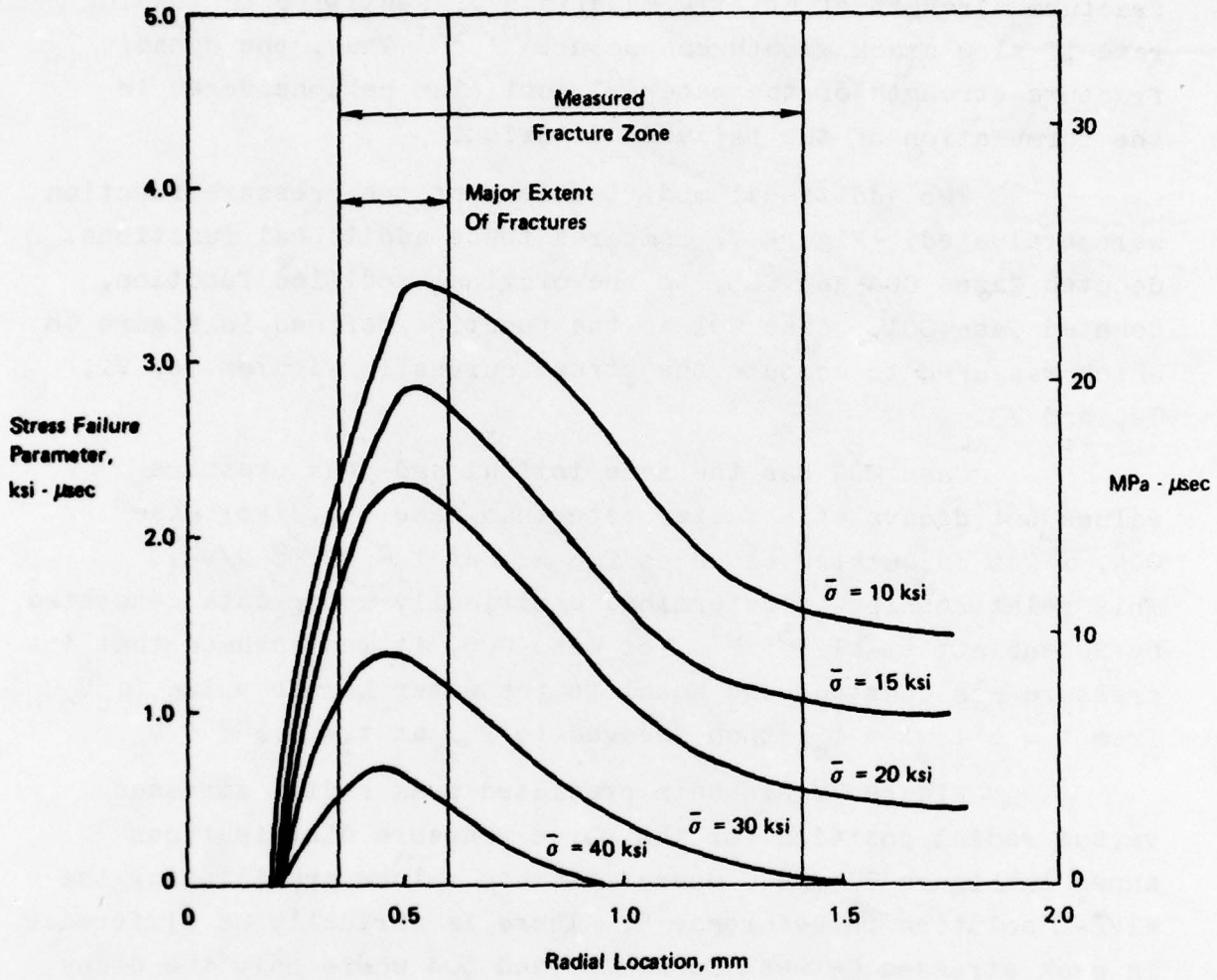

Figure 76. Stress Failure Parameter versus Lower Limit Stress $\bar{\sigma}$ and Radial Position for a 0.080 in. (2.0 mm) Drop Impacting ZnSe at 1120 fps (341 m/s)

in velocity. Merely incorporating time into the failure criterion does not appear to be sufficient. There is evidence that the fracture strength of brittle materials is sensitive to loading rate if slow crack growth can occur.[8, 9] Thus, the dynamic fracture strength of the material must also be considered in the formulation of the failure criterion.

Two additional modifications of the pressure function were evaluated. Figure 77 compares these additional functions, denoted Cases 004 and 005, to the original modified function, denoted Case 001. Case 001 is the function defined in Figure 68 which was used to compute the stress curves in Figures 70, 71, 72, and 73.

Case 004 has the same initial and peak pressure values but decays at a faster rate than Case 001. For Case 004, α was calculated based on $P = P_\infty$ at $t_1 = 0.158\ d/V_o$. This relationship was determined empirically using data generated by Rosenblatt et al.[5, 6] For Case 005, it was assumed that the pressure was constant and equal to the water hammer value ($\rho_o V_o C_o$) from $t = 0$ to $t = t_c$, then decayed to P_∞ at $t_1 = 0.158\ d/V_o$.

Figure 78 presents predicted peak radial stresses versus radial position for the three pressure distributions shown in Figure 77 and compares them to values predicted by the WAVE-L solution in Reference 5. There is virtually no difference in peak stresses between Cases 001 and 004 where only the decay constant was changed to produce a faster rate of pressure decay. This tends to indicate that the peak stress at any radial location is not dependent on the decay part of the pressure curve, but seems to be more strongly influenced by the magnitude of the initial pressure, or possibly the peak pressure.

Reducing the peak pressure to the water hammer value as in Case 005 resulted in a slight decrease in the predicted peak stress at each radial location as would be expected, but

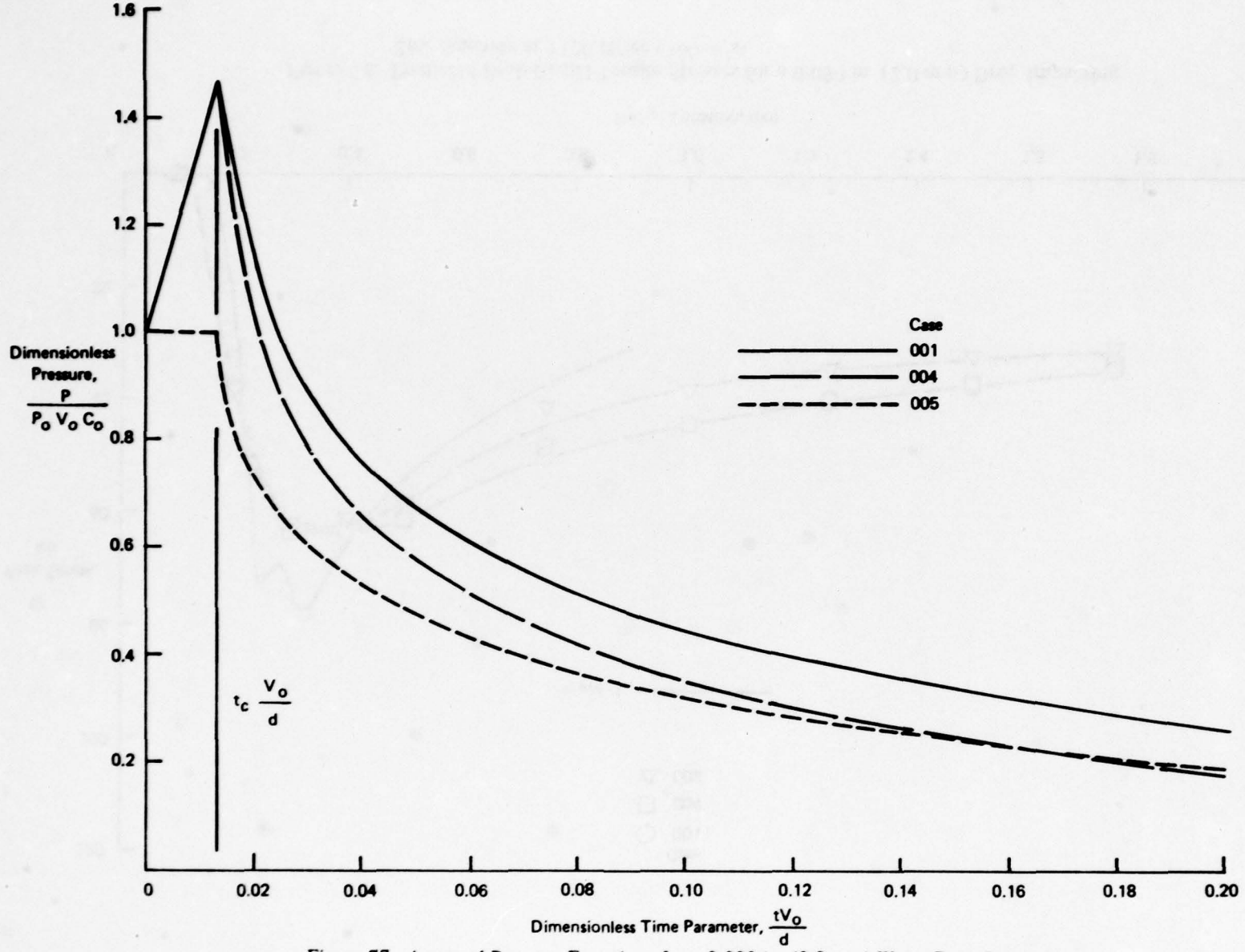

Figure 77. Assumed Pressure Functions for a 0.080 in. (2.0 mm) Water Drop Impacting Zinc Selenide at 1120 ft/sec (340 m/s)

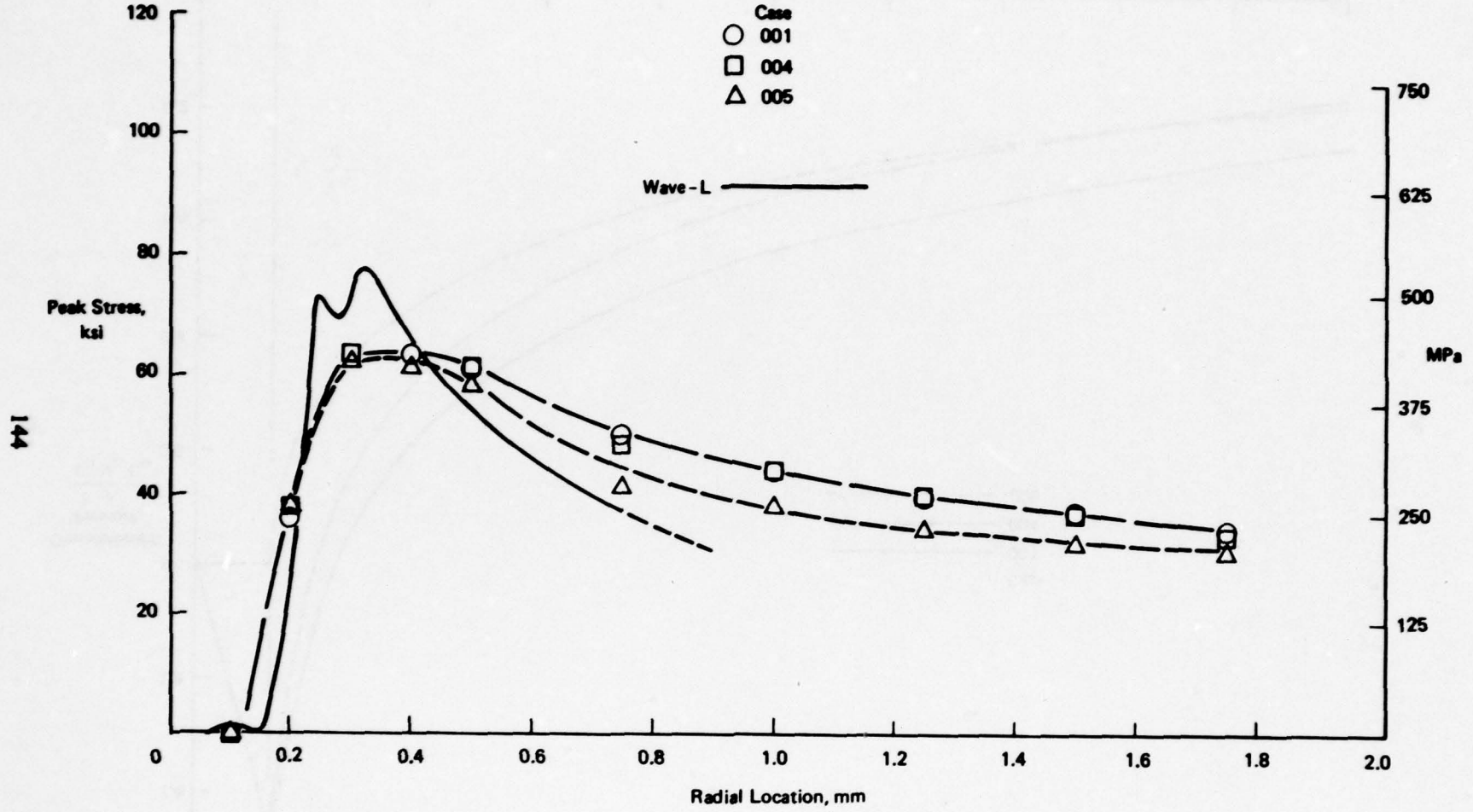

Figure 78. Predicted Peak Radial Tensile Stresses for a 0.080 in. (2.0 mm) Drop Impacting Zinc Selenide at 1120 ft/sec (340 m/s)

the general shape of the curve remained unchanged. The results from all three cases show relatively good agreement with the WAVE-L results at smaller radial locations, but diverge at radial locations greater than 0.016 in. (0.40 mm).

The primary difference between the two analytical models lies in the description of the pressure function. In the WAVE-L model, pressure is a function of both time and space (P(r,t)). In the analytical model modified in this program, the pressure is uniform over the loaded area and varies only with time (P(t)). This latter model is simpler than the WAVE-L model and requires much less computer time for a solution. It should aid in the formulation of damage prediction. For example, the model can be used to study the trade-off between drop diameter and impact velocity to produce comparable states of stress.

SECTION IV

CONCLUSIONS

A. Experimental Investigation

Damage threshold velocities, defined as the lowest velocity of impact by a 0.080 in. (2.0 mm) diameter drop which produced a fracture detectable by optical microscopic examination, were found to be as follows:

(1)	Zinc Selenide	- between 450 and 500 fps (137 and 152 m/s).
(2)	Zinc Sulfide	- approximately 575 fps (175 m/s).
(3)	Silicon	- approximately 900 fps (274 m/s).
(4)	Magnesium Fluoride	- between 900 and 1120 fps (274 and 340 m/s), but closer to 1120 fps.
(5)	Spinel	- approximately 1300 fps (396 m/s).
(6)	Sapphire	- between 1500 and 1750 fps (457 and 535 m/s).

As the velocity was increased above the damage threshold, the number of fractures formed by a single drop impact increased and, if the velocity were high enough, a complete ring fracture pattern was formed. These patterns consisted of fractures which formed a ring around an undamaged area. Complete ring fracture patterns were formed on zinc selenide at 500 fps (137 m/s), zinc sulfide at 730 fps (222 m/s), silicon at 1120 fps (340 m/s), spinel at 1750 fps (535 m/s), and sapphire at 2000 fps (610 m/s).

The circular nature of the ring patterns formed by the transgranular fractures on polycrystalline zinc selenide and zinc sulfide have been previously described.[1] The ring patterns on silicon, spinel, and sapphire were characteristic of the crystal lattice and orientation of these single crystal specimens. Silicon exhibited a square pattern representative of the 4-fold symmetry about the a, b, or c-axis of its cubic

lattice. Spinel exhibited an equilateral triangular pattern representative of the 3-fold symmetry about the [111] direction of its cubic lattice. Sapphire exhibited a hexagonal pattern representative of the 6-fold symmetry about the c-axis of its hexagonal lattice. The hexagonal fracture pattern did not appear to be foreshortened as would be expected if the c-axis was tilted 60° from the normal to the specimen surface as was reported by the vendor. Magnesium fluoride exhibited two intersecting sides of a square pattern consistent with the 4-fold symmetry of its cubic lattice.

Reducing the grain size of zinc selenide significantly increased its resistance to damage from water drop impact. In fact, the resistance to drop impact damage of fine-grained zinc selenide approached that of zinc sulfide of comparable grain size based on the size of the annular, ring-fractured areas. However, based on the number of cracks within the annular areas, zinc sulfide was still significantly more erosion resistance than fine-grained zinc selenide.

The extent of damage to zinc selenide from single drop impact decreased with the angle of impact between angles of 90° and 45°, at a constant impact velocity of 730 fps (222 m/s). The inner radius of the annular pattern of ring fractures remained essentially constant while the outer radius decreased as the impact angle decreased. The appearance of the ring fracture patterns suggest that, to a first approximation, damage is controlled by the component of the impact velocity that is perpendicular to the specimen surface.

The overlapping single drop experiments performed with zinc selenide showed that previously formed ring fractures are surprisingly resistant to increases in damage when subsequent drops impact the same area. Once a hexagonal array of ring fractures has been formed, it is almost impossible to detect the location

of impact of a subsequent drop. Upon repeated drop impact, the existing ring fractures do ultimately grow deeper as evidenced by a decrease in optical transparency. This behavior indicates the complexity of the propagation of stress waves once the initial pattern of ring fractures has formed and points out the problems inherent in analytically modeling the early stages of the erosion process for this type of material.

Comparison of the results from the small drop rainfield experiments with zinc selenide and zinc sulfide to those from prior standard rainfield experiments (Ref. 1) provides several interesting conclusions on the effects of drop size. The relationship between erosion damage and loss of transmittance for the same material was different in the two rainfields. For a given loss of transmittance, the specimen exposed to the small drop rainfield suffered more subsurface damage by extension of the ring fractures and less surface damage by pitting than did the specimen exposed to the standard rainfield. The erosion resistance of zinc sulfide, relative to that of zinc selenide, was less in the small drop rainfield than in the standard rainfield. A simple equivalency of total mass of water impacted per unit area is not adequate to correlate damage rate in the two rainfields. Predictive equations will have to incorporate drop diameter effects.

The single drop impact experiments proved that an antireflection coating with a thickness of only a few microns can modify the response of the substrate to water drop impact. A thorium fluoride coating prevented damage to zinc sulfide, although the coating fractured and/or completely debonded at the site of impact. A proprietary coating on gallium arsenide also prevented damage to the substrate, although it too was removed in an annular area surrounding the center of impact. A lanthanum fluoride coating, which appeared to suffer no damage in the single drop experiments, did not improve the erosion resistance of zinc sulfide in the small drop rainfield. Both single drop and rainfield experiments demonstrated that lack of adhesion

of the coatings to the substrates is a problem which requires more attention.

Single drop impact experiments demonstrated that a thin outer layer of zinc sulfide did protect the zinc selenide layer to which it was bonded if the layer was sufficiently thick. However, the presence of the interface did affect the response of the zinc sufide layer to drop impact. At an impact velocity of 730 fps (222 m/s), ring fractures penetrated through a 0.005 in. (0.13 mm) thick layer as compared to a penetration of only 0.00028 in. (0.007 mm) in thick, homogeneous zinc sulfide. At an impact velocity of 1120 fps (340 m/s), ring fractures penetrated through a 0.020 in. (0.50 mm) thick layer as compared to a pentration of only 0.008 in. (0.20 mm) in thick, homogeneous zinc sulfide. A bilayered specimen with a 0.020 in. (0.50 mm) thick zinc sulfide layer gave performance comparable to that of thick, homogeneous zinc sulfide in the small drop rainfield.

The potential of the bimedia concept was demonstrated with a specimen which used a layer of rubber to simulate the response of a liquid between an outer layer of zinc sufide and a zinc selenide substrate. Impact of 0.080 in. (2.0 mm) diameter single drops at 730 fps (222 m/s) produced smaller annular, ring-fractured areas on the zinc sulfide outer layer of the bimedia specimen than were produced on thick, homogeneous zinc sulfide; however, more cracks were present within the annular areas on the bimedia specimen. The larger than normal grain size of the zinc sulfide layer on the bimedia specimen probably contributed to the greater number of cracks. The bimedia concept shows promise and should be investigated further.

B. Theoretical Predictions

The modification of the analytical drop impact model to incorporate a decay with time in the impact pressure resulted in more realistic stress-time curves than were computed by the original model in which pressure was assumed to remain constant. At a given radial location, the initial part of the stress-time curve for the variable pressure case was similar to that for the constant pressure case, except the peak tensile stress was about 25% lower. Use of variable pressure also significantly reduced the magnitude of the relatively long duration tensile stress which followed the peak tensile stress pulse at larger radial locations.

The modified model predicted tensile stresses of 11.5 to 14.5 ksi (80 to 100 MPa) in zinc selenide impacted by a 0.080 in. (2.0 mm) diameter water drop at 500 fps (152 m/s). This is just above the damage threshold velocity which was found experimentally to be between 450 and 500 fps (137 and 152 m/s). The fact that the predicted tensile stresses for this case were close to the ultimate strength of 8.5 ksi (58.6 MPa) for zinc selenide demonstrated the validity of the modified analytical model.

As impact velocity was increased above the damage threshold velocity, quasistatic fracture strength became a less suitable failure criterion for zinc selenide. Failure was predicted to occur at much greater radial locations than were found experimentally. Incorporation of the duration of the stress pulse into the failure criterion by assuming a stress failure parameter equal to the value of the impulse (area under the stress-time curve) above a critical stress $\bar{\sigma}$ provided an improvement. For any selected value of $\bar{\sigma}$, the curve of the stress failure parameter versus radial location peaked within the band of radial locations where the major extent of fracturing was found experimentally to occur.

However, there was no unique value for either the stress failure parameter or the critical stress, $\bar{\sigma}$, which predicted failure for the three velocities investigated (500, 730, and 1120 fps or 152, 222, and 340 m/s).

To keep constant with velocity the value for the stress parameter which defined the boundaries of the fractured zone, the selected value of $\bar{\sigma}$ had to be increased with an increase in velocity. Merely incorporating the duration of the stress into the failure criterion does not appear to be sufficient. The dynamic fracture strength of the material must also be considered in the formulation of the failure criterion.

Additional modifications of the analytical model are not felt to be warranted at this time. The model as now formulated is simple and requires minimal computer time. Agreement between computed stresses and experimental results is as good as can be determined given the current state of failure criterion for dynamic loading. The model should prove to be a useful tool to study such things as the damage threshold velocity of materials and the trade-off between drop diameter and impact velocity for a given amount of damage.

REFERENCES

1. Hackworth, J.V. and Kocher, L.H., "Exploratory Development of Rain Erosion Resistant Infrared Window Materials," AFML-TR-77-84, May 1977.

2. Doerffler, W.W., Boord, T., Mar, H.Y.B., and Brown, J., "Erosion Resistant AR Coatings for IR Windows," AFML-TR-77-8 Feb. 1977.

3. Wahl, Norman E., "Supersonic Rain and Sand Erosion Research; Part I - Design, Construction, and Operation of a Mach 3 Rotating Arm Apparatus," AFML-TR-69-287, Part I, September 1969.

4. Blowers, R.W., "On the Response of An Elastic Solid to Droptlet Impact," J. Inst. Math. Applics., 5, 167, 1969.

5. Rosenblatt, M., Eggum, G.E., DeAngelo, L.A., and Kreyenhagen, K.N., "Numerical Investigation of Water Drop Erosion Mechanisms in Infrared-Transparent Materials." AFML-TR-76-193 December 1976.

6. Rosenblatt, M., Sto, Y.M., and Eggum, G.E., "Numerical Analysis of Water Drop Impact on a Brittle Target," ASTM Conference on Erosion: Prevention and Useful Applications, October 1977.

7. Taler, F.R. and Butcher, B.M., "A Criterion for Time Dependence of Dynamic Fracture," Sandia Laboratories, 1968.

8. Crouch, A.G. and Jolliffe, K.H., "The Effect of Stress Rate on the Rupture Strength of Alumina and Mullite Refractories," Proc. Brit. Ceram. Soc., 15, 37-46, 1970.

9. Kotchick, D.M. and Tressler, R.E., "Surface Damage and Environmental Effect on the Strain-Rate Sensitivity of the Strength of Sapphire and Silicon Carbide Filaments," J. Mat. Sci., 10, 608-612, 1975.

*U.S.Government Printing Office: 1979 — 657-002/559